

2009

A Non-Invasive Semiconductor Optical System To Measure Skin Tension

Anna Charron Dugas

Louisiana State University and Agricultural and Mechanical College

Follow this and additional works at: https://digitalcommons.lsu.edu/gradschool_theses

 Part of the [Engineering Commons](#)

Recommended Citation

Dugas, Anna Charron, "A Non-Invasive Semiconductor Optical System To Measure Skin Tension" (2009). *LSU Master's Theses*. 1649.
https://digitalcommons.lsu.edu/gradschool_theses/1649

This Thesis is brought to you for free and open access by the Graduate School at LSU Digital Commons. It has been accepted for inclusion in LSU Master's Theses by an authorized graduate school editor of LSU Digital Commons. For more information, please contact gradetd@lsu.edu.

**A NON-INVASIVE SEMICONDUCTOR OPTICAL SYSTEM TO
MEASURE SKIN TENSION**

A Thesis

Submitted to the Graduate Faculty of the
Louisiana State University and
Agricultural and Mechanical College
in partial fulfillment of the
requirements for the degree of
Master of Science in Biological and Agricultural Engineering

in

The Department of Biological and Agricultural Engineering

by
Anna Charron Dugas
B.S., University of Nebraska-Lincoln, 2002
December 2009

ACKNOWLEDGEMENTS

I would like to thank my principal advisor, W. Todd Monroe, Ph.D., for his guidance, assistance, and patience in supporting me through this project. I appreciate the support Dr. Monroe has given me in the logistics of dealing with commercial clients, funding, patent application, and my part time student/ full time staff status. I would also like to express gratitude to Daniel L. Thomas, Ph.D. for his advisement and patience as my employment supervisor and thesis committee member. I am grateful for the confidence and opportunities that Dr. Thomas has bestowed upon me in the last few years. I want to thank Frank Greenway, M.D. for his assistance and support, as well as, serving on my thesis committee. I am thankful for his collaboration with Meridian Medical, Inc. and encouragement of their support.

I would also like to give a special thanks to Yin-Lin (Jack) Chiu for his assistance in instrumentation design; Thomas McClure for his assistance in probe fabrication; Warren Hull and the CxC Engineering Communication Studio for use of the 3D rapid prototyping system; Kenneth Matthews, Ph.D. in Medical Physics for his assistance with the Velmex automated precision stage; and Joey Schwertz for assisting me with some of the AutoDesk® Inventor™ drawings seen in this thesis. I thank the members of Monroe lab and the Biological and Agricultural Engineering faculty and staff for their support and encouragement. I also thank my forty volunteers for the human subject testing for their time and bravery.

Finally, I am grateful and blessed for my family and friends who supported me through my graduate school adventure. And last but not least, I would to like thank my husband, Joseph, for his constant encouragement, support and assistance during the pursuit of my degree.

TABLE OF CONTENTS

ACKNOWLEDGEMENTS	ii
LIST OF TABLES	v
LIST OF FIGURES	vi
LIST OF ABBREVIATIONS	ix
ABSTRACT	x
CHAPTER 1. INTRODUCTION	1
The Importance of Skin Mechanics	1
CHAPTER 2. BACKGROUND AND LITERATURE REVIEW	5
2.1 Skin Biomechanics	5
2.2 Current <i>in Vivo</i> Methods of Skin Tension Measurement	14
2.3 Skin and Its Optical Properties	17
2.4 Project Objectives and Intellectual Merit	24
CHAPTER 3. CUTISFIRM INSTRUMENTATION DESIGN AND VALIDATION ...	31
3.1 Introduction	31
3.2 Materials & Methods	35
3.2.1 The Sharp GP2D120 Infrared Proximity Sensor.....	35
3.2.2 The Vacuum Probe System	40
3.2.3 The Electronic Control System	45
3.2.4 Methods for Cutisfirm Device Calibration	48
3.2.5 Methods with Artificial Skin Models	51
3.2.6 Methods with <i>in Vivo</i> Skin	53
3.3 Results	55
3.3.1 Calibration and Tolerance Determination of the Deformation	55
3.3.2 Exploration of the Color Variation using the GP2D120 Sensor	58
3.3.3 Effect of Negative Pressure on the Distance Measurement	60
3.3.4 Examination of the Viscoelasticity of Polyurethane Elastomers	62
3.3.5 Examination of the Viscoelasticity <i>in Vivo</i> on the Back of the Hand	65
3.4 Discussion	72
CHAPTER 4. CONCLUSIONS AND FUTURE CONSIDERATIONS	82
4.1 Conclusions	82
4.2 Future Considerations	82

REFERENCES	85
APPENDIX A: COMMERCIAL DEVICES FOR SKIN TENSION MEASUREMENT..	90
APPENDIX B: DRAWINGS OF THE CUTISFIRM DEVICE	93
APPENDIX C: WIRING DIAGRAMS AND PART INFORMATION	97
APPENDIX D: DATA TABLE FROM DORSAL HAND SKIN STUDY	114
APPENDIX E: BASIC STAMP 2PX OPERATIONAL PROGRAM	116
APPENDIX F: BASIC STAMP 2 OPERATIONAL PROGRAM	135
APPENDIX G: uM-FPU MATH CO-PROCESSOR IDE PROGRAM.....	138
APPENDIX H: MICROSOFT OFFICE EXCEL VBA PROGRAM	141
VITA	160

LIST OF TABLES

Table 1.1 The Top Five Surgical Cosmetic Procedures in 2007	4
Table 3.1 List of Valspar Paint Color Samples Used in Color Variation Study	59
Table 3.2 Distribution of Ages and Gender in Human Subjects	65
Table 3.3 Population Averages of Data Components for the Different Hand Positions ...	68
Table 3.4 Deformation Differences between Hand Positions	68
Table 3.5 Material Properties of Sorbothane ®	75

LIST OF FIGURES

Figure 1.1. The Median Age Increase of the U. S. Population from 1980 to 2006	2
Figure 2.1. Diagram of Human Skin Cross-section	5
Figure 2.2. A Schematic of the Structure of Collagen	7
Figure 2.3. An Arm of a Patient with Elastoderma	8
Figure 2.4. Langer's Lines	10
Figure 2.5. Effect of Forearm Measurement Zone Using the Dermal Torque Meter	11
Figure 2.6. Example Effect of Arm Position on Skin Tension Measurement	12
Figure 2.7. Example Effect of Probe Placement Angle on Skin Tension Measurement....	13
Figure 2.8. Strain-time Relationship of the Cutometer Suction Device	14
Figure 2.9. Classifications of Commercial Skin Tension Measurement Devices	15
Figure 2.10. Light Passing through a Slice of Material	18
Figure 2.11. The Sharp GP2D120 IR Proximity Sensor	19
Figure 2.12. Light Path of the Sharp GP2D120 IR Proximity sensor	20
Figure 2.13. A Diagram of Light Scattering in Skin	21
Figure 2.14. Absorption Spectra of Lipids and Oxy-/Deoxy-hemoglobin	23
Figure 2.15. Preliminary Vacuum Testing on Skin	25
Figure 2.16. Examples of the light obstruction method for measuring skin deformation...	27
Figure 2.17. A Design of the Skin Testing Probe	27
Figure 3.1. Images of the Skin Testing Probe Proposed Design	32
Figure 3.2. Vacuum Operation in a Cutisfirm Prototype	33
Figure 3.3. A Working Prototype of the Cutisfirm Skin Tension Measurement System ...	34
Figure 3.4 Example Output Characteristics of GP2D120 IR Proximity Sensor.....	36

Figure 3.5	Beam Width Characteristics of the Sharp GP2D120 IR Proximity Sensor....	37
Figure 3.6	Image of IR Beam Spot from Proximity Sensor in a Cutisfirm Prototype ...	38
Figure 3.7	Signal Output of Sharp GP2D120 IR Proximity Sensor	38
Figure 3.8	Circuit diagram of the signal conditioning used with the GP2D120	39
Figure 3.9	Signal Conditioned Output of the Sharp GP2D120 IR Proximity Sensor	40
Figure 3.10	Vacuum Supply System for the Cutisfirm Prototype	41
Figure 3.11	Vacuum Pressure Profile for a 10-Second Test	41
Figure 3.12	Hargraves C103E-12 Pump Flowrate Profile	42
Figure 3.13	Freescale Semiconductor MPXV6115VC6U Integrated Pressure Sensor	43
Figure 3.14	Calibration Graph of the MPXV6115VC6U Pressure Sensor	43
Figure 3.15	Airtrol V-800 Miniature Vacuum Regulator	44
Figure 3.16	Cutisfirm Suction Probe with Quick Release Tube Fitting Attached	45
Figure 3.17	BASIC Stamp BS2px and BS2 Microcontrollers and uM-FPU V3.1 chip....	46
Figure 3.18	5.7” Amulet On-board LCD Touchscreen	48
Figure 3.19	Signal Output Difference with Pump Power Isolated	49
Figure 3.20	Calibration Setup for the Sharp GP2D120 IR Proximity Sensor	50
Figure 3.21	Probe-insert Setup for the Calibration of the GP2D120 IR Sensor	50
Figure 3.22	Probe Setup for Artificial Skin Model Testing	52
Figure 3.23	Beam Reflector is Makeup Concealer	52
Figure 3.24	Setup for Measuring Tension Effects on a Polyurethane Elastomer	53
Figure 3.25	Images of Skin Deformation on the Back of the Hand	54
Figure 3.26	Calibration Curve for the Sharp GP2D120 IR Sensor	56
Figure 3.27	Dynamic Stage Study on GP2D120 IR Sensor Performance	57
Figure 3.28	Speed and Tolerance Comparisons in Dynamic Stage Study	58

Figure 3.29 Effect of reflector color on the GP2D120 IR Proximity Sensor	60
Figure 3.30 Distance Output under Different Electrical Configurations	61
Figure 3.31 Distance Output of the Electronic Noise Compared to Hand Skin Data	62
Figure 3.32 Polyurethane Elastomer Hardness Effects	63
Figure 3.33 Effect of Tension on the 50 OO Polyurethane Elastomer Sheet	64
Figure 3.34 Example Dorsal Hand Skin Deformation Measurements	66
Figure 3.35 Description of Data Components of the Skin Study	67
Figure 3.36 The Data Components T, E, V, R from Human Subject Testing	69
Figure 3.37 Age and Gender Correlation for Total Skin Deformation (T)	70
Figure 3.38 Age and Gender Correlation for Recoil Skin Deformation (R)	70
Figure 3.39 Age and Gender Comparisons of Non-significant Data Components	71
Figure 3.40 The Non-significant Effect of Concealer Application	74
Figure 3.41 Strain-Energy Densities for 50 OO Polyurethane Elastomer in Tension ...	77
Figure 3.42 Time of Recovery Determination by Linear Approximation	78
Figure 3.43 Age and Gender Comparison in Lotion Application Frequency	80

LIST OF ABBREVIATIONS

ABS	Acrylonitrile Butadiene Styrene
BM	Basement Membrane
CCD	Charge-coupled Device
E	Elastic Deformation Response
ECM	Extracellular Matrix
GUI	Graphic User Interface
ID	Inner Diameter
IR	Infrared
LED	Light Emitting Diode
NIH	National Institutes of Health
PTFE	Polytetrafluoroethylene
PU	Polyurethane
R	Recoil Deformation Response
RD	Cumulative Recoil Distance
R/E	Elastic Recovery
R/T	Biological Elasticity
SC	Stratum Corneum
SD	Secure Digital Card
T	Total Deformation Response
ToR	Time of Recovery from Vacuum
V	Viscous Component of Deformation
V/E	Viscoelastic Ratio

ABSTRACT

The objectives of this project are to design, construct, validate and test a low-cost, non-invasive and painless device to measure skin tension. Skin is a complex, multi-layered, anisotropic material with non-linear viscoelastic behavior during stress application. The intricate balance of different semi-elastic fibers and continuous regeneration has brought difficulty to the accurate measurement of its mechanical properties. Commercial skin tension measurement products have been described, but are too expensive to be readily accessible for skin research and clinical utilization. The device to be developed in this project differs from existing devices in that it measures skin deformation under vacuum using a non-invasive, low power, reflective light sensor. The results in this report show that this “Cutisfirm” skin tension measurement system is an effective product for measuring dynamic mechanical properties of skin. The Cutisfirm device was able to measure quantified changes in skin and artificial skin models within the 95% tolerance level of $\pm 0.139\text{cm}$ and up to 1.875cm/sec movement velocities. Results show changes in dorsal hand skin measured *in vivo* between open and closed fist positions as a function of gender and age in a diverse population subset. The Cutisfirm skin tension measurement system could be a potential candidate for a mass-produced, affordable device option for general clinical use.

CHAPTER 1: INTRODUCTION

The largest and most rapidly growing organ of the body, skin, is a complex, multi-layered, anisotropic material with non-linear viscoelastic behavior during stress application. The intricate balance of different semi-elastic fibers and continuous regeneration has brought difficulty to the accurate measurement of its mechanical properties.

The Importance of Skin Mechanics

Several reasons are available to justify the need for an accessible and accurate measurement system for skin mechanics. First, there is an increased focus on the human aging process which includes the gradual degradation of skin and changes in its mechanical properties. (Daly and Odland 1979; Leveque, de Rigal et al. 1980; Hull and Warfel 1983; Sumino, Ichikawa et al. 2004; Waller and Maibach 2005; Waller and Maibach 2006; Diridollou, de Rigal et al. 2007) The increased focus on aging is due to the United States human population getting older. According to the U.S. Census Bureau, the median age of the country was at 36.4 years in 2006 and is expected to increase along the general trend established since 1980. The median age is projected to be greater than 37 years by 2010. (See Figure 1.1) So as the human population ages, there will likely be greater numbers of skin-related medical conditions that clinicians must diagnose and treat. A device to characterize changes in skin's response to mechanical stress may be a useful diagnostic tool or one to evaluate therapy efficacy in aging patients.

Another justification for the need of accessible skin mechanics measurement devices is for the growing population of patients seeking direct adipose removal through cosmetic surgery. According to the American Society for Aesthetic Plastic Surgery, there has been a 114% increase in the number of annual surgical cosmetic procedures since 1997. (ASAPS 2007) Liposuction,

the removal of adipose tissue, is the most common cosmetic surgery reported in 2007. (See Table 1.1) Liposuction via tumescent (wet) technique has been characterized to not increase skin laxity by Henry et al. (Henry, VanLook et al. 1996) However, there have been reports showing that subcutaneous fat or hypodermis plays a major role in skin's mechanical response to stress; therefore more information could be learned from the effects of different methods of liposuction on skin mechanics. (Diridollou, Berson et al. 1998; Pierard 1999; Hendriks, Brokken et al. 2003; Mann, Palm et al. 2008)

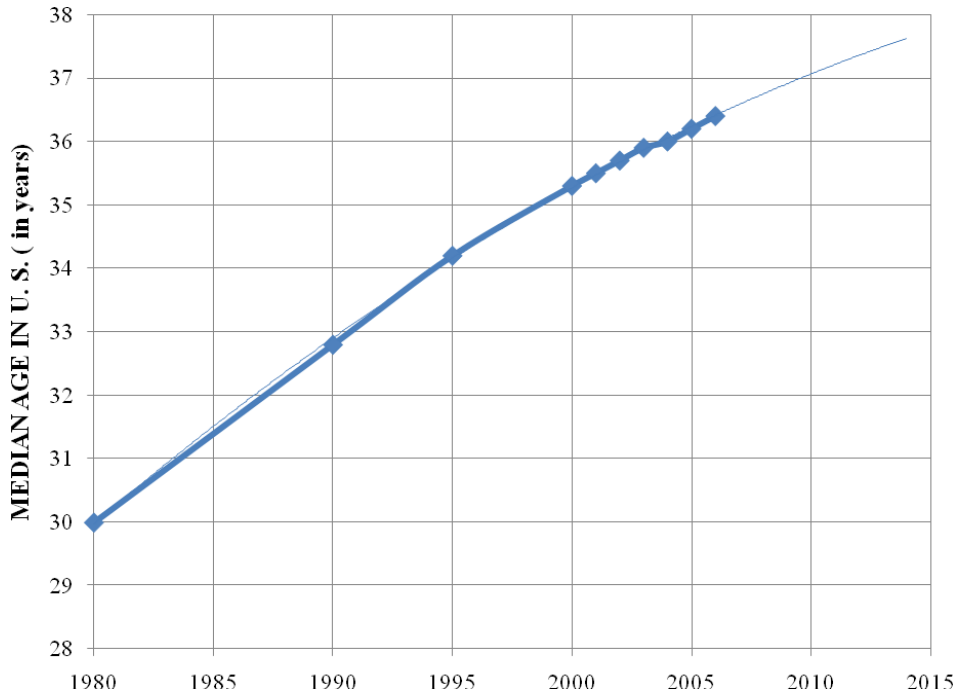


Figure 1.1: The median age increase of the U. S. population from 1980 to 2006. Data was taken from “Table 7. Resident Population by Age and Sex: 1980 to 2006,” reported by the U.S. Census Bureau. (Release date: May 17, 2007)

Accessible skin mechanics measurement devices can also be used for monitoring skin changes in pregnancy and rapid weight loss in surgical procedures such as post-bariatric surgery and abdominoplasty as described below.

Post-pregnancy healing: During pregnancy, several changes can occur in the skin resulting from the hormone alterations created by the gravid state. Although most skin conditions such as pigmentary and vascular changes return to normal postpartum, some of the structural changes remain in a lesser form. The most common structural change, striae gravidarum or “stretch marks,” occurs in 90% of pregnant white women, and some black and Asian women. (Elling and Powell 1997) Striae gravidarum is thought to occur as a result of skin thinning during increased layer-wise tension, causing the disruption of collagen fibers. Although stretch marks will reduce in appearance post-pregnancy, many will remain and never fully clear in several women. The study and treatment of striae gravidarum, as well as another common structural change molluscum fibrosum gravidarum (skin tags), could benefit from physician available devices which are able to accurately measure skin mechanics during and post-pregnancy.

Post-bariatric surgery: Bariatric surgery (e.g., the gastric bypass procedure) has been noted to be one of the most effective treatments for morbid obesity as well as related metabolic diseases. The American Society for Metabolic & Bariatric Society reports that in 2006, an estimated 177,600 people had bariatric surgery in the U.S. (ASMBS 2007) As a result of successful bariatric surgery and diet adjustment post surgery, rapid weight loss will occur, often leaving patients with excess or droopy skin. The excess skin is removed with subsequent body contouring surgery (body, breast, arm, and thigh lifts). Skin tension measurement devices could be used to monitor the treatment and structural healing in skin for post-bariatric surgery.

Abdominoplasty or the “tummy tuck”: This is a surgical procedure that is often done when skin and fat around the abdomen is loose. Loose skin on the abdomen is commonly caused by rapid weight loss, or pregnancy. (ASAPS 2008) Abdominoplasty is considered in the top 5 of

cosmetic surgeries. (See Table 1.1) Skin tension measurement devices could be used along with the diagnostic process and to explore healing post-abdominoplasty.

Table 1.1 The Top Five Surgical Cosmetic Procedures in 2007

ASAPS 2007 Statistics on Cosmetic Surgery		
Procedure	Reported	Percentage
Liposuction	456,828	31.8%
Breast augmentation	399,440	27.8%
Eyelid surgery	240,763	16.8%
Abdominoplasty	185,335	12.9%
Breast reduction	153,087	10.7%
Total	1,435,453	

In general terms, the measurement of skin mechanics could be used to observe the overall health of the organ and the individual enclosed by it. The mechanics of the skin could be monitored for an individual through a course of a medical or cosmetic treatment for any number of reasons besides the aforesaid topics. Monitoring the progress of UV skin damage, wound repair, the disease scleroderma, and reproductive aging/menopause changes are just a few of the other treatments that regular use of skin tension measurement instruments in clinics could prove useful in improving healthcare. Skin mechanics is often directly correlated to a measure of skin firmness or skin tension and these terms will be used interchangeable in the following document.

CHAPTER 2: BACKGROUND AND LITERATURE REVIEW

2.1 Skin Biomechanics

Skin is the largest single organ of the body which makes up about 5.5% of body mass. (Edwards and Marks 1995) The main functions of skin are to provide a protective and supportive covering for the body, to remain tense but allow free motion of joints, to counteract gravitation, and to be pliable enough for effective contact with surfaces for tangential touch sensation. (Serup 2002) It succeeds at these functions because of its organized, stratified structure composed of four main living layers: the epidermis, the basement membrane, the dermis, and the hypodermis (subcutaneous fat). (Hendriks 2001; Oikarinen and Knuutinen 2002) Figure 2.1 depicts the four main layers of human skin in a cross-sectional view. The dermal layer is the origin of the hair and sweat glands, which is also shown in Figure 2.1.

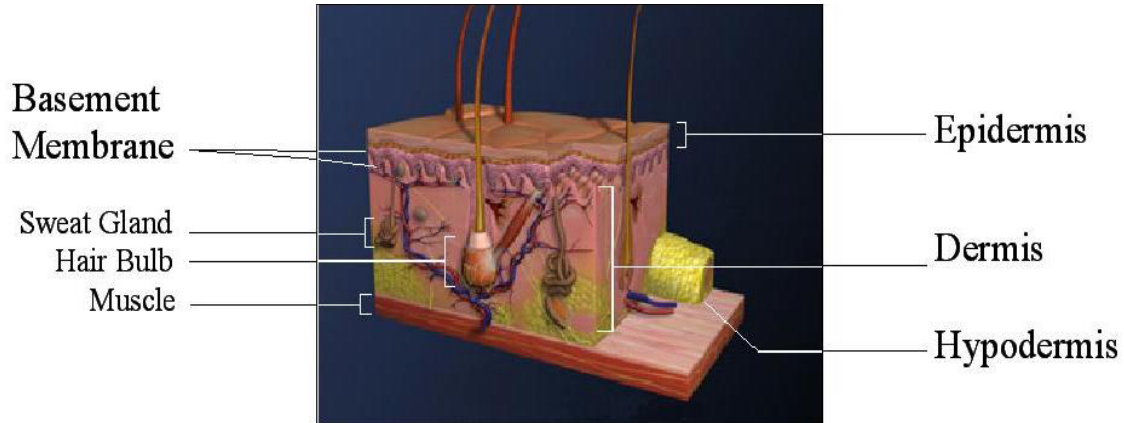


Figure 2.1: Diagram of human skin cross-section. The four major layers of living skin (outermost to innermost) are the epidermis, basement membrane (epidermal-dermal junction), dermis, and hypodermis (subcutaneous fat). The dermal layer is the origin of hair and sweat glands. Also in the dermis, collagen and elastin fibers make up the extra-cellular matrix and contribute to the mechanical nature of skin. (Image obtained from 3DScience.com.)

The superficial epidermis is approximately 75-150 microns in thickness and typically considered to be made of three layers, the stratum corneum (outermost), the stratum granulosum,

and the stratum spinosum. The inner two layers of the epidermis are primarily composed of keratinocytes, which are the cells that flatten and overlap to become the stratum corneum. (Hendriks 2001) Though very important for transdermal penetration and transport, the epidermis is less important in material mechanics than the other three main skin layers since the extra-cellular matrix surrounding the keratinocytes, melanocytes, and other cells is less fibrous and contains more adhesion molecules for assisting in the movements of keratinocytes to the skin surface. (Viac, Schmitt et al. 1994; Fox 1999)

The basement membrane (BM), also referred to as the dermal-epidermal junction or the basal lamina, separates the epithelial cells of the epidermis and the mesenchymal connective tissue of the dermis. It is a flexible, sheet-like structure approximately 50 to 100nm thick made of collagen IV, glycoproteins, and polysaccharides. (Fox 1999; Oikarinen and Knuutinen 2002) The BM primarily organizes the proteins in the adjacent cell membranes to induce cell differentiation and polarity changes and it assists with cell migration. The type IV collagen in the BM forms a network that stabilizes the layer and can contribute slightly to the mechanics of skin. (Hendriks 2001; Oikarinen and Knuutinen 2002)

The dermis is the most important layer to the mechanics of skin. It contains several components such as hair follicles, blood and lymph vessels, sweat glands, and nerve endings, as well as an extra-cellular matrix composed of collagen, elastin, and some reticulin. (Fox 1999; Hendriks 2001; Oikarinen and Knuutinen 2002) Collagen is the primary component of the dermal extracellular matrix (ECM) where it makes up 70 to 80% of the dry mass in skin. Collagen is composed of fibers which are approximately 300nm long and staggered for structural stability and lay mainly parallel to the layers of skin. Collagen fibers are glycine-rich proteins made of alpha-chained polypeptides in a triple helical structure. (See Figure 2.2) The triple

helical structure is stabilized by the cross-linking of these alpha chains which occurs due to the hydroxylation of the amino acids proline and lysine. Collagen is synthesized in the fibroblast cells in the dermis. There are many different types of collagen. Types I and III make up 95% of the collagen in skin, however, other collagen types, IV, V, VI, and VII are present and play a role in matrix assembly. The types of collagen differ in the alpha-chained polypeptides that form them.

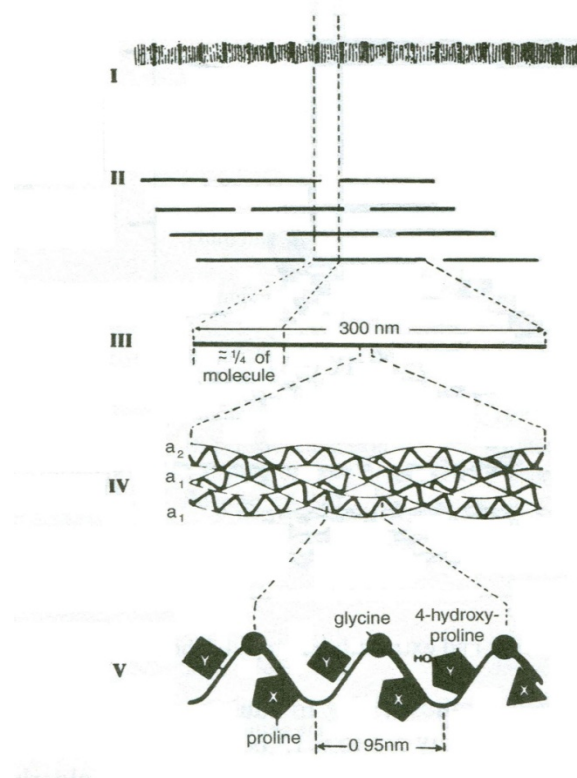


Figure 2.2: A schematic of the structure of collagen from largest structure to smallest. Collagen (I) is made of fibers aligned in a quarter-stagger pattern (II). Each fiber, approximately 300nm long (III), is made of three alpha-chained polypeptides which are formed into a triple helical structure (IV) due to cross-linking via amino acid hydroxylation.(V) (Oikarinen and Knuutinen, Chap. 1 Bioengineering of the Skin: Skin Mechanics, pg 5)

Collagen plays a major role in the mechanical characteristics of skin due to its prevalence in dermal ECM and its overlapping fibrous structure. Collagen is thought to control overall

stretching or distensibility of the skin since it is characterized by high tensile strength (1.5-3.5MPa), low extensibility, and high stiffness. (Serup 2002) Over time, existing collagen fibers become thicker and less soluble due to increased covalent bonding of adjacent polypeptide chains. This collagen fiber thickening reduces the flexibility and elasticity of dermis as the skin material ages. Aging of skin is also associated with a decline in overall collagen synthesis or rejuvenation which is otherwise known as age-related atrophy. (Oikarinen and Knuutinen 2002)

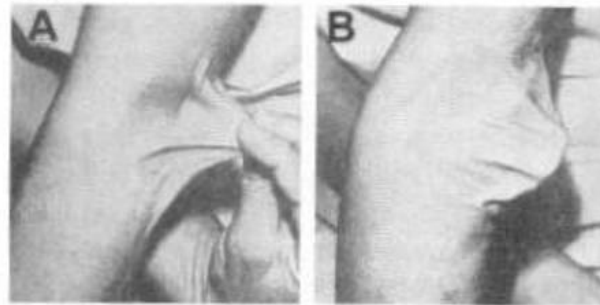


Figure 2.3: An arm of a patient with elastoderma, demonstrating the laxity (A) and delayed recoil (B) of the skin. Elastoderma is a skin condition formed by a local accumulation of abnormal elastic fibers in the lower dermis. (Oikarinen and Knuutinen, Chap. 1 Bioengineering of the Skin: Skin Mechanics, pg 10)

The other main component of the dermal layer which significantly impacts skin mechanics is elastic fiber. Elastic fibers are primarily composed of elastin (an alanine-rich, 70kDa, triple-helical polypeptide) formed covalently into a three-dimensional network. These fibers make up 1 to 2% of the dry mass in skin. The elastic fibers crisscross throughout dermal layer, where the oxytalan fibers run perpendicular to the epidermis and the elaunin fiber exist parallel to the skin layers. Elastic fibers are thought to be a key factor in the retraction of the skin after an applied force since they often exhibit almost complete reversible strains. (Serup 2002) The importance of the 3-D network of elastic fibers in skin mechanics is well depicted in elastoderma (Figure 2.3) which is a skin condition where a local accumulation of abnormal

elastic fibers creates skin laxity and delayed return of the skin after tension is applied.

(Oikarinen and Knuutinen 2002) These fibers, like collagen, also get thicker and shorter as skin ages.

The deepest major layer of skin is the hypodermis or subcutaneous fat. This layer is frequently excluded from the list in generalized articles and texts, but hypodermis layer has been found to play an important role in the mechanics of skin, in particularly with elasticity and extension. The hypodermis is a fibrous-fatty layer which is loosely connected to the dermis and it constitutes at least 10% of bodyweight. (Hendriks 2001) This layer is highly variable in thickness over the body and varies greatly with age, sex, race, and diet of the individual. (Diridollou, Berson et al. 1998; Pierard 1999) The primary purpose of the hypodermis in mechanics is to provide a cushion for impact and constant pressures.

Skin is a complex material comprised of linear elastic materials (collagen and elastin) arranged in preferential and sometime random directions, and confined aqueous regions (mainly epidermis and hypodermis) that exhibit viscous damping of external and internal forces. Also, the difficulty in reproducing measurements of stresses and strains in skin arises from its micro-anatomical variations not just through its multiple layers, but its variation across the body. This material makeup yields the mechanical behavior of skin, a non-homogenous, anisotropic, and non-linear viscoelastic material.

Figure 2.4 shows an illustrated pattern of Langer's lines depicted by Karl Langer in 1861. Langer's lines share a relationship with skin's directional variations called anisotropy. (Barbenel 2006) Physicians have used Langer's lines to decide where to make incisions during surgery since cuts parallel along lines generally heal better and faster. Along these Langer's lines, collagen and elastin fibers are stretched more than when the fibers are perpendicular and this allows for

maintaining skin firmness while improving joint flexibility and body movement. (Hendriks 2001)

A difficulty arises when considering Langer's lines in mechanical measurement since these lines vary from person to person slightly. (Barbenel 2006) However when visually monitored they can be used as a guide to skin's anisotropic, mechanical behavior.

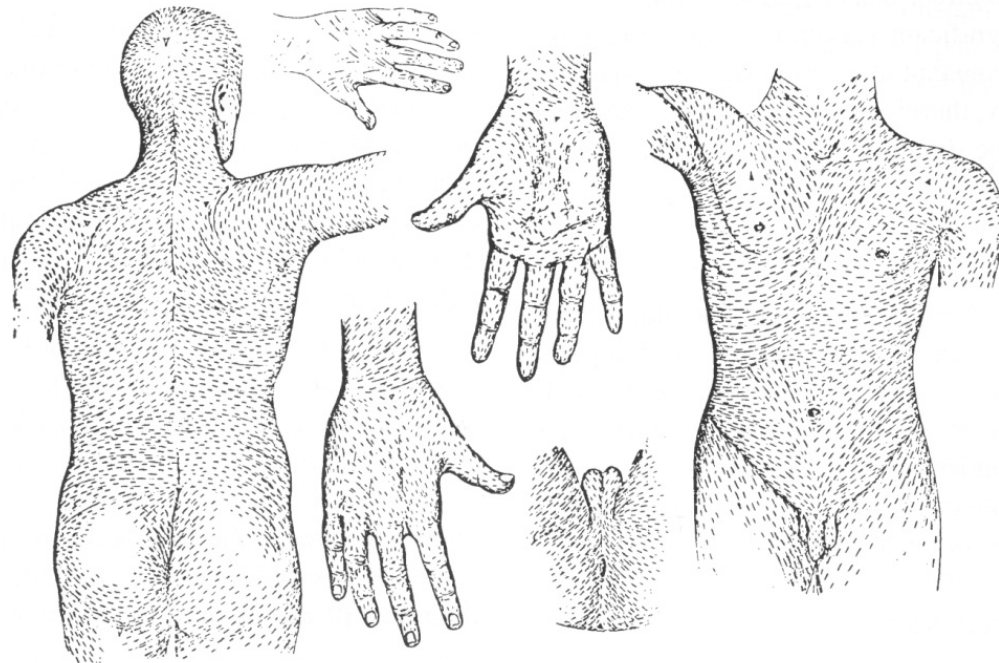


Figure 2.4: Langer's lines. Originally reported by Karl Langer in 1861, these are lines where skin exhibited the least flexibility. These lines were said to correspond to the arrangement of collagen fibers in order to improve body movement. (Barbenel, Chap. 64 Handbook of Non-Invasive Methods and the Skin, 2nd ed., pg 565)

Other significant anatomical variations in the mechanical behavior of skin are the overall change in tension and skin thickness across the body. To counteract gravitation on the body, skin covering the appendages is under greater tension than the skin on the body core. In Figure 2.5, data from a Dermal Torque Meter shows that as torque is applied to different areas on the forearm, the instrument meets more resistance on the distal ends of the forearm and is able to turn fewer degrees. (Rigal 2002) This observation coincides with how the skin is able to help

counteract gravity and assist in blood recirculation. Thus, the position where skin tension is measured needs to be monitored for reproducible data.

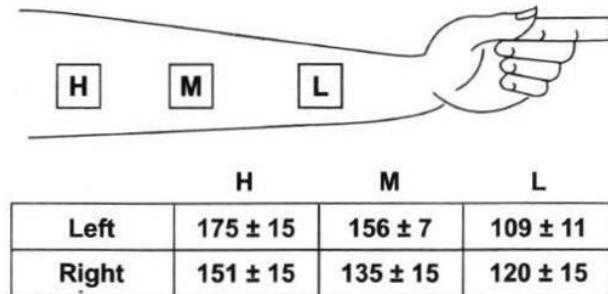


Figure 2.5: Effect of forearm measurement zone using the Dermal Torque Meter. The data is reported as relative angle of torque in degrees where the larger the value, the more flexible and less tense the skin is. Therefore, the data shows that the distal forearm regions are more tense than regions near the elbow. (Rigal, Chap. 5 Bioengineering of the Skin: Skin Mechanics, pg 73)

Skin tension measurement on the limbs will vary greatly with the position of the joints nearby. The underlying musculature impacts the forces to the skin and alters the skin's stretching ability. In Figure 2.6, the Dermal Torque Meter has been used on forearms held in different positions. The skin is reported to be the most relaxed when the forearm muscles are the most relaxed (90° elbow). As the arm of the person is extended, the forearm muscles extend which gives a smaller angle of torque (increased tension). If the person clinches a fist, the forearm muscles are contracted and this also increases the tension of the skin. (Rigal 2002)

One other anatomical complexity in the mechanical behavior of skin is its viscous or fluid-like characteristics. Skin exhibits damping or viscous effects during stress levels above normal preload due to the aqueous components in the material. If skin is subjected to consecutively applied loads or cycles, significant hysteresis will occur in the stress-strain curves. (Hendriks 2001) Therefore, the stress history is important to monitor during skin tension measurement.

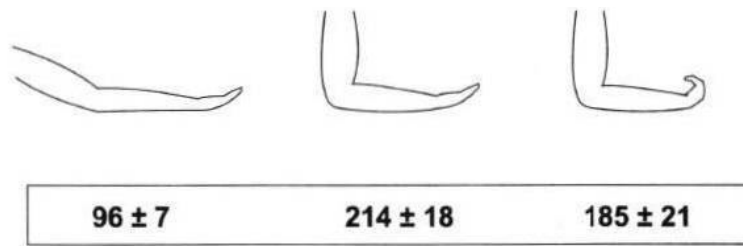


Figure 2.6: Example effect of arm position on skin tension measurement using the Dermal Torque Meter. The data is reported as relative angle of torque in degrees where the larger the value, the more flexible and less tense the skin is. Therefore, the data shows that as the forearm is relaxed by the bending of the elbow, the skin tension become more lax, however when a fist is clinched the forearm increases in tension, likely due to muscle below the skin. (Rigal, Chap. 5 Bioengineering of the Skin: Skin Mechanics, pg 74)

Skin mechanics is also impacted by external factors. Changes in temperature (thermo-contraction) and hydration (internally and externally) must be closely observed to achieve consistent skin tension readings. Surface thermal measurements using a temperature probe (thermistors) and hydration using a TEWL (Trans-Epidermal Water Loss) measurement are often taken along with tension measurements for improved consistency in data. (Rigal 2002) Both temperature and hydration are mainly affected by the environment history and diet of patient.

In addition to the aforementioned biological variables in skin, instrumental errors can be created from the flexibility of the skin when the tension measurement probes are applied. Figure 2.7 shows how the angle of probe pressed on the skin can affect torque angles using the Dermal Torque Meter. (Rigal 2002) Probe angle and placement onto the skin as well as probe attachment to the skin is the source for frequent errors in skin tension measurement using torsion and suction devices. (Serup 2002)

After considering the difficulties and complexities of skin tension measurement *in vivo*, mathematical models have been developed to characterize skin's mechanical properties. The mathematical models of skin are often derived from the measurements taken with different types

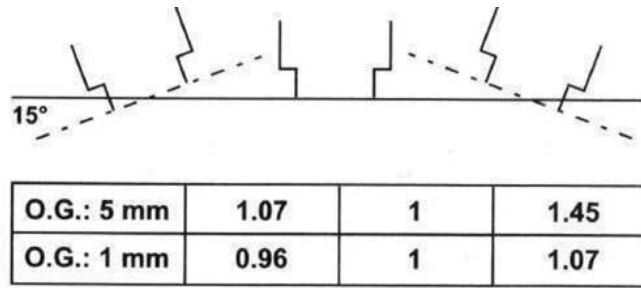


Figure 2.7: Example effect of probe placement angle on skin tension measurement using the Dermal Torque Meter. The data is expressed as a ratio of the torque measured at an angle over the torque measurement at perpendicular to the skin, where an accurate result equals a ratio of 1. (Rigal, Chap. 5 Bioengineering of the Skin: Skin Mechanics, pg 73)

of *in vivo* and *in vitro* devices. (See Figure 2.8) For defining skin mathematically, the principles such as Hooke's laws of elasticity have been used to model regions of tension where skin behaves elastically. (Diridollou, Patat et al. 2000; Serup 2002) Some reports consider the viscoelastic models, such as Maxwell and Kelvin-Voigt in skin measurement characterization. (Boyer, Zahouani et al. 2007; Jachowicz, McMullen et al. 2007) A combination of the Maxwell and Kelvin-Voigt models, termed the Burger Model, has been used to describe skin's reaction to torsion forces from the Dermal Torque Meter and specifically taken into account the impact of creep from continuous and repetitive stress. (Rigal 2002) Other reports contain more complex models using finite element modeling to more specifically define time-dependence and creep in skin mechanics. (Larrabee 1986; Larrabee and Galt 1986; Larrabee and Sutton 1986; Wu, Cutlip et al. 2006) To design an effective skin tension measurement device, consideration must be given to what information (qualitative, quantitative, and to what degree) is important to the study. Figure 2.8 describes the skin model of strain-time relationship of a commercial device, the Cutometer. (Berndt and Elsner 2002) This Cutometer skin biomechanics model will be similar to the model used to interpret the data resulting from the device built for this project, because of the similar data output structure, deformation (strain) vs. time.

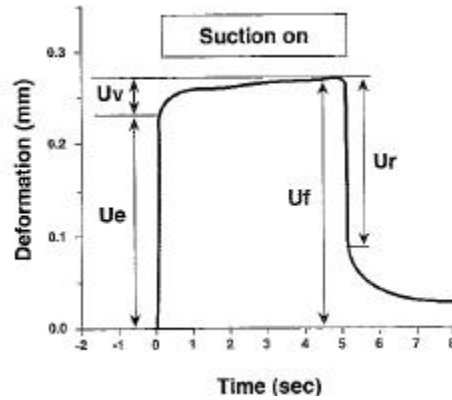


Figure 2.8: Strain-time relationship of the Cutometer suction device obtained on vulvar skin using a 2mm diameter probe cycling 500mbar of vacuum 5sec on, 3sec off. The parameters used to describe the strain: U_e = instantaneous deformation height, U_v = viscoelastic and viscous height change (creep), U_f = final deformation height, and U_r = instantaneous recovery height change. (Berndt and Elsner, Chap. 7 Bioengineering of the Skin: Skin Mechanics, pg 95)

2.2 Current *in Vivo* Methods of Skin Tension Measurement

Commercial and research devices are available to measure skin tension. Some of the commercial devices found in recent literature are detailed in Appendix A. The marketed devices for *in vivo* skin tension measurement can be classified into six categories based on function: applied suction, elastic shear propagation, indentation, pinching and pulling, torsion, and durometry. This section provides an overview of these methods. (See Figure 2.9)

Suction devices consist of a probe or tube with an opening placed cross-sectionally onto the skin. A vacuum pressure is applied inside the probe, causing in the skin exposed to the vacuum chamber to deform inward. The height of the skin deformation is measured and compared to the vacuum pressure applied, accounting for the diameter of the tube's orifice. The resulting data shows to the elastic and viscoelastic regions of skin plotted in stress-strain or strain-time curves. (Berndt and Elsner 2002)

Elastic shear propagation devices produce pulsatile pressure waveforms which create vibrations or waves of pressure along the surface of the skin. In these devices, the speed of the

elastic shear wave propagation is measured and correlates to skin viscoelasticity in a proportional manner. (Vexler, Polyansky et al. 1999)

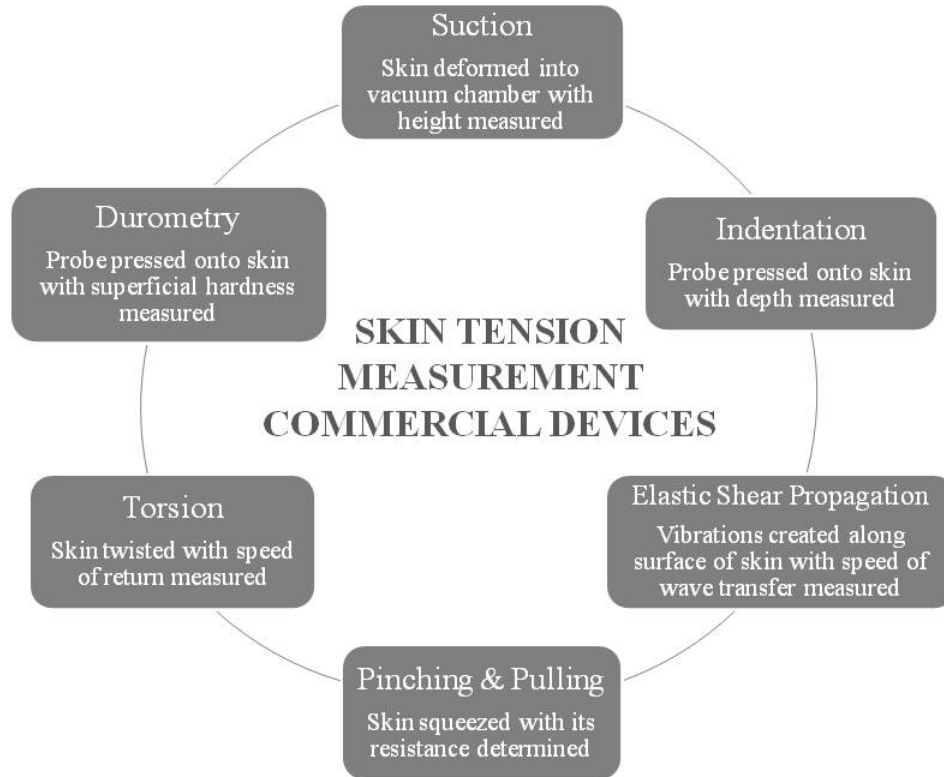


Figure 2.9: Classifications of commercial skin tension measurement devices.

In indentometry, a probe is pushed (positive pressure) onto the skin surface so that the skin deforms interior to the body. Indentation probes have been used for the measurement of cartilage stiffness during arthroscopy with some success. (Korhonen, Saarakkala et al. 2003; Arokoski, Surakka et al. 2005) Indentation probes have also been utilized in skin tension measurement using single, constant pressures, (Graves and Edwards 2002; Dawes-Higgs, Swain et al. 2004) as well as multiple, impact pressures. (Pugliese and Potts 2002) Accurate indentation methods on skin are complicated by underlying muscle movement more so than in suction methods for skin tension measurement. (Graves and Edwards 2002)

Pinching and pulling devices impact mostly the superficial layers of the epidermis. Pinching devices, such as the pinch elastometer described in Harrison et al. could be used for skin tension measurement. (Harrison, Bush et al. 2007) A pinching device would be used to clasp a section of skin and the resistance of the skin to the pinching motion will correlate to the firmness of the skin. Pulling devices, such as the Extensometer (see Appendix A) are attached firmly to the skin and stretch the surface of the skin in a transverse or superficially planar direction. (Vescovo, Varchon et al. 2002) The resistance of the skin to pulling is related to the firmness of the skin's exterior layers. The mechanisms of the stress-strain relationships in the pinched and pulled skin devices are more difficult to determine than in the other functional types of skin tension measurement machines, because of the complex, multi-axial stress application.

Torsion devices are commonly used to measure skin tension, especially when the firmness of the epidermis is of concern. Torsionmeters measure the elastic response of the skin to a twisting motion on the surface. The dermal torque meter described by Rigal in the Bioengineering of the Skin: Skin Biomechanics (2002, CRC Press) is a torsion device in which a concentric ring and an interior disc are affixed firmly to the skin. Then the disc inside the ring is rotated to a given angle and released to allow for a rotational return in response to the skin's elastic nature. The ability of the skin to return to its original orientation is measured in terms of angle, where a larger angle would relate to an increased laxity in the skin and a smaller angle would result from a firmer skin.

The final device functional type to be mentioned is a durometer. Durometers are used to measure the hardness of a material. The Rex Durometer, which is the international standard for measuring the hardness of rubber, plastic, and nonmetallic materials, has also been used to measure skin hardness. (Romanelli and Falanga 2002; Kissin, Schiller et al. 2006) The Rex

Durometer is used similar to the indentation device where the probe is pressed on the skin, but the measurement received is in terms of relative degrees of hardness from Shore 0 to 100. The initial hardness is recorded during the first second of firm contact with skin. The data resulting from durometer measurements can be used to compare the progression of treatments or skin conditions. However, the true correlation between the hardness measurement and the stress-strain relationship is not well developed.

Based on the principles of function for each type of skin tension device, suction devices will provide the simplest mechanics in a device along with the most informative data for the effects of tension on full-thickness skin. Therefore, the device to be designed in this work will be a suction device. See Section 2.4 for a comparison of popular commercial suction devices with the design in this project.

2.3 Skin and Its Optical Properties

When a slice of matter is exposed to light, it can interfere with the light beam via reflection, refraction, absorption, and scattering. (See Figure 2.10) Since biological tissue is a generally opaque media, the effect of refraction is masked by the effect of absorption and scattering. (Niemz 2007) Therefore, a light beam targeted at skin for penetration is affected primarily by absorption and scattering, with scattering being the dominant effect. Materials in skin that absorb are chromophores, such as hemoglobin and melanin. (Kollias 1995) Whereas, the scattering materials of the skin are the structures that differ in their index of refraction from the rest of the medium, which are cell membranes, and the stratum corneum. (Kollias 1995)

Light absorbance in tissue is the transfer of energy from the incidence light to the material in the form of heat motion or molecular vibrations. (Niemz 2007) A transparent material will allow light to pass through without energy loss or absorption, whereas an opaque

material will absorb the light energy. However, the transparency or opacity of a material is dependent on the wavelength of the incidence light. (Niemz 2007)

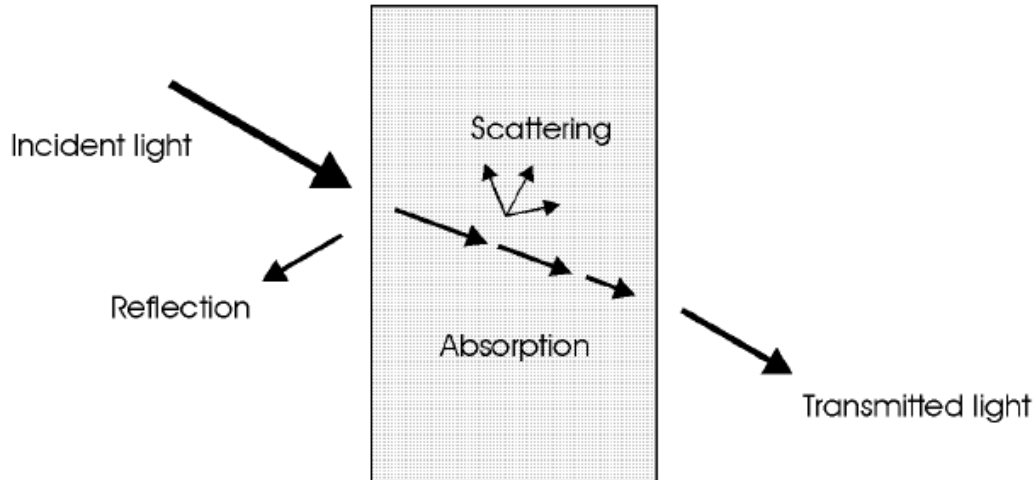


Figure 2.10: Light passing through a slice of material results in some of the light being reflected, absorbed, or scattered. The material properties affect the proportion of light that is diverted from direct transmittance. (Taken from Niemz 2007, Chapter 2, pg 9)

In this project, the wavelength range of focus is 780-920nm that is emitted by the Sharp GP2D120 IR proximity sensor used to determine skin deformation. To understand the impact of the infrared light sensor on skin, reflection, absorbance and scattering will be explored for the 780-920nm wavelengths.

The Sharp GP2D120 sensor used for skin height measurement in the suction probe emits light in the near infrared region. Since this sensor will be used to measure light intensity reflected from the skin's surface, the reflection of the incident IR light will be the primary focus considered in this section. Reflection is defined as the returning of electromagnetic radiation from a surface which is incident or at a different angle than the directional flow of the radiation. (Niemz 2007) The angle of the reflective radiation (θ') tends to be equal and normal to the angle of incidence (θ), which is the angle between the incoming radiation and the barrier surface along

a plane of incidence. However in diffuse reflection, several photon beams are reflected in and out of the plane of incidence. Diffuse reflection occurs with biological tissues due to their rough and unpolished surfaces. (Niemz 2007)

The stratum corneum (SC) is the barrier surface in which the IR sensor reflection occurs with the skin. The surface itself is very porous and full of obstructions such as hair and gland openings leading to the diffuse reflection of light. However, the stratum corneum is rather reflective due to the significant difference in its refraction compared to air (1.55 for the SC versus 1.0 for air). The reflection measured perpendicular to the incident light has been reported to be approximately 5% of the incidence light intensity over a range of wavelengths. (Kollias 1995) Dry and scaly skin increases diffuse reflection of the SC because of the increased roughness of the surface, whereas wetting the skin with mineral oil will smooth the SC and reduce the diffusion of reflected light.

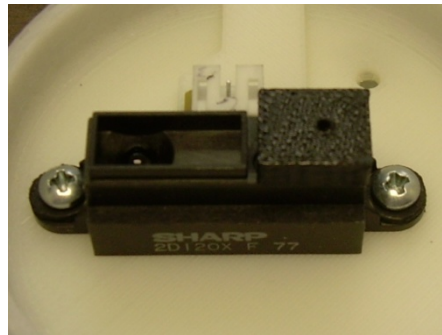


Figure 2.11: The Sharp GP2D120 IR proximity sensor with filtering cap over the LED emitter.

The Sharp GP2D120 IR proximity sensor in Figure 2.11 is designed for detecting the distance to rough unpolished surfaces such as paper or tissue at a 4-30cm distance. The low power ($<5\mu\text{W}$) LED emitter bulb dispenses light in a general forward direction with significant

divergence in the beam. After placing a filtering cap with a 1mm hole centered over the LED, the beam width is approximately 5.6mm in diameter at the 8cm surface distance. Therefore, the light beam from the emitting LED diverges at an angle of 0.88 degrees from the normal using the filtering cap. The diverging beam increases the reflective potential of the skin since the photons interact with the boundary at several incident angles. However, the detector of the Sharp GP2D120 sensor is in plane with the LED emitter at approximately 20mm in distance from the lens centers. This configuration leads to the general incidence angle of the sensor at 8cm from skin to be 11 degrees and 13 degrees at the 7cm distance. (Figure 2.12) This range of incidence angles has been observed by the author to be more suitable for rough, unpolished surfaces than for a highly reflective mirror with significant difference in output readings (~25% reduction in output for the mirror when compared to the output from yellow paper at the same distance).

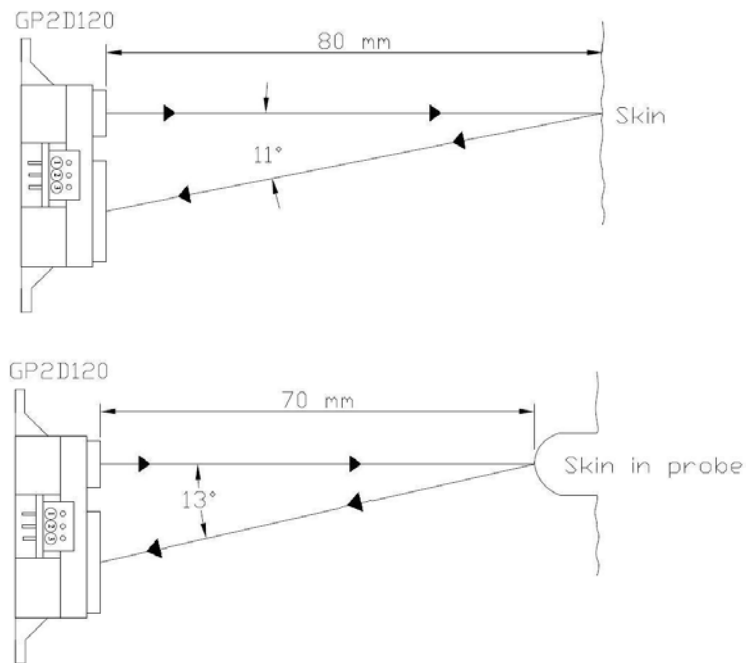


Figure 2.12: Light path of the Sharp GP2D120 IR proximity sensor. At 8cm, the incidence of reflection that is detected by the sensor occurs at approximately 11 degrees. The incidence angle increases two degrees when the skin is moved to 7cm from the sensor.

In order for this sensor to be suitable for skin reflection measurement, the voltage output from the detector must be sensitive enough to overcome the diverging photon beams to detect minor changes in proximity ($<1.5\text{mm}$). The Sharp GP2D120 IR proximity sensor has a distance-tailored IR CCD array linear detector which, with additional signal noise conditioning, is able to achieve this sensitivity. This aspect is discussed in more detail in Section 3.2.1.

Scattering is another factor that may contribute to the Sharp GP2D120 sensor being an effective measurement tool on the skin. Scattering occurs when an incident photon changes its direction of travel due to a change in the medium. (Kollias 1995) A scattering event occurs when photons collide with the different layers and components of the skin. Figure 2.13 depicts how light scatters from the different elements in the skin. Most of the scattering events in the skin occur in the dermis.

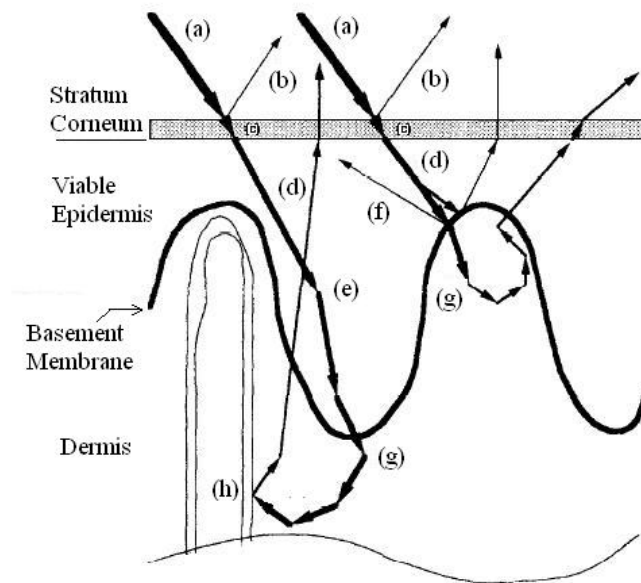


Figure 2.13: A diagram of light scattering in skin. The arrows indicate the direction of photons and the arrow thicknesses represent the relative light intensity. (a) Incident light; (b) Light reflected by the stratum corneum; (c) Light traversing the SC; (d) light traversing epidermis with some scattering from melanosomes (e); (f) scattering from basement membrane; (g) frequent scattering events from collagen fibers or (h) blood vessels in the dermis. (Kollias 1995)

Collagen fibers in the dermis have different refractive indices than the surrounding material. This material change relates to why the photons are redirected. (Kollias 1995) Blood vessels present in the dermis also scatter incident light significantly. The epidermal-dermal junction or basement membrane is the next layer of skin by intensity to cause light scattering. The change from the mostly aqueous epidermis to the fibrous dermis creates a refractive index change and creates scattering events. Although light scattering is less pronounced in the epidermis, melanosomes or melanin particles redirect light through the outer layer. Melanosomes have refractive indexes of 1.65 which is quite different to the approximate 1.33 index of the rest of the epidermis. (Vangemert, Jacques et al. 1989; Kollias 1995; Schmidt 1999)

Scattered light within the skin can return back to the surface if the scattering events upon the photons redirect to around 180 degrees. Therefore, scattered light that enters the skin from the Sharp GP2D120 IR sensor could potentially be measured by the IR detector. However, photons usually need to go through several scattering events in order to return to the skin's surface. For instance, if the average deflection angle is 10 degrees, approximately 18 interactions of the photon with the medium would be needed to turn it around. The larger and longer the light path, the more apt the scattered photons will undergo absorption or dissolve into the medium.

A concern with using the Sharp GP2D120 proximity sensor is that a portion of the light radiation will enter the skin and be absorbed. Since light energy often is transferred into heat energy in absorption, there is a need to consider potential thermal effects of the sensor in the skin. The power output of the Sharp GP2D120 IR proximity sensor was measured using an optical power meter (Model 1815-C, Newport, Irvine, CA). At 850nm, the Sharp GP2D120 IR sensor emits $<5\mu\text{W}$. When the 1mm-hole filtering cap is placed on the LED emitter of the

sensor, the power is $2.63\mu\text{W}$ at 8cm and $2.72\mu\text{W}$ at 7cm (the distance range projected of skin height measurement in the suction probe). Therefore, the sensor's IR output has a Class 1 hazard rating for nonionizing radiation from both the ANSI Z136.1 *Safe Use of Lasers (1993)* and IEC 60825-1 classification systems. A Class 1 laser system does not pose a hazard under normal operating conditions. Therefore, the Sharp GP2D120 IR proximity sensor should be safe for use in the skin tension measurement device.

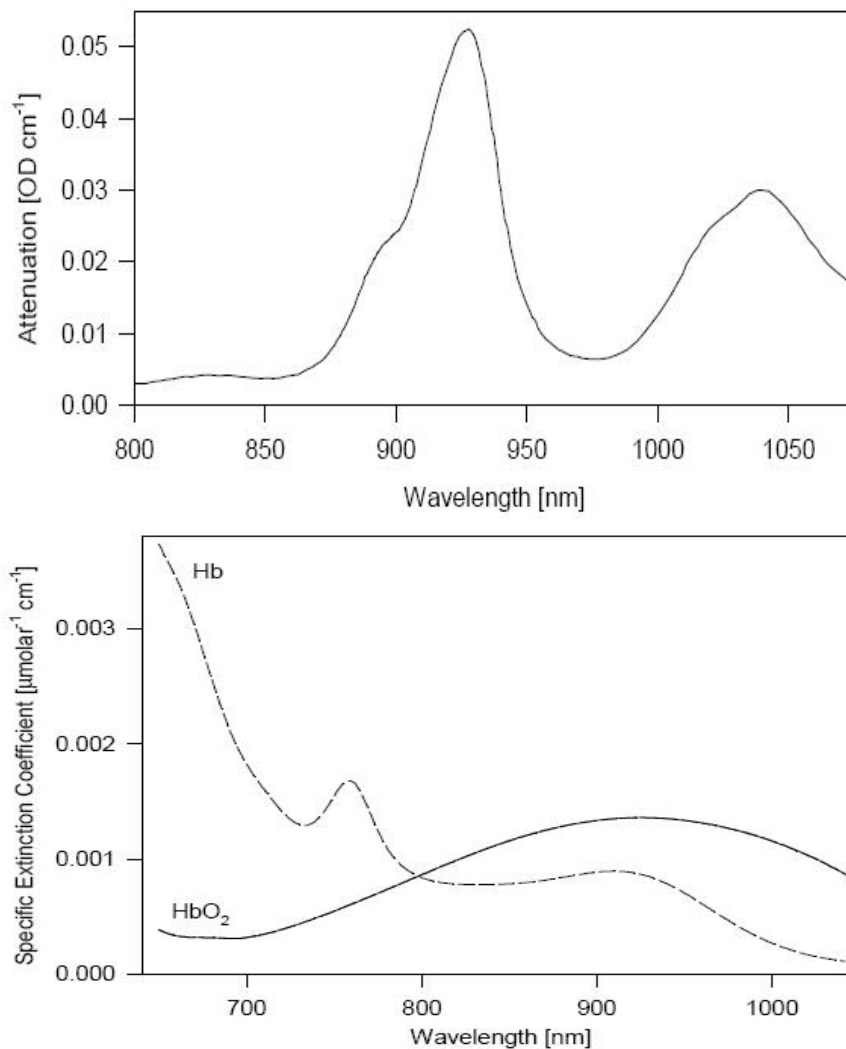


Figure 2.14: Absorption spectra of lipids and oxy- /deoxy-hemoglobin (respectively). (Schmidt 1999)

Although the Sharp GP2D120 IR sensor will not pose a thermal safety risk, some of the photons from the emitter will still be absorbed into the skin. The constituents of biological tissue which contribute towards absorption in the near infrared region are primarily lipids and hemoglobin. (Wilson and Jacques 1990; Schmidt 1999) Figure 2.14 characterizes the absorption spectra of lipids and hemoglobin.

The 780-920nm wavelength range of the sensor would likely absorb in the lipids of the cell membranes/barriers. For the small amounts of the weak energy that enter the dermis from the sensor, the oxygenated or deoxygenated hemoglobin found in the blood vessels would also be likely to absorb those photons. Therefore, light energy absorption will take place in the skin and mostly likely be targeted in the lipids of cell membranes, but the low light energy from the IR sensor should not cause thermal tissue damage.

2.4 Project Objectives and Intellectual Merit

Objective 1: Design a skin tension measurement device. A suction device has been designed to measure the effect of tensioning on the viscoelastic nature of skin. Suction force application devices are the most common and are more mechanically simple to design compared to indentation devices. (Jemec, Selvaag et al. 2001; Pedersen, Hansen et al. 2003; Grove, Damia et al. 2006; Khatyr, Imberdis et al. 2006) Also, preliminary experiments indicate that the suction concept will provide meaningful information on the relative tension of skin. Briefly, a 15in Hg (50.8kpa) vacuum is applied to the skin via a 12mm ID tube affixed to the surface by double-stick adhesive tape. The skin very quickly forms a dome inside the tubing during vacuum and the tape adhesive did not appear to slip (measured residual marking upon removal of tube). When the negative pressure is released, the skin is visually observed to rapidly return to the

normal level (see Figure 2.15). No bruising occurred, so the capillaries under the dermis layer of the skin are not compromised in the suction test at the 15in Hg (381mm Hg) vacuum pressure.

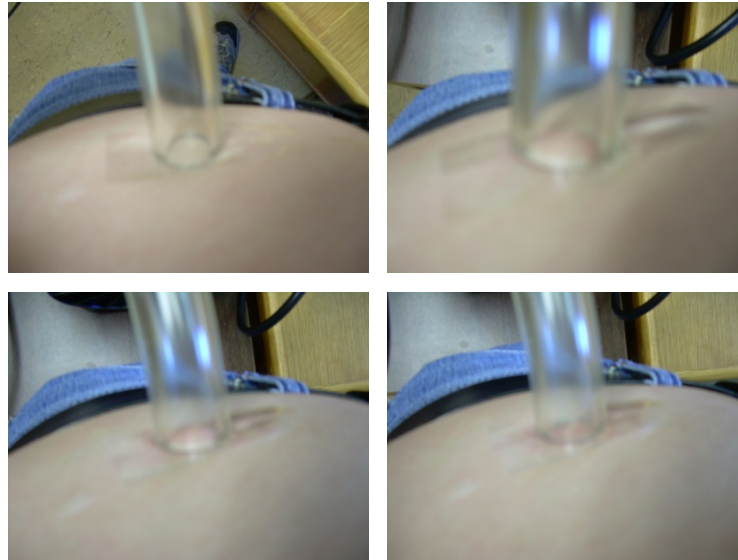


Figure 2.15: Preliminary vacuum testing on skin using 15in Hg (381mm Hg) vacuum pressure and 12mm ID Tygon tubing: Image (a) shows tubing attached to skin prior to suction, (b) shows skin deformation or “doming” after initial 15in Hg suction applied, (c) shows skin flushing after 5 seconds of suction, and (d) shows skin after suction is terminated, with no lasting bruising or other discoloration.

Because the suction method is common with several commercially-available products, the main differences from existing devices and the proposed device are briefly reviewed:

A) Vacuum force is kept constant and differences in skin height will be used to determine skin viscoelasticity: The most popular commercial devices reported, the Cutometer SEM 575 (Courage + Khazaka, Köln, Germany) and Dermalab (Cortex Technology, Hadsund, Denmark), are suction devices which use varying pressure to raise the skin to a certain height or use optical beam obstruction techniques to determine changes in height during the applied suction. (Berndt and Elsner 2002; Serup 2002) The design in this project reverses this function to vary the skin height measurement based on a constant vacuum pressure, which should be easier to keep

constant than skin height. The skin height then is determined with a remote sensing device. The constant vacuum pressure system, along with the remote distance sensing device, could create a more consistent and realistic deformation measurement than the existing varying pressure systems. Also, the resulting data may be more straightforward to model and analyze since the deformation of the skin is the direct result of its stress response, not a response to gradually changing the pressure inside the chamber. The remote sensing height measurement may also allow for more sensitive skin deformation rate analysis which could add more information to the breadth of knowledge on the viscoelastic nature of skin and in particular the immediate elasticity of the material.

B) The height measurement of skin deformation during suction will be measured by an above and centered remote sensing system. The Cutometer SEM 575 and DermaLab devices use horizontal optical path obstruction systems to measure height of skin deformation under suction. That is, as the skin height reaches the level of the side-mounted sensors, the light path between the sensors (across the diameter of the vacuum tube) is obstructed by the skin. This light obstruction is detected and then pressure setting at that time is recorded. (see Figure 2.16)

C) The device designed in this project uses an Infrared (IR) proximity sensor (GP2D120, Sharp Microelectronics Inc., Camas, WA) to detect the height change of the skin as a constant vacuum pressure is applied. The Sharp light sensor is composed of an IR emitter bulb (850nm \pm 70nm) and a tailored IR CCD array linear detector and the unit is designed to detect objects at a distance from approximately 4cm to 30cm. Commonly used in robotics for non-tactile obstruction sensing, the Sharp GP2D120 also contains signal conditioning to reduce the impact of other wavelengths of light, such as ambient light. Figure 2.17 shows the placement of the Sharp GP2D120 sensor in the vacuum probe. The emitter of the sensor is placed in the center of

the probe and the emitter's IR beam path is denoted by the red cone. The CCD array linear detector receives the reflected light from the skin, determines that angle of incidence, and then converts the measurement into a voltage output. A color "reflector" is used on the skin to reduce the potential variability as a result of different pigments in skin.

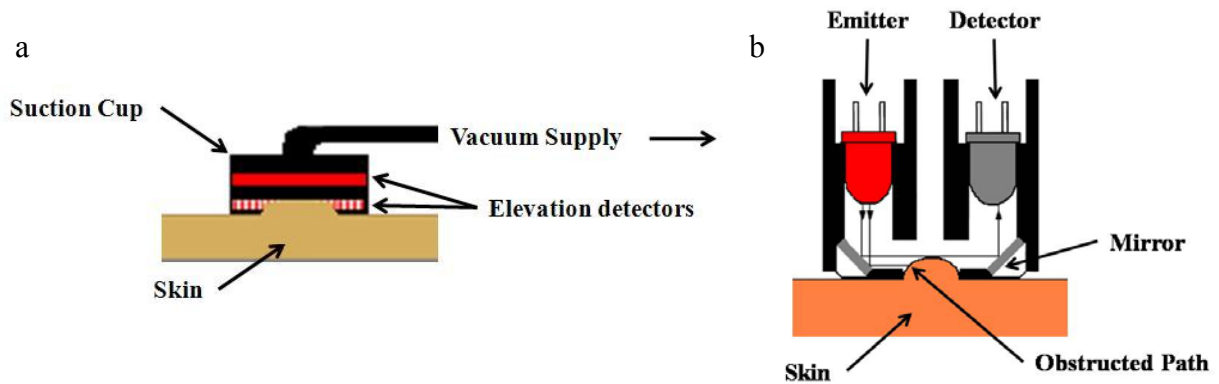


Figure 2.16. Examples of the light obstruction method for measuring skin deformation height where the first image (a) is based on the DermaLab and the second (b) is based on the Cutometer.

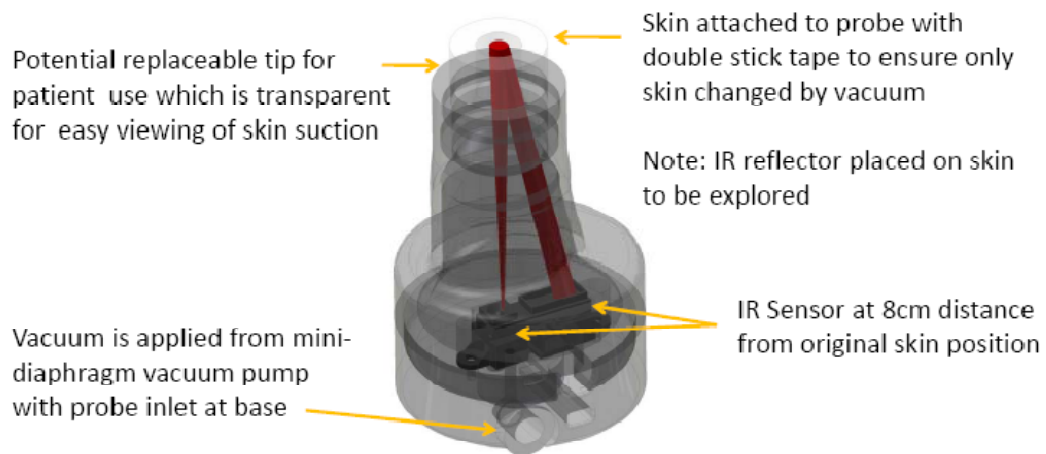


Figure 2.17: A design of the skin testing probe inverted to show the functioning of the Sharp GP2D120 IR proximity sensor. The red cones represent the approximate path of the IR beam where an emitter LED produces the IR photons that are reflected off of the skin and then received by the IR detector. The change in path length is converted into a voltage change by the sensor.

D) The device has been designed to be portable with data recording capabilities with or without a computer. The BASIC Stamp BS2px (Parallax, Inc., Rocklin, CA), a low-cost programmable microcontroller is used to interface the height sensor, vacuum, and control/trigger systems. The microcontroller is also interfaced with a data storage module. Data is stored onto a microSD card for later analysis using a custom computer algorithm designed in the Microsoft Office Excel VBA program.

The vacuum supply pump is a 12-volt miniature diaphragm pump (C103E-12, Hargraves Technology Corp., Mooresville, NC) that is attached to the probe by vacuum tubing. A small vacuum air allowance valve (V-800, Airtrol Components, Inc., West Berlin, WI) activates when the optimum negative pressure is reached and the valve maintains the pressure limit. A solenoid valve (EVO-3-6-H, Clippard Instrument Laboratory, Inc., Cincinnati, OH) is activated when the timed test is finished to release the vacuum supply quickly.

All the electronics and sensors are housed in enclosures that are attached remotely to the skin probe via a vacuum tube and wiring connected to the sensor and a trigger. The trigger mechanism is a thumb button switch on the top of the skin probe. This button allows the device operator to initiate the vacuum pressure and sensor for a preset time of testing. The microcontroller system will then control the vacuum shut off to reduce user error in timing control. An overall power switch has been installed on the enclosure as a safety override during the probe's operation and well as quick release fittings for manual removal of the vacuum supply. Research and design efforts from the first project aim have provided feasibility data on a novel and cost-effective means to determine changes in skin.

Objective 2: Validate of the function of the device in skin tension measurement. Probe prototypes in ABS plastic have been created on a 3-D rapid prototyping printer at the

Engineering Communications Studio, College of Engineering, LSU. The ABS prototype design and a simple PVC-fitting probe have been used to test general design structure, vacuum effectiveness and to assist in instrumentation positioning. Other tests that have been performed on the prototypes are vacuum control, adhesive connection to skin, effectiveness in skin height measurement, safety, and user ergonomics.

Objective 3: Observe of the prototype device in operation using artificial skin models.

The distention measurement during suction in a prototype has been tested using a semi-linearly elastic material to determine repeatability of the device. The distension of polyurethane elastomer blocks, exhibiting hardness levels of Shore 3000 to 7000 (equivalent hardness levels of a racquet ball to a rubber band), has been explored. Polyurethane elastomers have been used in previous reports as artificial models to skin since they exhibit similar degrees of deformation seen with skin. (Beaulax Co. 2006; Jachowicz, McMullen et al. 2007)

The suction device has also been tested on a rigid, non-deformable surface (PE plastic) to determine the internal pressure curve versus time of the vacuum system. This data has been used to account for system noise appearing in data output when the device is used on skin. The pressure curve analysis also reveals the effective speed of the vacuum system and validates the use of the miniature diaphragm pump.

Objective 4: Explore the operation of the skin tension measurement device *in vivo*.

Confirmation of the suction device's effectiveness in its sensitivity, repeatability, and accuracy has been performed on 40 patients (20 males/20females). Testing on the adhesive connection of device using the double sticky tape and the accuracy of probe placement angle has been explored along with the general functioning of the system.

The developments from this project should yield a patentable design and the construction of a skin tension measurement device which will measure the mechanics of full-thickness skin. The introduction of IR optics in the measurement of skin deformation under suction should allow for a more simplistic design, thereby decreasing the cost of manufacturing and decreasing the market price of the device in comparison to its existing commercial competitors. The ultimate goal of this design project is to produce an effective skin tension measurement device which can be more affordable and perhaps easily accessible to dermatologists, plastic surgeons, general practitioners, and skin researchers so that the mechanics of full-thickness skin *in vivo* can be explored in further depth and more patients can be monitored pre- and post-skin alterations.

CHAPTER 3: CUTISFIRM INSTRUMENTATION DESIGN AND VALIDATION

3.1 Introduction

Skin is a complex, multi-layered, anisotropic material with non-linear viscoelastic behavior during stress application. These characteristics of the organ complicate the objective to accurately determine its mechanical properties, in spite of its general accessibility for measurement. The measurement of skin mechanics is useful to observe the health of the organ and the individual enclosed by it. Skin mechanics is often directly correlated to a measure of skin firmness. Knowledge of the firmness of the skin can be monitored for an individual through a course of a medical or cosmetic treatment. Monitoring the progress of aging, UV skin damage, wound repair, changes during pregnancy, the disease scleroderma are just a few of the treatments that regular use of skin tension measurement instruments in clinics could prove useful in improving healthcare.

Significant advances have been made in skin measurement device development and skin mechanics modeling. (Refer to Chapter 2) However, modern dermatology practices still lack the regular use of skin mechanics measurement instruments for the common diagnoses. This deficiency is likely the result of device inaccessibility. Few commercial devices are available and are expensive. The objective of the following chapter is to explain the design and validation of a quality skin tension measurement device where mass production and affordability is plausible. The “Cutisfirm” skin tension measurement device has been developed using a commercially available, inexpensive proximity sensor to detect dynamic skin elasticity changes under suction.

The Cutisfirm skin tension measurement system consists of a plastic probe, which houses an optical proximity sensor, and a vacuum chamber that will interface with the skin. The probe

has been designed in Autodesk® Inventor™ Professional 2008 and (See Appendix B for detailed drawings of the probe.) a prototype has been made in ABS plastic using a Stratasys Dimension 3D printer. (See Figure 3.1)

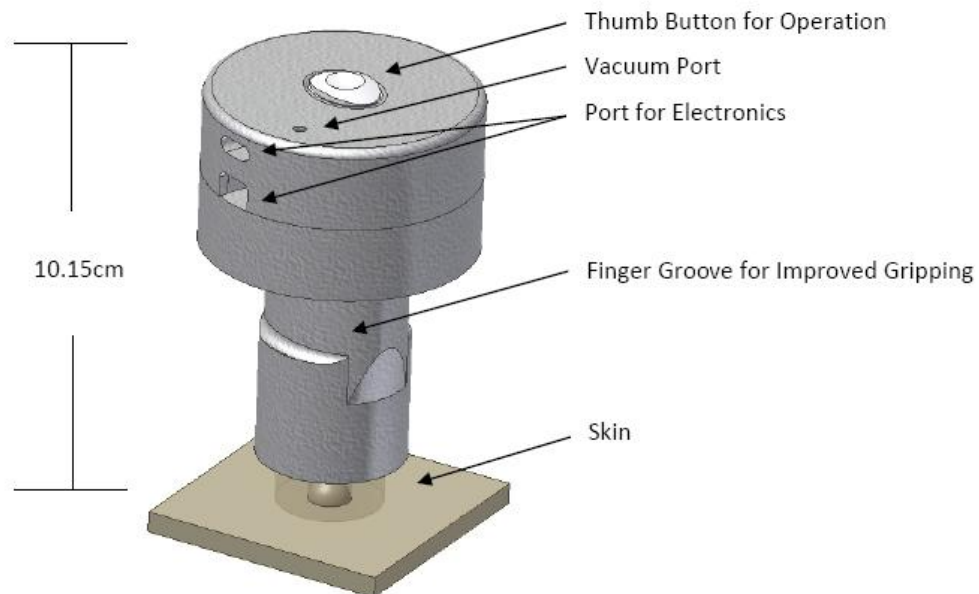


Figure 3.1: Images of the skin testing probe proposed design. Housed inside the probe is the Sharp GP2D120 IR proximity sensor which will produce an IR beam that will be reflected off of the skin and then received by its CCD linear array IR detector to determine skin deformation.

The external width of the Cutisfirm probe is optimized for a physician to comfortably hold the probe with his/her thumb on top and index and middle fingers pinching the probe in the finger groove. A translucent removable tip is attached to the end of the probe. (See Figure 3.2)

This translucent tip will allow the physician to observe the skin deformation. The tip is designed to be removable for easy cleaning and sanitizing. The probe is attached to the skin using double-sided sticky tape (3M High Performance Double Coated Tape 9086, St. Paul, MN) to prohibit superficial skin slippage into the suction chamber. The skin isolation resulting from affixing the probe allows for more consistent readings in skin height deformation.

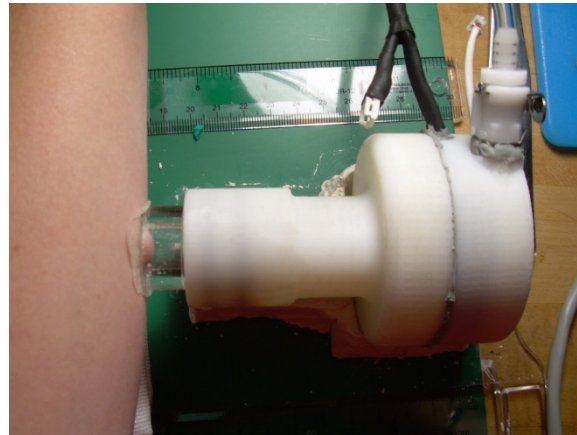


Figure 3.2: Vacuum operation in a Cutisfirm prototype. The probe has been created by a 3-D rapid prototype printer in ABS plastic (white) and machined Acrylic (clear). The probe is attached to skin via double stick tape to isolate the testing site to the skin which is initially exposed in the vacuum chamber. Ten inches of Hg (254mm Hg) vacuum has been supplied allowing for the doming of forearm skin to approximately 10mm.

The device uses the Sharp GP2D120 infrared (IR) proximity sensor (Microelectronics Inc., Camas, WA) to detect the height change of the skin as a suction of a constant pressure is applied by a miniature diaphragm vacuum pump. A miniature vacuum air allowance valve activates when the optimum negative pressure is reached and the valve maintains the pressure limit. A three-way solenoid valve is then utilized to release the vacuum once the timed test is complete. For control and skin height data collection, a uM-FPU V3.1 math co-processor and BASIC Stamp 2px microcontroller module have been utilized to interface with the height sensor, vacuum, and control/trigger systems as well as data storage during testing. Data is then stored

via a microSD card for later analysis using a program designed in Microsoft Office Excel VBA. All the electronics and sensors are designed to fit in a small enclosure for portability. The enclosure is attached remotely to the skin probe via a vacuum tube and an electrical cord connected to the sensor and a trigger.



Figure 3.3: A working prototype of the Cutisfirm Skin Tension Measurement System. A Sharp GP2D120 IR proximity sensor is housed in a suction probe made of PVC fittings and a clear acrylic nozzle for skin attachment. The probe is attached to pump/value control electronics boxes.

The working prototype used in testing of artificial models and *in vivo* is pictured in Figure 3.3. Another probe prototype made of PVC fittings has been constructed to achieve efficient vacuum function. The printed probe prototypes are made of porous ABS, and since they are printed layer-by-layer, they were not able to be used in vacuum operation effectively. The PVC probe, however, contains the same internal volume and the IR sensor is still centered and placed 8cm from the skin's surface. The skin is also still attached to the clear nozzle with

double-sided sticky tape. The probe design which has been drawn should achieve vacuum when manufactured from molten or injection molded plastic.

3.2 Materials & Methods

This section is divided into two topics: materials and experimental methods. The materials portion of this section provides a detail overview of the components or parts in the prototype design. (See Appendix C for wiring diagrams and part specification sheets.) The methods are an overview of the experimental designs used to obtain the results reported in section 3.3.

3.2.1 The Sharp GP2D120 Infrared Proximity Sensor: The skin deformation within the suction probe is measured using the Sharp GP2D120 infrared (IR) proximity sensor (Microelectronics Inc., Camas, WA). This inexpensive (\$12.50) light sensor is commonly used in robotics for non-tactile obstruction sensing. The Sharp range sensor is composed of an IR emitter bulb ($850\text{nm} \pm 70\text{nm}$) and a tailored IR CCD array linear detector and the unit is designed to detect objects at a distance from approximately 4cm to 30cm. During the operation of the sensor, a divergent IR beam is emitted from the IR LED bulb to a surface (e.g., skin) and the CCD array linear detector receives the reflected light from that surface, determines that angle of incidence, and then converts the measurement into a voltage output. (Refer to Figure 2.12, pg 22 for visual description of the angle of incidence.) Figure 3.4 shows the voltage output characteristics of the Sharp GP2D120 sensor in the range of potential probe lengths. (See Appendix C for the Sharp GP2D120 specification sheet showing full voltage output profile.) The voltage output is a nonlinear function of the distance and is best represented by a second order equation in its overall appearance. The IR proximity sensor is reported by Sharp to detect $\pm 0.3\text{cm}$ in height changes effectively, which is evident in Figure 3.4 even with beam attenuation

using filtering caps. However, the sensitivity of the IR proximity sensor can be improved to <0.2cm with further signal conditioning using a passive, low-pass filter system.

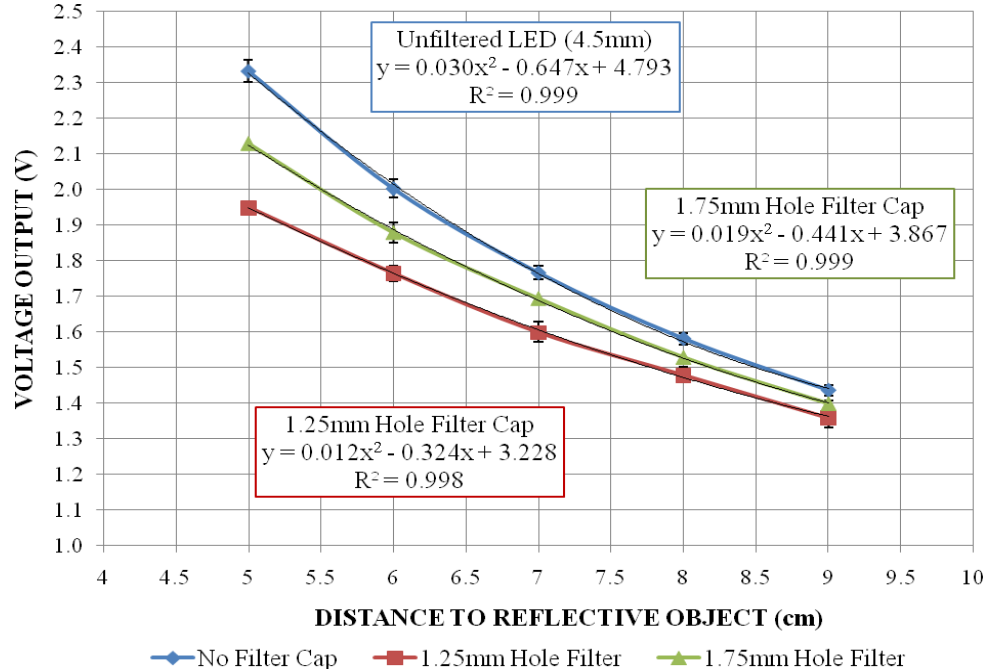


Figure 3.4: Example output characteristics of GP2D120 IR proximity sensor in the range of potential probe lengths. The different lines represent the optional beam attenuation profiles that could be used on the sensor. Data was obtained using yellow paper at known distances and the voltage read by a multimeter. (Error bars depict standard deviation)

The IR beam produced by the Sharp GP2D120 sensor is attenuated by placing a cap with a small aperture onto the IR emitter (filtering cap). The attenuation is necessary for beam focusing and positioning onto the center of the suctioned skin dome within the probe. Figure 3.5 displays beam width measurements using different aperture sizes of the cap placed on the IR emitter. The caps used are made of ABS plastic and coated with opaque, carbon black oil paint. Beam spots for each aperture have been collected on images from the different distances by an IBM PC Camera with the color filter removed. The images have been scaled and the beam spot diameter measured in Image J (NIH Open Source Image Analysis with JAVA).

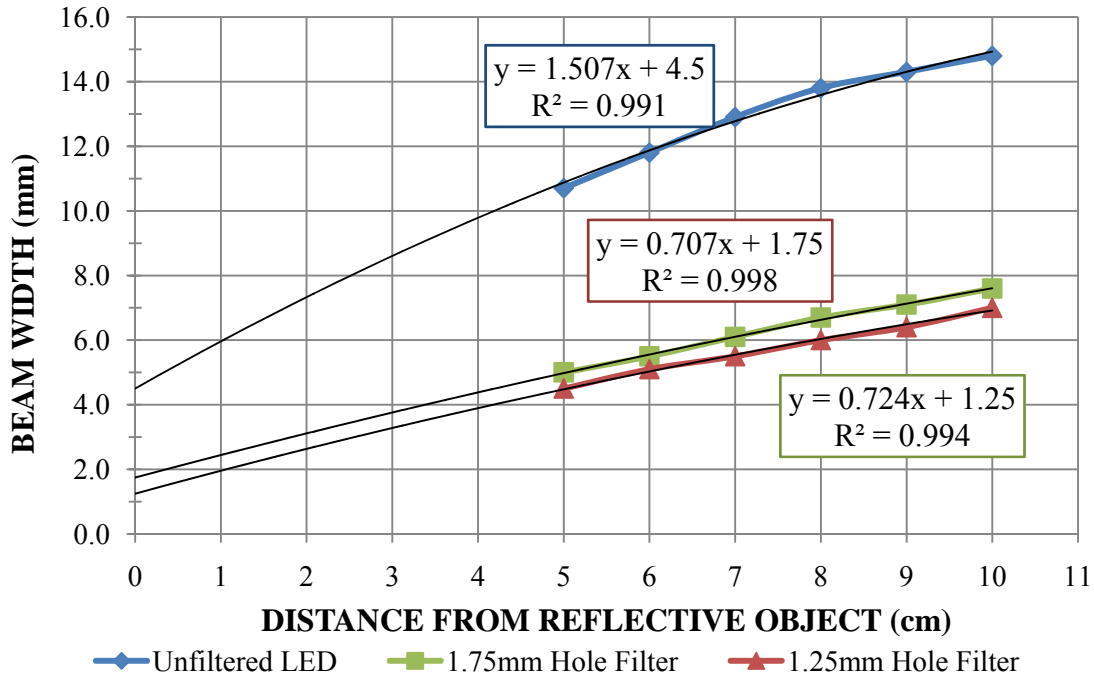


Figure 3.5: Beam width characteristics of the Sharp GP2D120 IR proximity sensor using caps with different apertures. Caps of ABS plastic (1.25mm and 1.75mm holes in the center of beam) are placed on the IR emitter side of the sensor, then the size of the beam spot on paper was captured by the IBM PC Camera (color filter removed) and the photo was analyzed via Image J (NIH Open Source Image Analysis with JAVA)

The Sharp GP2D120 is also reported to contain internal signal conditioning to reduce the impact of other wavelengths of light, such as ambient light. As an extra precaution, the IR proximity sensor has been encased in a probe material that is not transparent to the longer visual and IR wavelengths to prevent any potential outside light interference. The Sharp GP2D120 IR proximity sensor is placed into this opaque probe with an attenuating cap with a 1mm diameter-hole. The typical light output for the Sharp GP2D120 sensor has been imaged using an IBM PC Camera and shown in Figure 3.6.

In operation, the Sharp GP2D120 IR proximity sensor outputs a signal with a 10ms pulse width. The sensor also employs an oscillator circuit to speed up the measurement frequency of the detector so that the measurement response time is 39-40ms. In Figure 3.7, there is evidence

of sensor sampling with the 30ms of noisy signal during measurement followed by 10ms of stable output.



Figure 3.6: Image of IR beam spot from proximity sensor in a Cutisfirm prototype. Using a webcam with the color filter removed, the approximate 850nm beam spot from the IR proximity sensor, with the 1mm-hole attenuating cap installed, is shone on a piece of yellow paper and seen through the clear acrylic tip of the probe.

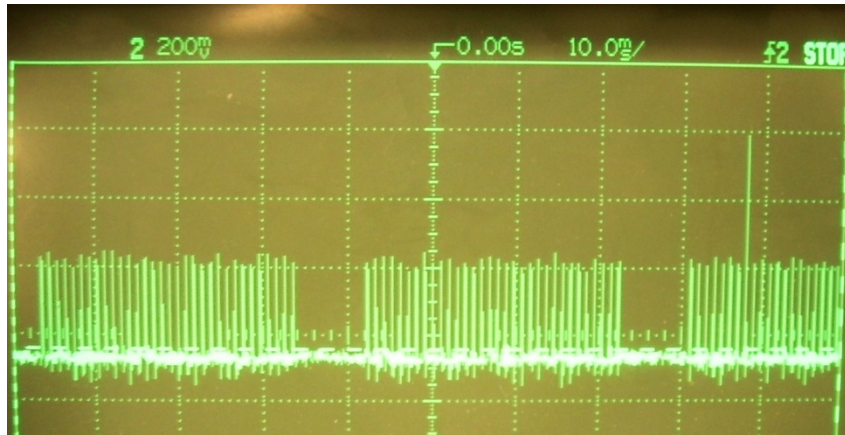


Figure 3.7: Signal output of the Sharp GP2D120 IR proximity sensor measured using the HP 54600B oscilloscope set at 200mV/vertical gridline and 10msec/horizontal unit. The figure provides evidence that the IR sensor outputs a pulsed signal for ~30msec with a ~10ms gap.

The sensitivity of the Sharp GP2D120 sensor in distance measurement is reported and observed to be $\pm 0.3\text{cm}$. By reducing the noisy signal during the measurement period, the voltage peaks seen in Figure 3.7, this sensitivity can be improved. In Figure 3.8, the schematic reveals

the dual low-pass filters system used in the working prototype of the device. The pre-sensor RC filter has a low-pass frequency cutoff of 23.4 Hz. The pre-sensor filter is necessary to reduce the effects of fluctuations in the supply current caused by the operation of other components attached to the same DC power supply. And, if the device is ever supplied with AC current, the 60 Hz supply noise should be filtered by the pre-sensor low-pass filter. The post-sensor RC filter has a low-pass frequency cutoff of 338.6 Hz which easily allows for the sensor reading, occurring at ~25 Hz, to pass through along with the frequency of voltage change during surface motion. The resulting signal from filtering is shown in Figure 3.9 and is nearly absent of the voltage spikes. Therefore, when the voltage output is collected, there is a reduced variation in the voltage readings, thus improving the sensitivity of the distance measurement with the IR sensor. With the signal conditioning, the sensor is able to detect distance changes to $\pm 0.139\text{cm}$ for 95% tolerance.

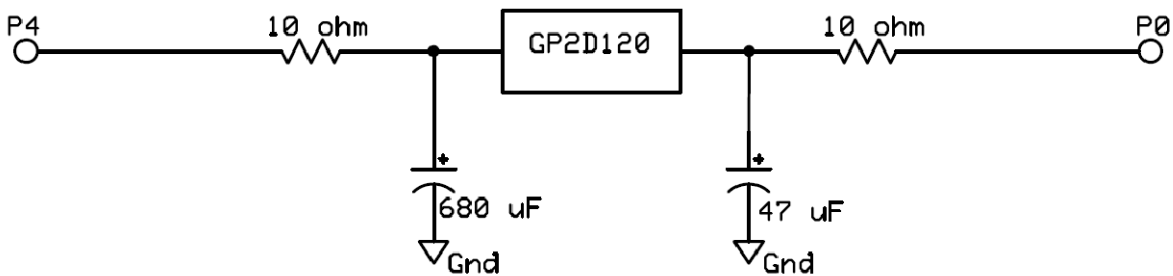


Figure 3.8: Circuit diagram of the signal conditioning used with the GP2D120 to reduce noise during the measurement period. The frequency cutoff of the pre-sensor filter is 23.4 Hz. The post sensor filter has a frequency cutoff of 338.6 Hz to allow for the sensor's signal output.

After signal conditioning the GP2D120 IR sensor, the voltage output is collected by the uM-FPU V3.1 math co-processor module (Micromega Corporation., Kingston, ON, Canada). The uM-FPU converts the voltage output of the sensor to 12-bit decimal values using its internal digital-to-analog converter. The decimal values are then converted into the measurement of skin deformation. See Section 3.3 for the details on the decimal value conversion.

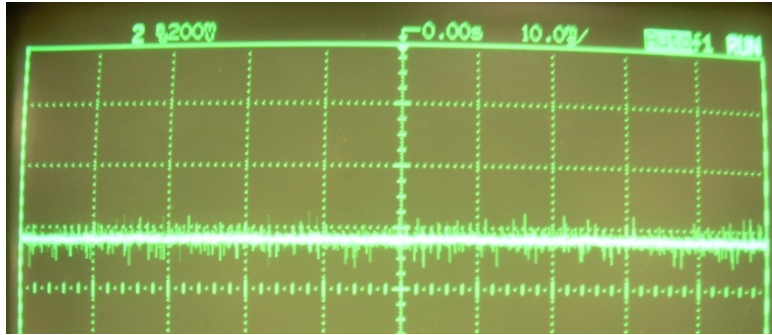


Figure 3.9: Signal conditioned output of the Sharp GP2D120 IR proximity sensor using the dual low-pass filter system. The signal is measured using the HP 54600B oscilloscope set at 200mV/vertical gridline and 10msec/horizontal unit. As the reflective object is moved within the measuring range (4 to 30cm) this baseline reading moves relative to the voltage change. The disappearance of the peaks seen in Figure 3.7 shows the reduction of noise resulting from the sensor's oscillating circuitry.

3.2.2 The Vacuum Probe System: The vacuum supply for the suction probe is created by a 12-volt miniature diaphragm pump (C103E-12, Hargraves Technology Corp., Mooresville, NC) that is attached to the probe by vacuum tubing. A small vacuum air allowance regulator/valve (V-800, Airtrol Components, Inc., West Berlin, WI) activates when the targeted negative pressure is reached and it maintains the pressure target. A solenoid valve (EVO-3-6-H, Clippard Instrument Laboratory, Inc., Cincinnati, OH) is activated when the timed test is finished to release the vacuum supply quickly. (See Figure 3.10)

The combination of the three components yields the pressure curve in Figure 3.11. At 0 seconds, the pump is initiated by the electronic control system. The vacuum pressure or suction increases rapidly and becomes fully developed by 2.5 seconds. The maximum flowrate of the pump decreases from approximately 6 to 0.9 liters per min during this time. (See Figure 3.12) Once the targeted negative pressure has been attained, the Airtrol V-800 vacuum regulator assists in maintaining this pressure until 10 seconds is reached. Then the pump is terminated and the Clippard three-way solenoid valve is activated, causing a rapid release of the vacuum, within 1s.

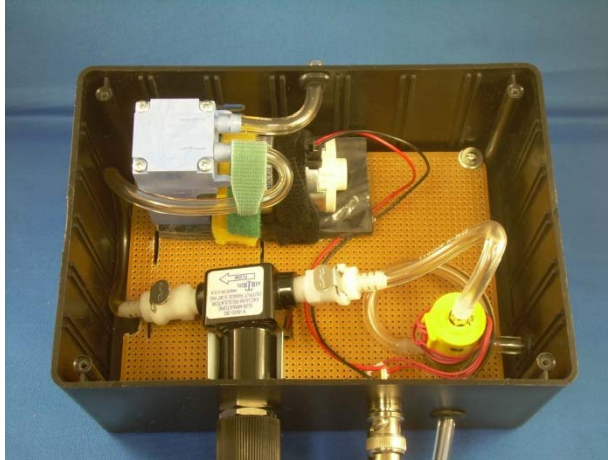


Figure 3.10: Vacuum supply system for the Cutisfirm prototype. The 12V miniature diaphragm pump (upper left) creates the vacuum pressure which is controlled with a vacuum regulator (lower left) and the vacuum is quickly released after testing by a three-way 6V solenoid valve (lower right).

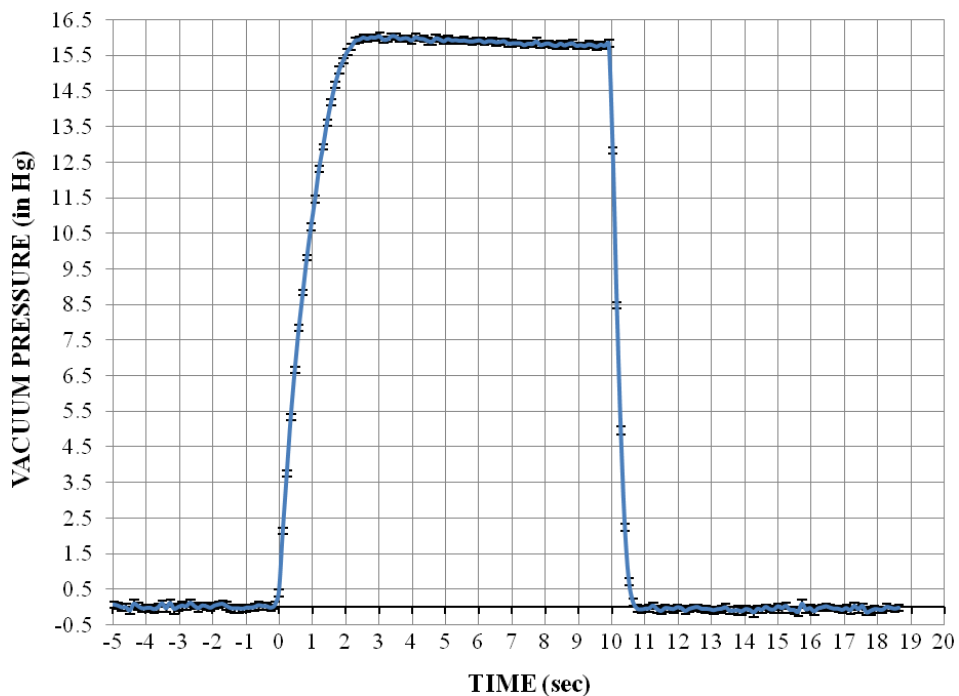


Figure 3.11: Vacuum pressure profile for a 10-second test using the Cutisfirm skin tension measurement device adhered to a rigid plastic surface. The negative pressure has been measured by an integrated pressure sensor placed near the suction probe in the system. (Error bars in S.E.M., n = 25)

The pressure is measured by an integrated silicon pressure sensor placed near the suction probe. The MPXV6115VC6U (Freescale Semiconductor, Chandler, AZ) is a calibrated, temperature self-compensated, signal-conditioned integrated chip sensor designed to detect pressures from -14.7 to +2.2psi (-30 to +4.45in Hg). (See Figure 3.13) The piezoresistive transducer converts the negative air pressure to voltage output. In the Cutisfirm device, this voltage output is collected by the uM-FPU V3.1 math co-processor and converted into 12-bit decimal values. Figure 3.14 shows the calibration curve used to determine the pressure in inches of mercury. The 12-bit decimal output of the sensor was compared to a calibrated P1600 pressure transducer attached to a XR440 Pocket Logger (Pace Scientific, Inc. Mooresville, NC). There is a linear relationship between the voltage output or converted decimal and the pressure. The tolerance of the sensor, in the conditions which it is subjected to from the Cutisfirm operation, is ± 1.12 in Hg ($N=25$, $1-\alpha = .95$, $\gamma = 0.05$). This tolerance is determined from the data shown in Figure 3.11.

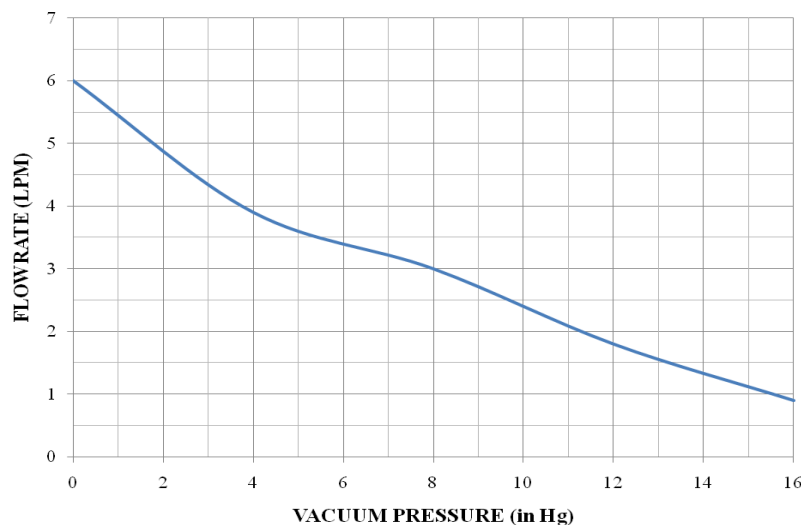


Figure 3.12: Hargraves C103E-12 pump flowrate profile projected for the first 2.5 seconds of a 10 second test using the Cutisfirm skin tension measurement device adhered to a rigid plastic surface. (Data taken from the C103E-12 specification sheet in Appendix C)

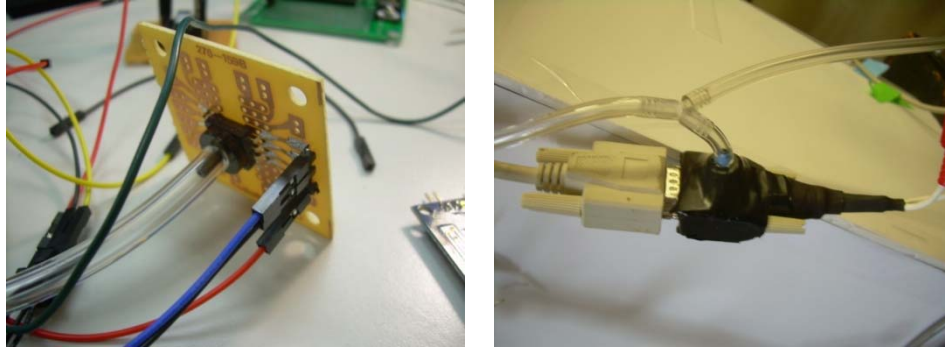


Figure 3.13: Freescale Semiconductor MPXV6115VC6U integrated pressure sensor. The left picture shows the surface mounted sensor attached to tubing during initial testing. The right picture shows the sensor integrated into the Cutisfirm skin tension measurement device.

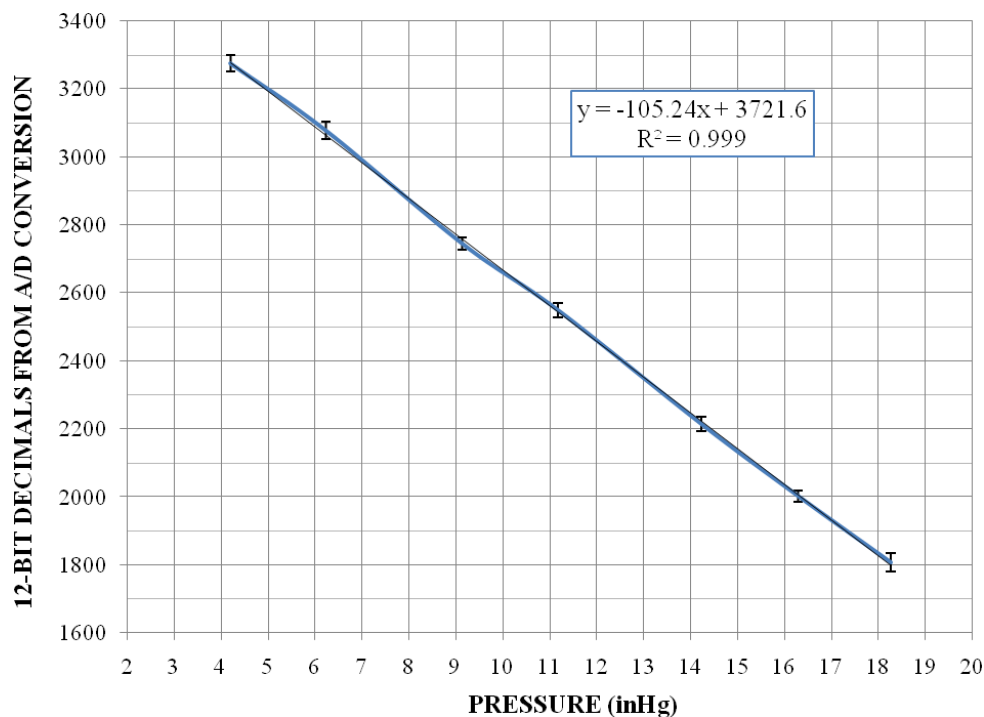


Figure 3.14: Calibration graph of the MPXV6115VC6U pressure sensor. The 12-bit decimal output of the sensor was compared to a calibrated P1600 pressure transducer attached to a XR440 Pocket Logger (Pace Scientific, Inc. Mooresville, NC).

Since the vacuum supply proposes the greatest risk of injury for the tested person with the Cutisfirm device, safety features have been incorporated into the vacuum probe system. The 12V miniature diaphragm pump has been selected because of its maximum vacuum pressure

limitation. The Hargraves C103E-12 pump has a maximum negative pressure of 20 inches of mercury (508mm Hg, 9.8psi). This pressure corresponds to 7.65 newtons (1.72lbs_f) of force applied to the exposed skin (12mm dia.) when using the Cutisfirm device. Therefore, even at its maximum, the pump will not create a damaging force to the skin exposed in the probe.

Another safety feature is the inclusion of a manually controlled vacuum regulator. The V-800-30-W/K Miniature Precision Vacuum Regulator (Airtrol Components, Inc., West Berlin, WI) is a constant bleed regulator which is adjustable from 0 to 30in Hg (0 to 762mm Hg) and a maximum flowrate of 28 liters per minute. The regulator is important in the vacuum system design, since it stabilizes pump supply at the target pressure. A manual knob on the regulator can be adjusted with the guidance of a Bourdon tube gauge to change the pressure supply between tests. The knob also can be adjusted if the tested person feels pain during testing.

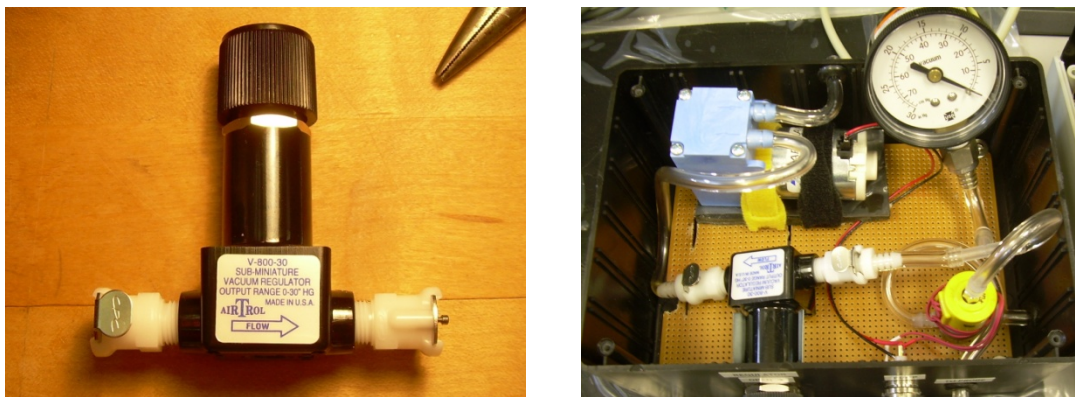


Figure 3.15: Airtrol V-800 miniature vacuum regulator. The regulator can be manually adjusted with the assistance of a Bourdon tube pressure gauge, seen on the right.

Other design features incorporated to increase the safety of the vacuum system are: the Clippard three-way solenoid valve is set open to the atmosphere as a default when the pump is not running; and manual quick release tubing fittings. The main connection to the suction probe

is a quick-release fitting. (See Figure 3.16) This fitting is incorporated so vacuum pressure can be removed from the probe immediately if the tested person feels pain from the suction.

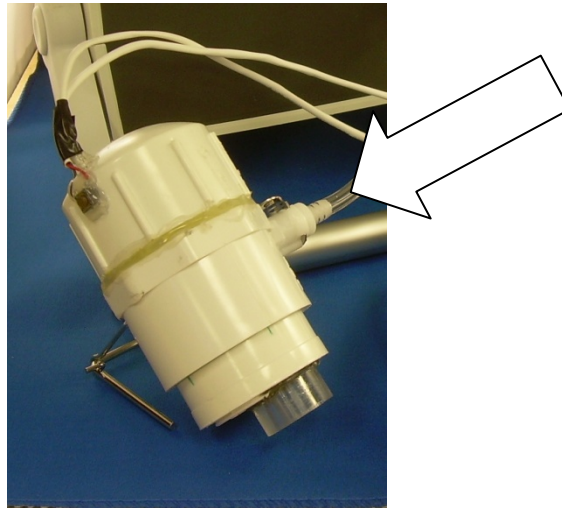


Figure 3.16: Cutisfirm suction probe with quick release tube fitting attached. (arrow) The quick release fitting has been incorporated in the design so immediate of removal the probe from the vacuum system could be accomplished if the person being tested feels pain during operation.

3.2.3 The Electronic Control System: All of the previously mentioned parts are interfaced by a central microcontroller system consisting of 2 – BASIC Stamp microcontroller modules and a math co-processor. The center of the control system is a BASIC Stamp 2px microcontroller. (Figure 3.17, left) The BS2px chip is a powerful microcontroller with the fastest processor (32MHz Turbo) of the BASIC Stamp product line. The BS2px provides 8 units of 2 kilobytes of EEPROM memory for ~4,000 program instructions and 38 bytes of RAM, along with 128 bytes of temporary RAM. This microprocessor has been chosen as the central “brain” because of its speed, memory capacity and user-friendly programming interface (PBASIC).

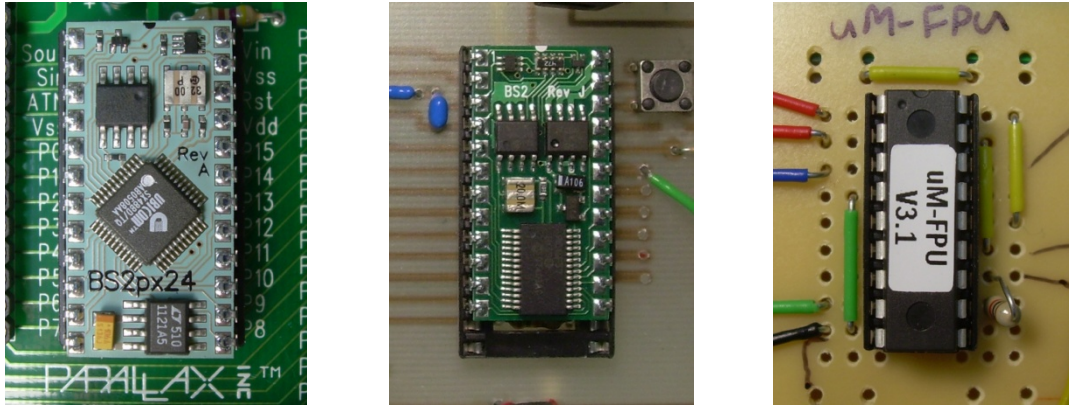


Figure 3.17: BASIC Stamp BS2px (left) and BASIC Stamp BS2 microcontrollers (middle) and uM-FPU V3.1 chip (right).

A secondary microcontroller is used to act as a timing controller for pump and solenoid valve. A microcontroller was utilized for this purpose instead of 555 timing circuitry, since the microcontroller is programming adjustable. Also, a single microcontroller covers much less space on the motherboard than a series of 555 timers. The BASIC Stamp 2 module was selected as the secondary microcontroller. (Figure 3.17, middle) The 24-pin chip consists of a 20MHz processor with 2 kilobytes of EEPROM and 32 bytes of RAM. Similar to the BS2px, it also has 16 I/O pins and 2 dedicated serial pins for an electronic interface with a user-friendly programming language. The BS2 is a consistent counter or timer since is dedicated to just turning on I/O pins and counting milliseconds using a ceramic-resonator time base ($\pm 1\%$ accuracy in milliseconds).

The last component of the central electronic control system is the uM-FPU V3.1 32-bit floating point co-processor. (Figure 3.17, right, Micromega Corporation., Kingston, ON, Canada) This integrated circuit serves as the data collection and conversion module. The math co-processor is designed to work with a master microcontroller using SPITM or I²CTM interface. The chip is capable of two channel voltage input, 12-bit analog to digital conversion, and complex

data processing including string parsing, calculating matrices and Fast Fourier Transforms (FFT). The uM-FPU math co-processor is also capable of timing its data processing, which is why the processor has been incorporated into the Cutisfirm device. The chip is programmed using an uM-FPU V3 Integrated Development Environment (IDE).

The uM-FPU floating point co-processor has been interfaced with the BASIC Stamp 2px using a 2-wire SPI™ interface. The uM-FPU V3.1 chip is responsible for collecting the voltage from the GP2D120 IR proximity sensor and the MPXV6115VC6U integrated pressure sensor, converting those voltages to 12-bit decimal values, performing the necessary calculations to change the decimal values to the actual physical values for output, and timing those operations for each reading.

Data from the Cutisfirm skin tension measurement device is transferred to a microSD card after the uM-FPU chip has completed the processing. The data is written onto the microSD card using the uDRIVE-uSD-G1 Embedded “DOS micro-Drive” module. (4D Systems Pty Ltd., Sydney, Australia) This module is a compact unit which receives the data in serial (57,600 baud) directly from the uM-FPU chip and writes the data to the microSD card in FAT16 or FAT32 format.

The user interface of the Cutisfirm device is an LCD Touchscreen. For the working prototype, a 5.7” monochrome LCD Touchscreen was used. (Amulet On-Board, Amulet Technologies, Santa Clara, CA) The 320 x 240 pixel resolution screen is used for the human-device interface in place of a computer. (See Figure 3.18) The Amulet On-Board module is programmed using a simple html compiler. This electronic addition allows for the device to be more portable and stand-alone. Also, the touchscreen interface provides an engaging, user-

friendly operation. There is a smaller version (3.8”) of this LCD module which can be directly attached to the electronic enclosure box in future prototypes.

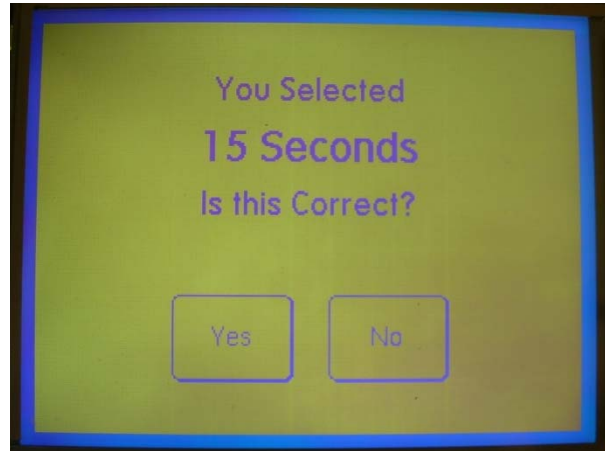


Figure 3.18: 5.7” Amulet On-Board LCD Touchscreen that has been used with the working prototype. The LCD touchscreen provides a user-friendly human-to-device interface which replaces the need for a computer during testing.

The electronics of the Cutisfirm device are powered by two independent 12V sealed lead acid (SLA) batteries (Panasonic® LC-127R2P 12V/7.2Ah, RadioShack Corporation). One of the SLA batteries is a dedicated power supply for the pump. The pump is isolated in order to reduce the noise in the data output signal which occurs when the pump is activated. (See Figure 3.19) The other SLA battery supplies power to the rest of the working prototype.

Further details of the electronic control system such as wiring diagrams and details on voltage regulators, relays, and other electrical components are presented in Appendix C.

3.2.4 Methods for Cutisfirm Device Calibration: The calibration of the Cutisfirm skin tension measurement system involves determining the distance measurement capabilities of the Sharp GP2D120 IR proximity sensor. The IR sensor is calibrated using an automated precision

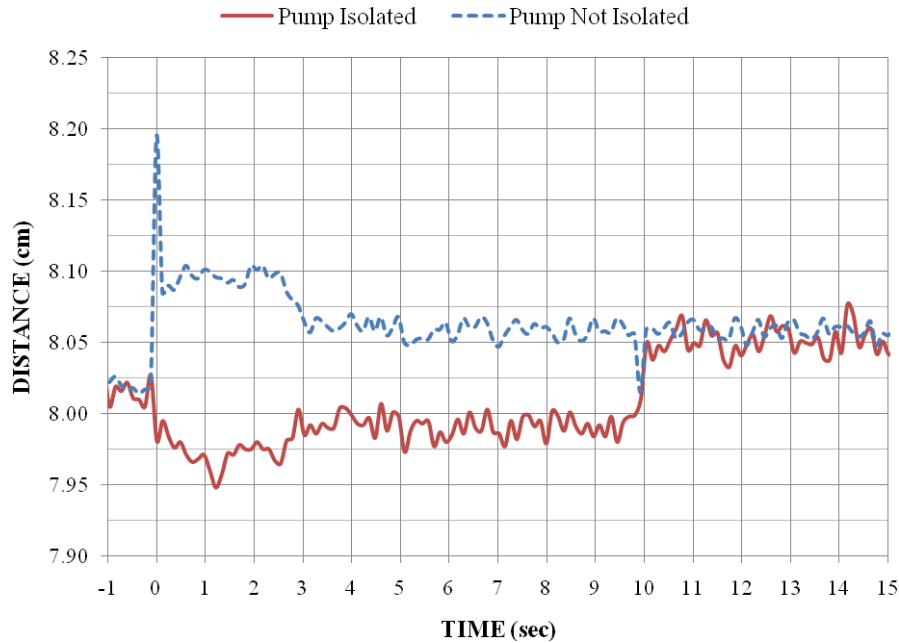


Figure 3.19: Signal output difference with pump power isolated from the Cutisfirm skin tension measurement device.

stage (UniSlide MA6000, Velmex Inc, Bloomfield, NY) to achieve accurate and precision distances and movements in the 7-8cm range of the probe. The output from the IR sensor is compared to known distances on the stage using yellow paper (initially), paint sample cards, and makeup concealer (spread on paper) as “reflectors” of the IR beam. The stage movement is controlled by a stepper motor and verified visually using a ruler affixed to the stationary stage base. (See Figure 3.20)

The Sharp GP2D120 IR sensor is also calibrated while inside the probe using the probe-insert setup shown in Figure 3.21a. Color effects on the output of the IR sensor are explored using the probe-insert setup. Valspar paint sample cards (Lowes) are cut into 8mm discs, and attached onto the stage insert bolt. (Figure 3.21b, c) The insert bolt is then moved inside the probe within the 7 to 8cm range of the probe measurement. (Figure 3.21d)

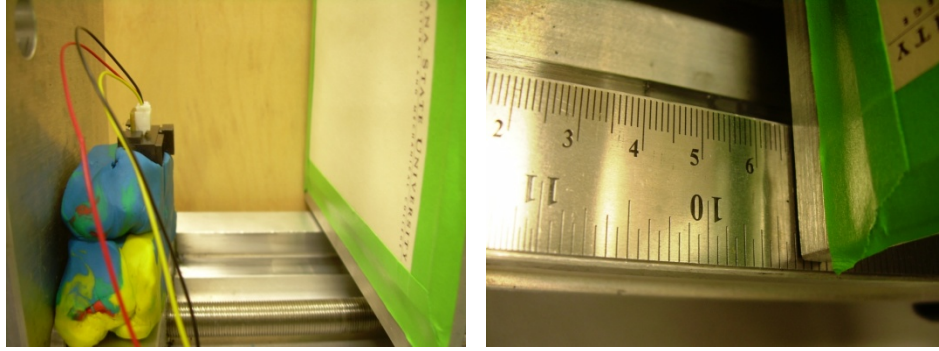


Figure 3.20: Calibration setup for the Sharp GP2D120 IR proximity sensor. (left) The IR sensor is affixed onto the stationary base of a precision stage and the reflecting surface for the IR beam, yellow paper, is attached to the moving portion of the Velmex UniSlide MA6000 stage. (right) Distance changes of the stage are verified using a ruler attached to the stationary base of the stage.

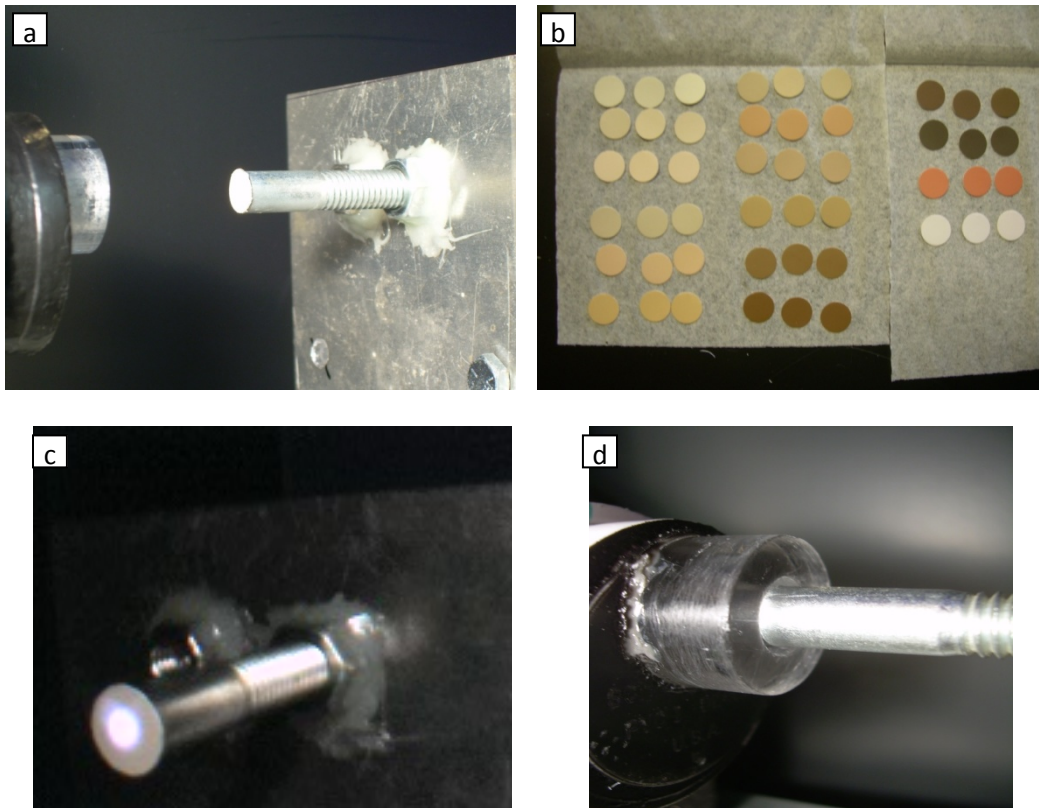


Figure 3.21: Probe-insert setup for the calibration of the GP2D120 IR sensor. (a) A view of the insert bolt and the probe end. (b) Paint sample card discs cut to be placed onto the insert bolt for color effect analysis of the IR sensor. (c) IR beam spot on a paint color disc, taken at sensor distance = 16cm with the IBM PC camera with lens IR filter removed. (d) The bolt insert position during calibration testing.

The dynamic reaction of the sensor is also determined using the probe-insert setup. The automatic precision stage and stepper motor controller are programmed to move within the measurement range of the probe at the speeds: 1cm/s, 0.47cm/s, and 0.24cm/s. The Cutisfirm device output is collected for the three speeds to determine if the targeted distance (where stage is stopped after motion) can be measured accurately. Device tolerance has been determined for the targeted distances: 7cm, 7.25cm, 7.5cm, 7.75cm, and 7.875cm.

3.2.5 Methods with Artificial Skin Models: The Cutisfirm skin tension measurement device has been tested on two different types of materials other than skin to obtain information on the accuracy and repeatability of the system. The first material is a rigid plastic made of 1” thick, Virgin Electrical Grade Teflon[®] PTFE (McMaster-Carr[®] Supply Company, Aurora, OH). This rigid, non-deformable surface is used to determine pressure curve versus time of the Cutisfirm vacuum supply inside the probe. This data is accounted for skin height changes versus time calculations when the device is used on skin. (See Figure 3.22, left) Also, the results from testing on the rigid PTFE surface are used to determine the stability of the deformation distance measurement signal.

The deformation measurement during suction of the Cutisfirm device is also tested using a semi-linear elastic material (more similar to skin) to determine repeatability and the tolerance of the device. Polyurethane elastomer blocks have been used (McMaster-Carr[®] Supply Company, Aurora, OH) and exhibit hardness levels of Shore 30 OO to 70 OO, which are the equivalent hardness levels of a racquet ball to a rubber band. (See Figure 3.22, right)

The procedure for measuring the artificial skin models using the Cutisfirm device is briefly stated as followed. High performance double coated sticky tape (50mm W x 7mil, 3M, St. Paul, MN) is trimmed to size (a disc the same size of the bottom surface of the probe nozzle)

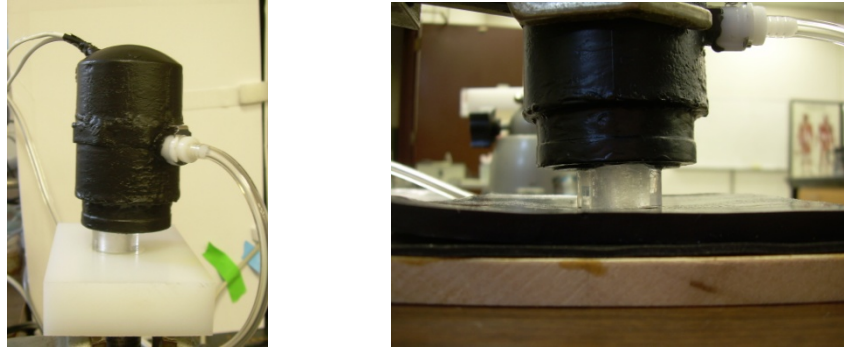


Figure 3.22: Probe setup for artificial skin model testing which is used in the validation experiments of the Cutisfirm skin tension measurement device. (left) A rigid, plastic surface is attached to the probe to determine the background signal and pressure curve of the system. (right) The probe is adhered to polyurathane elastometers of varying hardness to explore the sensitivity and accuracy of the deformation measurement.

and is attached to the testing material. A colored reflector is added to the center of the tape disc using makeup concealer (CG Smoothers® Concealer, #730 – neutralizer) as shown in Figure 3.23. Then the rest of the double-sided tape is exposed and the probe is placed onto the tape disc. The probe is then held by hand or by a lab stand brace while the instrument is cued through a series of menus on the LCD touchscreen. During the LCD menus, the IR sensor signal is calibrated to the length of the probe (8.0cm) and the operator is asked to select a testing time (5, 10, 15, 20, 25, 30, or 60 seconds). The pump is then activated and testing allowed to commence by pressing a manual button on the side of the probe. Ten-second suction tests have been used to determine the difference between different hardness levels of the polyurethane elastometers.

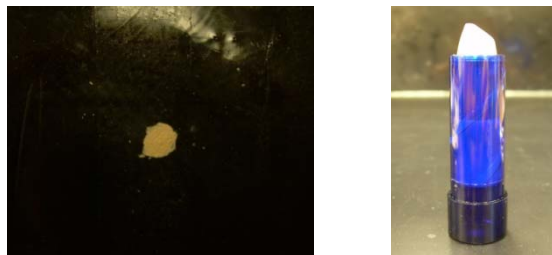


Figure 3.23: Beam reflector is makeup concealer shown on the polyurathane elastomer sheet (left) The CG Smoothers® concealer (#730 – neutralizer) is shown on the right.

The addition of tension to a polyurethane elastomer has also been explored. Calibration and fishing weights are used in the setup shown in Figure 3.24 to apply tension to the square elastomer sheet on all four sides. The applied tension ranges from 0N, 75N, 163N, and 238N. The material is placed in the setup and allowed to reach static equilibrium. Then the probe attached to the material with double-sided tape and operated as mentioned previously.

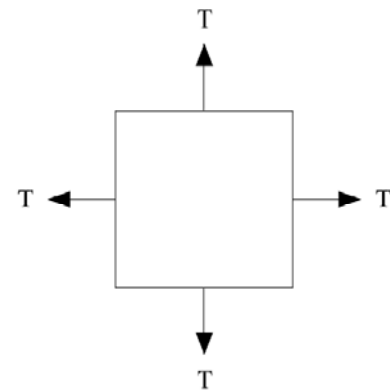
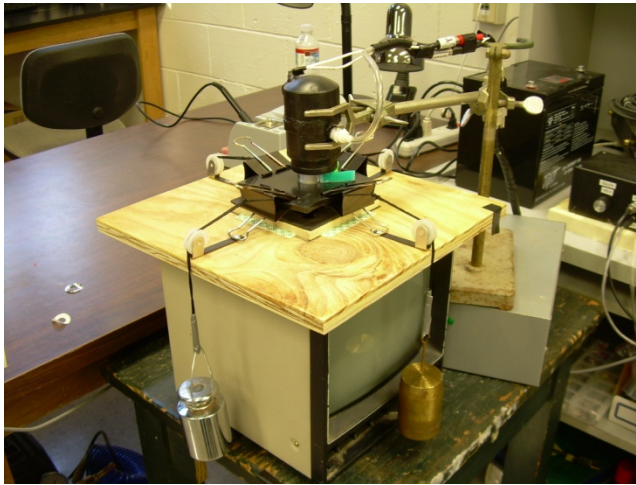


Figure 3.24: (right) Setup for measuring tension effects on a polyurethane elastomer sheet using the Cutisfirm skin tension measurement system. (left) The simple free body diagram of the static tension setup where $T = \text{mass of weight} * \text{acceleration of gravity}$.

3.2.6 Methods with *in Vivo* Skin: The Cutisfirm skin tension measurement system has been used to measure skin on the back of the hand. Lacking a commercial device for direct comparison, an experiment has been performed to show the relationship of body position to the change in skin tension. The dorsal side of the hand has been chosen for its accessibility and observable change in skin tension between the open and closed fist positions. Forty people (20 men, 20 women) from 18 – 66 years of age have been tested on the back of their right hand. Similar to the procedure with the artificial skin models, double-sided tape and makeup concealer

are added to the skin, and then the probe is attached and operated. The operation has been videotaped for review and approximate measurement of the skin deformation.

The skin on the back of the hand is tested while the hand is held in two positions: fist and relaxed. (See Figures 3.25a,b) In the fist position, the person holds a racquetball firmly and maintains a wrist deflection of approximately 30 degrees from the plane of the forearm by resting the arm on an elevated pillow. In the relaxed position, the forearm is laid on a pillow at elbow height and the hand is made to rest on a computer mouse. Five 10-second suction tests are done for each of the hand position. The probe is used on the same testing area between the two positions; however the probe is removed between positions for skin recovery. The resulting deformation measurements from the suction tests are compared between the positions.



Figure 3.25: Images of skin deformation on the back of the hand in different positions: fist hand (upper) and relaxed or flat hand (lower) taken by a video camera. The green ruler is used as a reference distance in image analysis using Image J (NIH Open Source Image Analysis with JAVA).

3.3 Results

The working prototype was used to determine overall function effectiveness of the Cutisfirm skin tension measurement system. The deformation distance measurement was calibrated and tolerance determined. The effect of the reflector color on the GP2D120 IR sensor output was determined. The Cutisfirm device was then used to measure polyurethane elastomers of varying hardness and finally on the hand skin of forty people to observe the system functioning as intended. The data obtained from these studies has shown that the Cutisfirm skin tension measurement device could work as an affordable alternative to the existing commercial skin tension measurement devices.

3.3.1 Calibration and Tolerance Determination of the Deformation: The calibration data for the GP2D120 IR proximity sensor is shown in Figure 3.26. The calibration curve correlated the decimal output values with the measured distances using a quadratic equation approximation. A linear approximation of the data would not be correct since the sensor did not behave linearly in its effective range of 4cm to 30cm. (See Figure 3.4 and Appendix C) The quadratic polynomial approximation was used instead of an exponential decay fit since the quadratic equation was more straightforward in the uM-FPU programming code and was also recommended by the chip manufacturer. The quadratic equation of the calibration was incorporated into the uM-FPU programming language so that the decimal values were converted from the GP2D120 sensor output and transformed into the skin deformation distances. (See Appendix E-3 for program written in the uM-FPU IDE.)

The tolerance of the skin deformation measurement and calculation has been determined through dynamic stage studies. In Figure 3.27a, the dynamic distance measurement at the stage speed of 0.47cm/sec has been shown. The targeted distances were 7cm, 7.25cm, 7.5cm, 7.75cm,

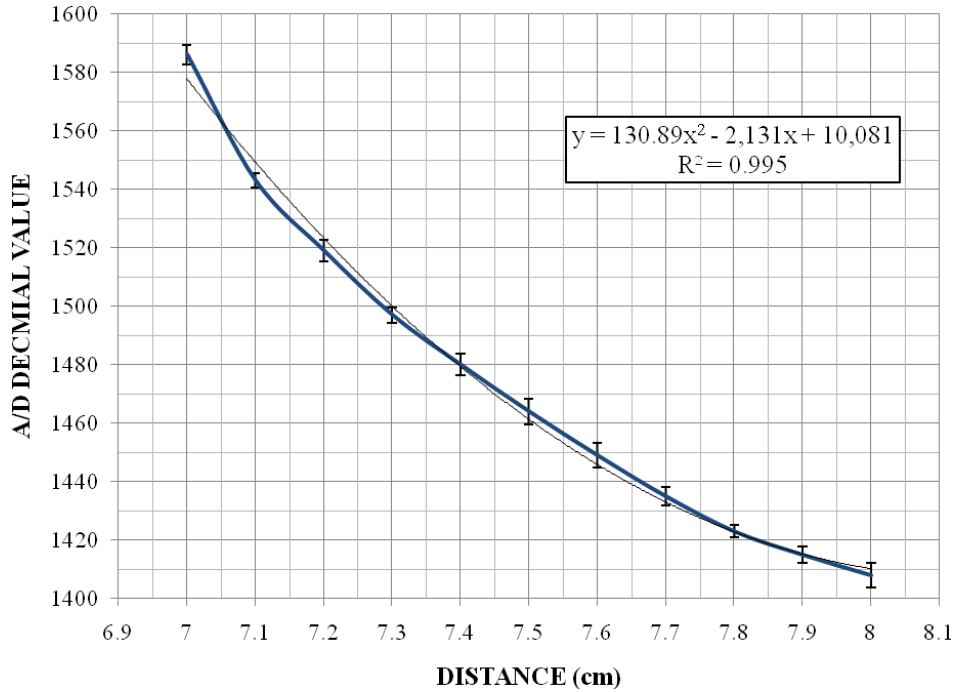


Figure 3.26: Calibration curve for the Sharp GP2D120 IR sensor using makeup concealer as the IR beam reflector. The error bars depict the total variance of the data (n=240). The curve has been approximated by a best fit quadratic polynomial.

and 7.875cm and the stage was halted for 1 second at those distances during testing. The stepper motor controller measured distances by steps, where 2000 steps equalled the movement of a centimeter. The average distances reported by the Cutisfirm devices were respectively (targetted), 6.987±0.035cm (7cm), 7.229±0.04cm (7.25cm), 7.491±0.19cm (7.5cm), 7.746±0.027cm (7.75cm), and 7.868±0.029cm (7.875cm). All tolerances for the 0.47cm/sec speed were less than average ± 0.126cm (n = 12, 1-α = 0.95, γ = 0.05). The Cutisfirm’s response to the difference speeds has been shown in Figure 2.7b for the 7.5cm distance target.

A comparison of the target distances and tolerances (error bars) between the three speeds of the dynamic stage studies has been shown in Figure 3.28. The largest 95% tolerance range was ± 0.139cm (.278cm) which occurred in the slow speed (0.24cm/sec) at the 7.00cm targeted

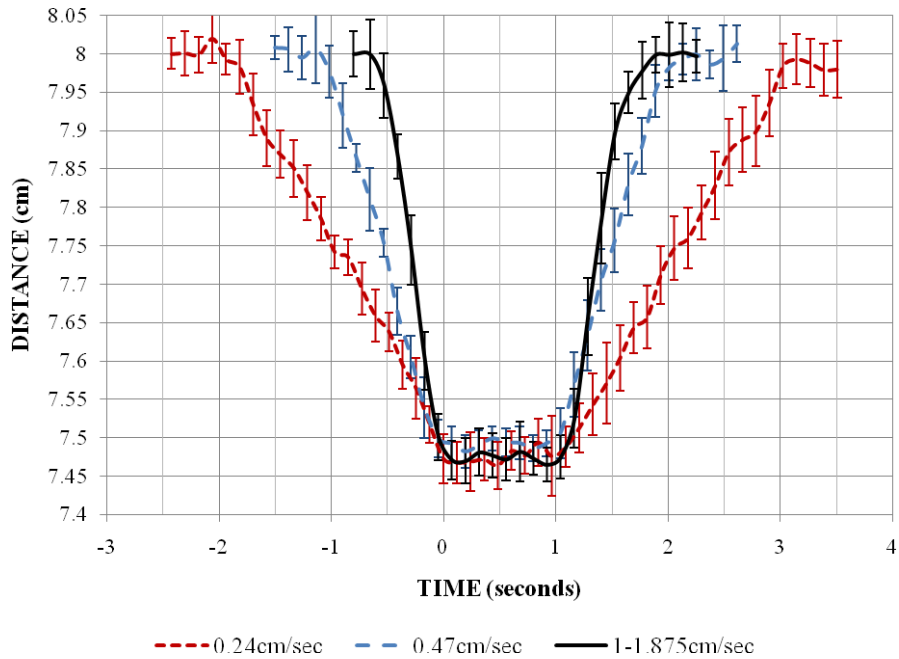
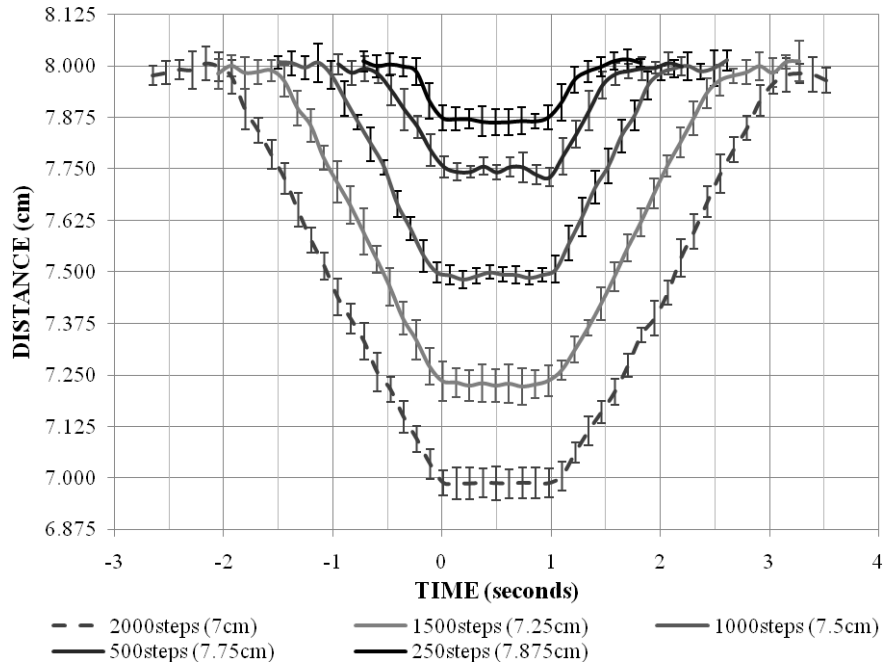


Figure 3.27: Dynamic stage study on the GP2D120 IR sensor performance. (a) The distance measurement of the Sharp GP2D120 IR proximity sensor during a dynamic stage study at 0.47cm/sec for the target distances: 7cm, 7.25cm, 7.5cm, 7.75cm, and 7.875cm. A target distance is held for 1 second before the precision stage (UniSlide MA6000, Velmex Inc, Bloomfield, NY) returns back to 8cm. (b) The comparison of the stage speeds for the targetted distance of 7.5cm. (Error bars for both graphs in \pm standard deviation, $n = 12$)

distance. The average overall tolerance of the speeds was $\pm 0.102\text{cm}$, meaning that 95% of all distance values outputted by the device were approximately the targeted distance value $\pm 0.102\text{cm}$. There was no significant difference in the tolerance of the sensor measurement between the speeds ($P < 0.05$). Therefore, the distance measurement of the device will be accurate in distance referencing in spite of speed changes in the skin as it succumbs to the negative pressure during testing.

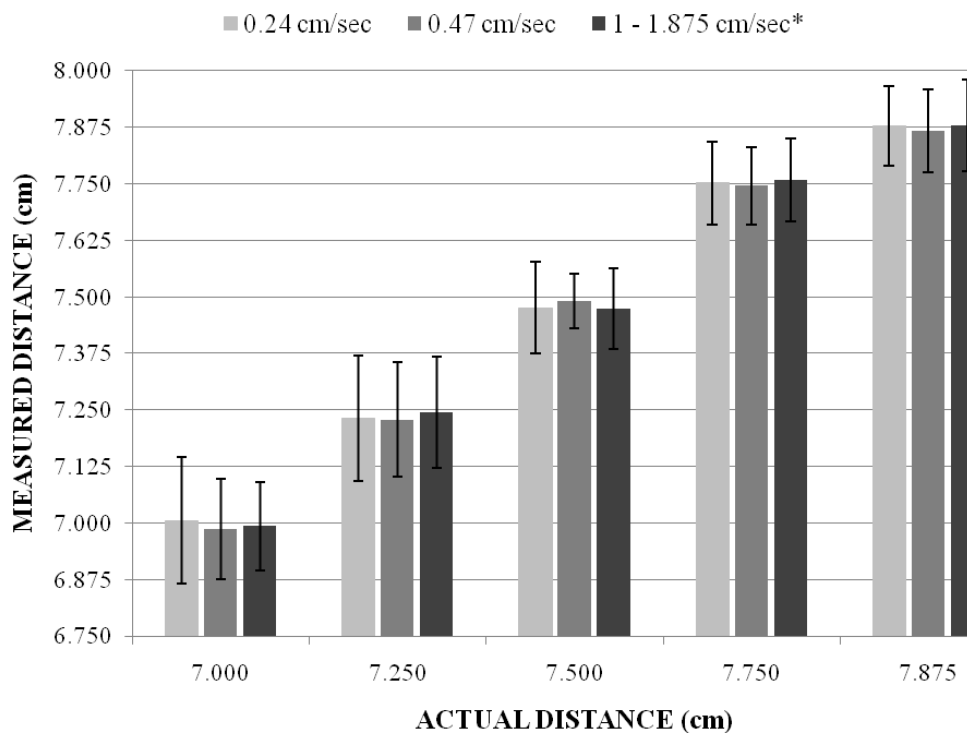


Figure 3.28: Speed (0.24, 0.47, and 1cm/sec) and tolerance (95%) comparisons in dynamic stage study for the distance measurements of the Sharp GP2D120 IR proximity sensor. The errors bars are in tolerance ($n = 12$, $1 - \alpha = 0.95$, $\gamma = 0.05$).

3.3.2 Exploration of the Color Variation using the GP2D120 Sensor: The effect of IR beam reflector color was observed for Sharp GP2D120 IR proximity sensor. Sixteen different paint sample cards (Valspar, Lowes, listed in Table 3.1) were selected to model skin tone

variations (refer to Figure 3.21, page 55) according to sample lightness measured by a color meter (ColorTec-PSM Colorimetry II V4.0, AccuProbe, Inc., Salem, MA). The IR sensor output in decimal has been observed over the known distances between 6.8cm and 8cm in Figure 3.29. A positive correlation was observed between IR sensor decimal-converted voltage output and the lightness of a reflector color. Therefore, color, and in particular, color lightness, of the IR beam reflector has been shown to impact the sensor output, and thereby, the distance measurement accuracy across different colored samples. A color reflector was implemented in further testing to remove the potential error caused from the color variation of the IR beam reflection surface.

Table 3.1 List of Valspar Paint Color Samples Used in Color Variation Study

Paint Color ID	Color Name	Lightness (<i>D65</i>)
	<i>white reference</i>	80.11
7004-2	Soft Silk	77.24
3003-10C	Cream in my coffee	74.72
2004-8C	Warm Cappuccino	73.87
3001-10C	Tagsale Linen	71.64
2004-8B	Mesa Sand	67.00
3003-10B	Hopsack	66.00
3002-8A	Lyndhurst Gothic Tan	64.84
3003-10A	Moose Mousse	61.32
2004-8A	Vienna Beige	59.31
3001-10A	La Fonda Boulder	58.91
2003-5C	Terra Earth	55.54
3002-9C	Cincinnati Hotel Carl Tan	54.71
3002-9B	Mocha Syrup	41.85
3002-9A	Mona's Mane	35.95
3003-9A	Humboldt Earth	34.03
6005-2C	Italian Leather	29.21
	<i>black reference</i>	11.69

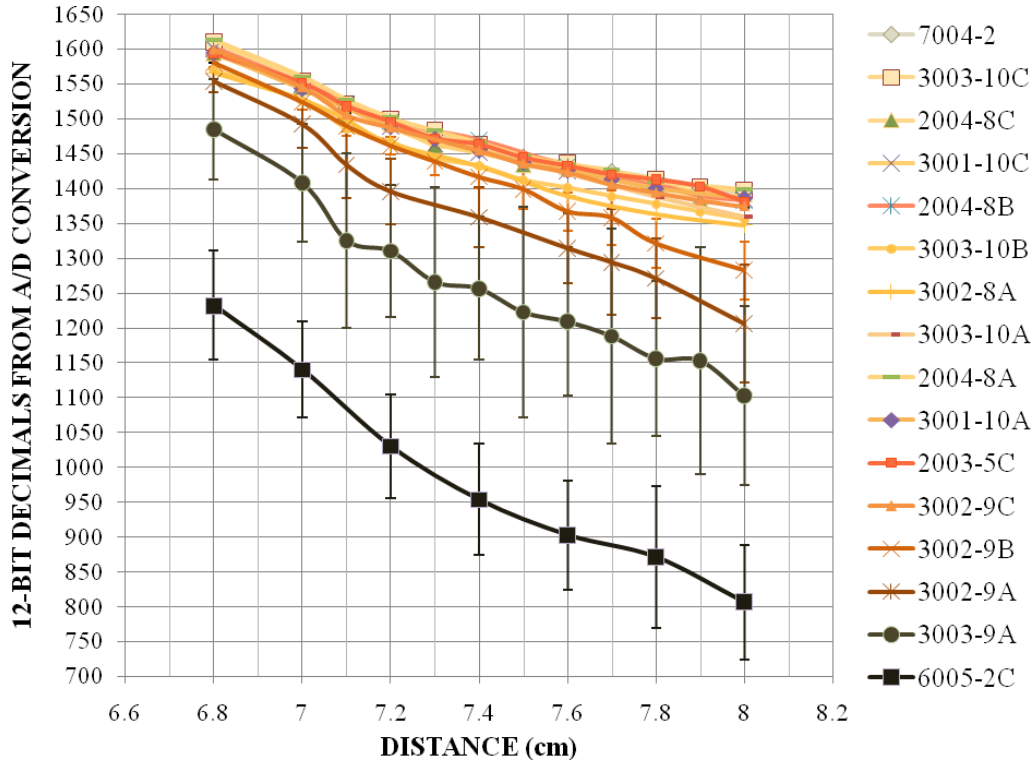


Figure 3.29: Effect of reflector color on the GP2D120 IR proximity sensor. Sixteen paint sample cards of varying tones of brown were used (Valspar, Lowes, listed in Table 3.1). The darker the brown shade, the lower the voltage output of the sensor (converted to 12-bit decimal).

3.3.3 Effect of Negative Pressure on the Distance Measurement: A rigid, non-deformable surface was used to determine if vacuum pressure and the electrical operation of the device would affect the distance measurement. A change in the distance measurement output during operation was observed and this change has been determined as signal noise from the system. The black line in Figure 3.30 represents the signal noise profile of the device when there was no deformation of the tested surface. This internal noise profile was determined from an average of fifty trials. By exploring different electrical configurations (e.g., no pump, no valve, or no IR sensor), it was observed that the noise created in the device largely resulted from current fluctuations of the pump and valve circuitry (relays) when they were initiated and stopped.

There also appeared to be some fluctuation in the distance measurement as the pressure changed in the probe (time 0 to 2.5sec), suggesting that the GP2D120 IR sensor was directly effected. Since the value of distance decreased from time 0 to 2.5 seconds, there was a voltage increase in the sensor during the start of the vacuum pressure in the probe. This increase in voltage could have resulted from an increase in reflected beam intensity caused by a less divergent emitted IR beam under vacuum.

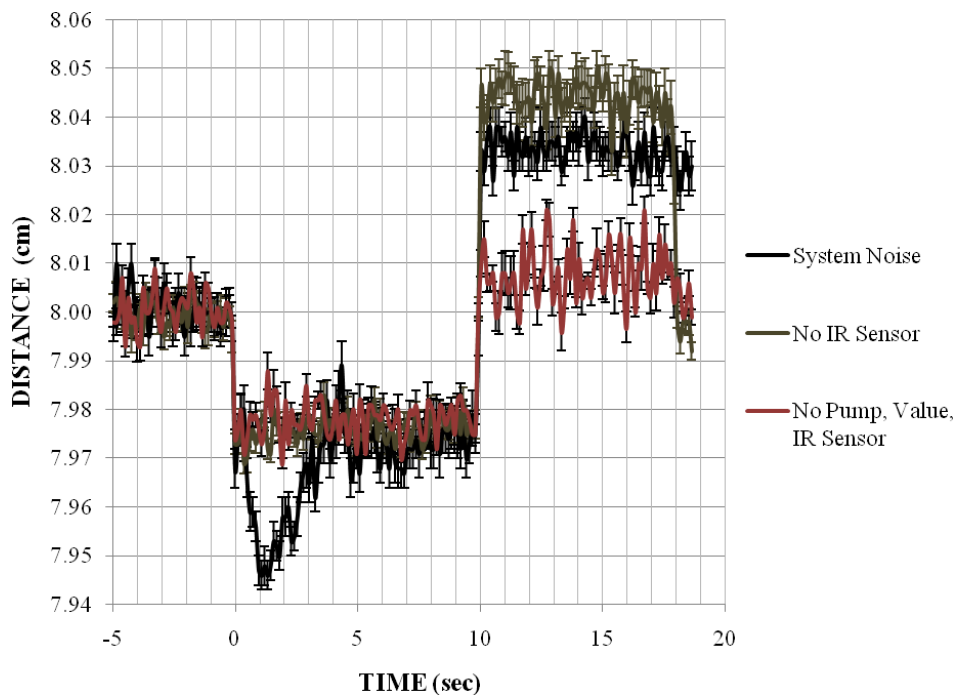


Figure 3.30: Distance output under different electrical configurations of the Cutisfirm skin tension measurement device. The black line represents the noise profile of the device when there is no deformation of the surface.

The overall internal noise profile of the Cutisfirm device was compared to an example result of dorsal hand skin testing. (See Figure 3.31) The signal noise was 5-fold and 8-fold less than the skin deformation of the fist hand and relaxed flat hand respectively. Therefore, the

signal noise was not determined to dramatically impact the results of the skin testing. The signal noise trend was then subtracted from the rubber and skin data reported in the following sections.

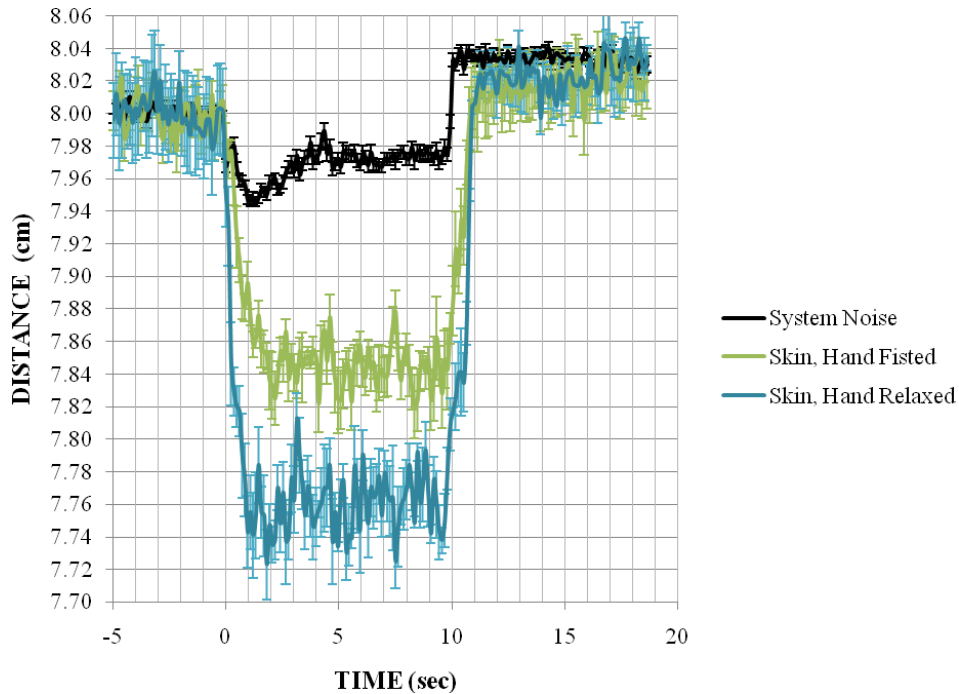


Figure 3.31: Distance output of the electronic noise compared to hand skin data.

3.3.4 Examination of the Viscoelasticity of Polyurethane Elastomers: Polyurethane (Sorbothane®) elastomer sheets were used to initially test the overall function of the Cutisfirm device. Five different sheets of soft rubber were tested by attaching the probe to the center of the 4-inch square sheets and the tested sheet was placed in suspension with negligible tension (allowed to rest on square wooden frame with no surface contact directly below the area of probe attachment). The results from the testing of the five different elastomer sheets have been shown in Figure 3.32. The softest material, 30 OO, exhibited the largest deformation, and the deformation distance of the other elastomer sheets also correlated to their hardness levels. There was an increase in the viscous component of the stress response in softer sheets. The viscous

component of the measurement occurred between times 2 and 10 seconds. This observation was supported by the fact that the polyurethane elastomers were made softer by incorporating more viscous or oily molecules into the materials.

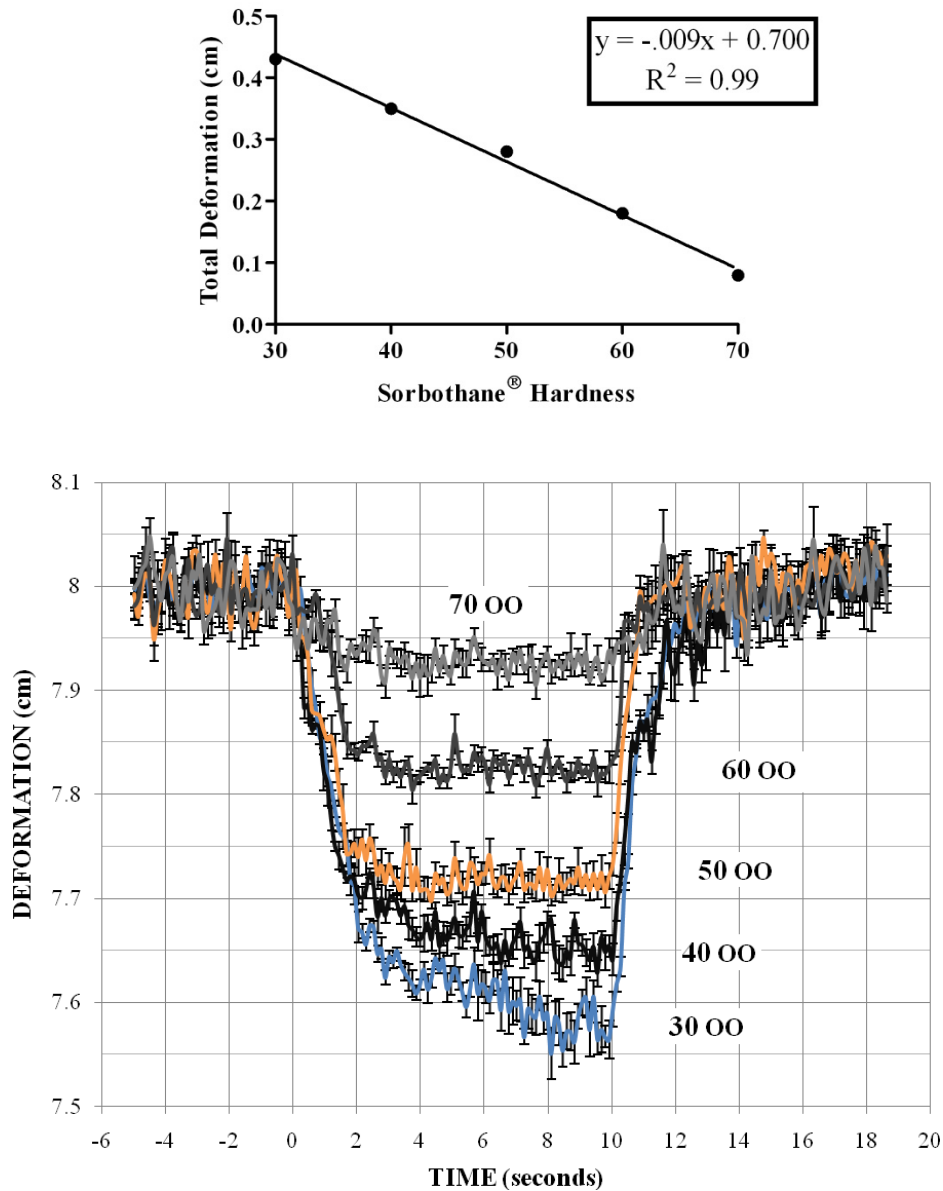


Figure 3.32: Polyurethane elastomer hardness effects. (a) The negative correlation of material hardness and the total deformation during vacuum. (b) The calculated deformation for polyurethane elastomers of varying hardness ratings. The signal noise was subtracted from the raw data. (Error bars depict standard error)

The polyurethane (PU) elastomer with medium hardness (50 OO) was then selected to explore the effect of tension application on the elastomer during deformation measurement with the Cutisfirm device. Calibration weights were hung from pulleys and clamped to the PU sheet in the configuration shown in Figure 3.24 on page 58. The application of 75N of tension caused a decrease in deformation of the material during testing. However, as the tension was increased to >160N, the deformation of the PU elastomer returned to the relaxed levels. This was due to the thinning of the material under the increased tension. At 163N, the thickness of the material reduced from 0.25cm to 0.226cm and at 238N, the material thickness became 0.203cm. The reduction in sheet thickness reduced the elastic modulus and allowed for more material deformation into the suction probe during testing.

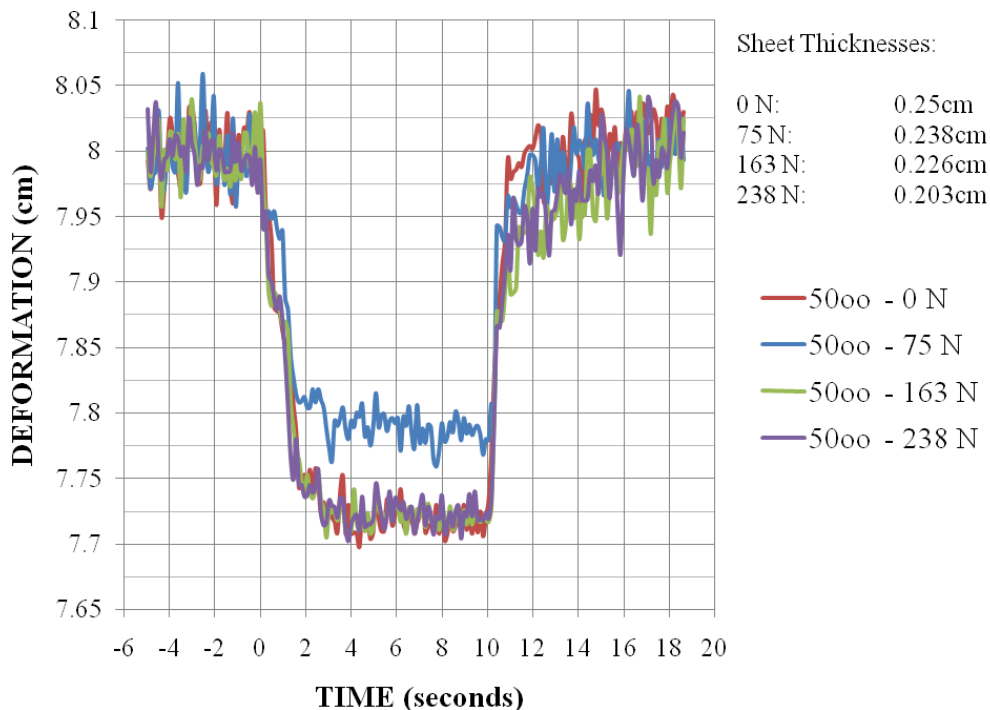


Figure 3.33: Effect of tension on the 50 OO polurethane elastomer sheet. As 75N of tension was applied to the sheet, the deformation decreased. However as the tension increased, the thickness of the material was reduced enough so that the level of deformation increased.

3.3.5 Examination of the Viscoelasticity *in Vivo* on the Back of the Hand: The Cutisfirm skin tension measurement system was tested on the dorsal skin of the hand for forty human subjects (20 men, 20 women) from the ages 18-66 years. (See Table 3.2) Lacking a commercial device for direct comparison, the study was performed to show the relationship of body position to the change in skin tension. Each person was tested with his/her hand held in the closed fist and relaxed (open) positions. Five consecutive 10-second tests were recorded for each hand position on the same skin area, with 5 minutes of recovery between the tests. Data from the five tests were then averaged and the average deformation distance was compared with time for each hand position. Representative cases of the dorsal hand skin deformation measurement in various aged males have been shown in Figure 3.34.

Table 3.2 Distribution of Ages and Gender in Human Subjects

AGE	MALE	FEMALE
18-19	0	1
20-24	6	6
25-29	5	2
30-34	1	0
35-39	2	2
40-44	2	4
45-49	0	4
50-59	2	0
60-66	2	1
SUMS	20	20
	TOTAL	40

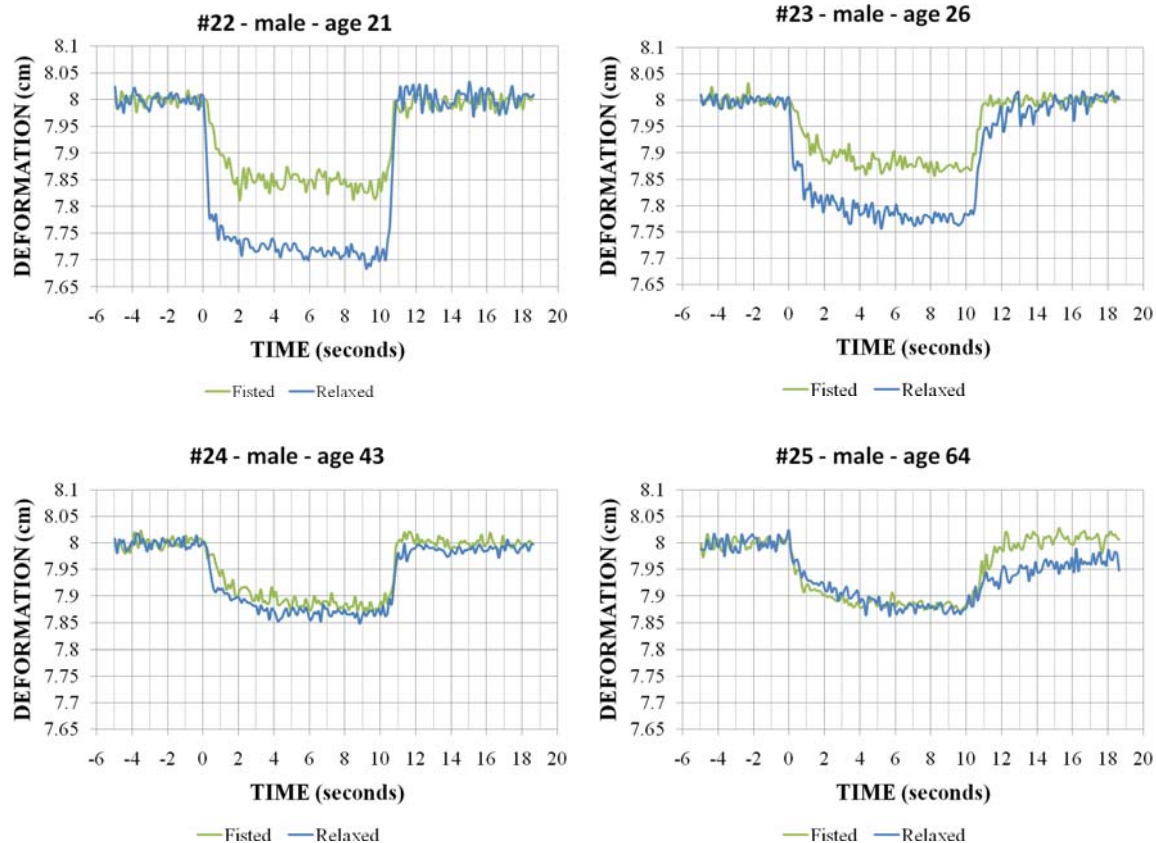


Figure 3.34: Example dorsal hand skin deformation measurements for 4 men between the ages of 21 and 64 years taken by the Cutisfirm skin tension measurement device.

The data in Figure 3.34 showed a general decreasing trend in the difference between the hand positions with increasing age in men. For further analysis, the data was broken up into different components which related to the biomechanical characteristics of the skin. These data components have been depicted in Figure 3.35 and were defined as:

- E = immediate deformation of the skin or the elastic response (cm)
- V = deformation creep caused by the viscous nature of the skin (cm)
- T = total deformation of the skin (cm)
- R. = elastic return of the skin or recoil (cm)
- ToR = time of recovery or the length of time for the skin to return to baseline (sec)

One other component, which was used to compare the recovery response, was the cumulative recoil distance (RD) or area of the curve with respect to baseline (cm*sec). Thus RD

was not a physical property of skin biomechanics, yet it did provide insight into the skin recoil dynamics with respect to the time of recovery.

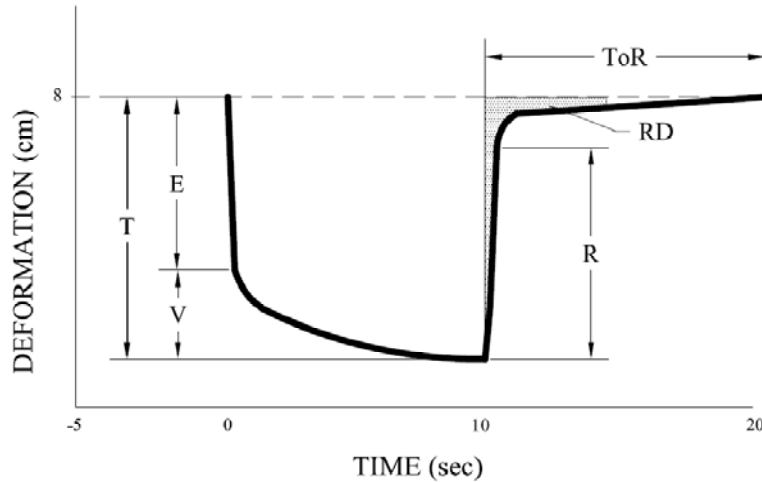


Figure 3.35: Description of data components of the skin study used to analyze the biomechanical properties of dorsal hand skin.

The data components were calculated from the deformation/time curves as follows: E was the difference in the deformation between time 0 and 2.5 seconds; T was the average deformation between 9 and 10 seconds; V was the difference between T and E; R was the difference in deformation between the 10 and 11-second time points; and ToR was the time from the 10-second suction release to the point at which the skin returns to the original distance (8cm). In the cases where the ToR was longer than the 8.6 seconds of extra data capture, a linear approximation of the deformation between 16 and 18 seconds was used to forecast the time of recovery. A table listing all of the data components for the forty subjects tested has been included in Appendix D.

The data components were compared between the relaxed and fistled hand positions for the tested population and shown in Table 3.3. The difference of the hand positions (relaxed

Table 3.3 Population Averages of Data Components for the Different Hand Positions

	E	V	T	R	ToR	V/E	R/E	R/T	RD
Relaxed	0.15 ± 0.011	0.02 ± 0.003	0.17 ± 0.01	0.12 ± 0.012	11.33 ± 2.01	0.21 ± 0.05	0.83 ± 0.053	0.70 ± 0.038	0.28 ± 0.028
Fisted	0.10 ± 0.008	-0.005 ± 0.002	0.11 ± 0.008	0.08 ± 0.009	8.07 ± 0.98	-0.01 ± 0.05	0.99 ± 0.178	0.72 ± 0.049	0.19 ± 0.021

(Error bars in standard error)

Table 3.4 Deformation Difference between Hand Positions (Relaxed Hand - Fisted Hand)

	E	V	T	R	ToR	V/E	R/E	R/T	RD
Difference	0.05 ± 0.009	0.02 ± 0.004	0.05 ± 0.009	0.04 ± 0.011	3.26 ± 2.17	0.23 ± 0.078	-0.16 ± 0.2	-0.01 ± 0.063	0.10 ± 0.030
Paired T-test	<0.0001	<0.0001	<0.0001	0.0007	0.1405	0.0060	0.4108	0.8125	0.0025
Significance (P < 0.01)	Yes	Yes	Yes	Yes	No	Yes	No	No	Yes

minus fisted) was used to compare the positions and shown in Table 3.4. Of the forty people tested, significance ($P < 0.01$) in the difference between the positions was found in the total deformation (T), the elastic response (E), the viscous portion (V), the recoil response (R), the viscoelastic ratio (V/E), and the cumulative recoil distance (RD) using the Student's T-Test (paired, two-tailed, $P <$ noted in Table 3.4). There was a general larger skin deformation in the relaxed hand position and this larger T also allowed for larger values in the E and R components for the relaxed hand position. (See Figure 3.36) The average viscous effect (V) in the skin deformation profile also was more pronounced in the relaxed hand position compared to the fisted position and this difference was also evident in the comparison of the viscoelastic ratios (V/E). Eighty percent of the population showed a greater cumulative recoil distance (RD) for the relaxed hand as well. To summarize the exploration of skin deformation in different hand positions, the relaxed position of the hand had an increased total deformation, and especially an increased viscous deformation for most of the tested population, while the fisted hand recoiled or returned to origin position faster, perhaps due to the increase in lateral tension of the skin. A

subset of the subjects tested (20%) experienced minimal or opposite differences between the hand positions, so different parameters (e.g. age, sex) were explored.

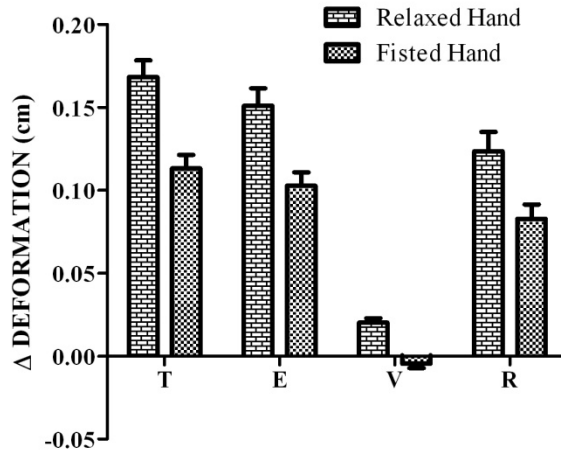


Figure 3.36: The data components T, E, V, R from human subject testing which were significantly different between the relaxed and fisted hand positions.

The total deformation differences in the hand positions were compared across age and gender. There was no correlation in the total skin deformation (T) for the overall population due to age, however in men 40 years or older there was a significant decrease ($P < 0.05$) in the total deformation determined using the Bonferroni post test from a 2-way ANOVA. (See Figure 3.37) A slight increase in the T component difference between the relaxed and fisted hand positions was observed in younger women compared to younger men; however there was no significant difference. (See Figure 3.37)

A significant difference ($P < 0.05$) was also observed in the older men group for the recoil response (R), seen in Figure 3.38. The data from the +40 year males showed that smaller recoil response in the relaxed position when compared to the fisted hand position. Similar comparisons were made with the other data components with the total tested population with all P values greater than 0.05 (2-way ANOVA, Bonferroni post test) in age or gender in Figure 3.39.

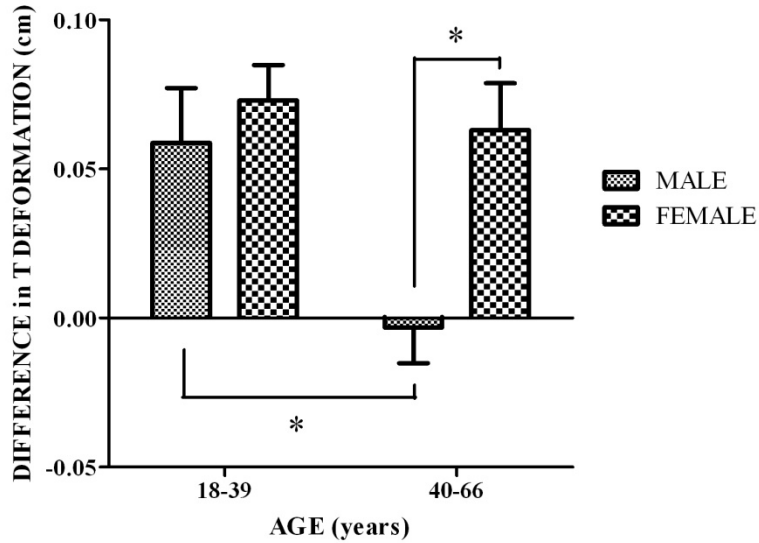


Figure 3.37: Age and gender correlation for the total skin deformation (T). The horizontal bars denoted with asterisks represent statistically significant differences between age or gender groups.

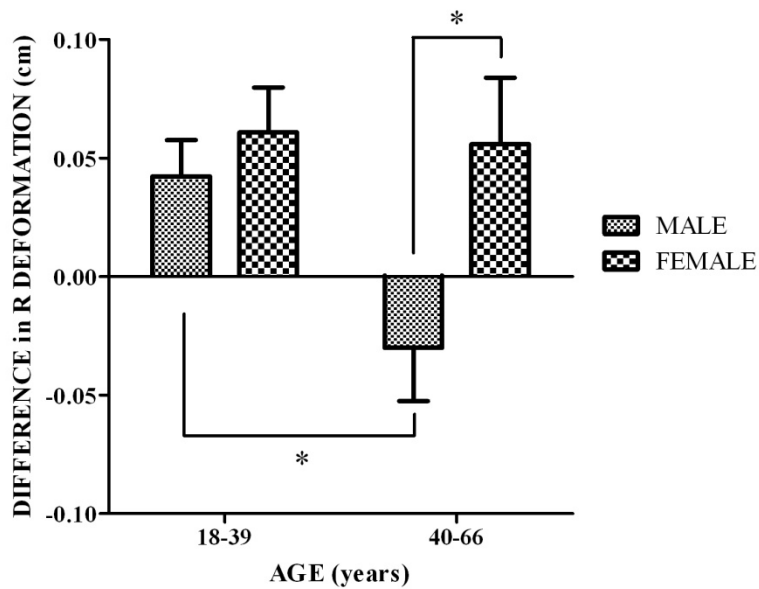


Figure 3.38: Age and gender correlation for recoil skin deformation (R). The horizontal bars denoted with asterisks represent statistically significant differences between age or gender groups.

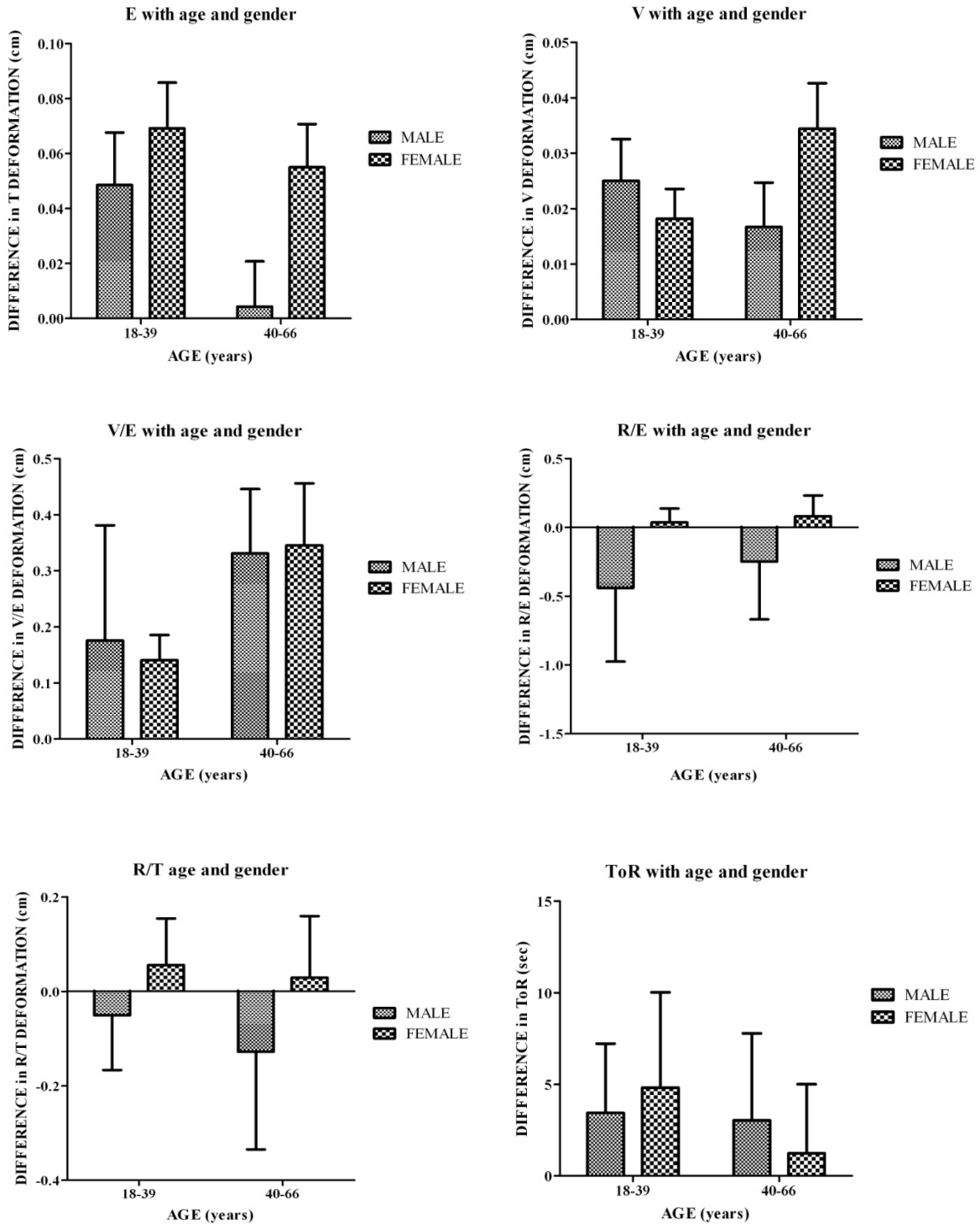


Figure 3.39: Age and gender comparisons of non-significant data components from the human subject testing ($P > 0.05$).

3.4 Discussion

The Cutisfirm skin tension measurement system was designed and a prototype created to validate that a quality skin tension measurement device could be devised where mass production and affordability was feasible. The Cutisfirm device has been developed using an inexpensive robotic proximity sensor to detect dynamic skin elasticity changes under suction. The prototype to house the Sharp GP2D120 IR proximity sensor was originally designed in Autodesk® Inventor™ Professional 2008 and then synthesized in ABS plastic by a 3D printer. This prototype was used to test the physical size, the ergonomics, and the structural stability of the design. The printed probe however was not effective for use in vacuum experiments, since the ABS plastic material was very porous as a result of its synthesis technique and it was too intricate internally for effective coating with epoxy. Therefore, a substitute probe made of PVC pipe fittings was devised for the experiments using vacuum. A probe nozzle of clear acrylic was added to the probe for its attachment to the testing material. The orifice size of the nozzle, 12mm, was designed for testing on full thickness skin and to allow an unimpeded path for the IR beam from the Sharp GP2D120 IR proximity sensor. The probe prototype was then attached to electronic and mechanical hardware to achieve precisely timed vacuum tests and skin deformation measurement with data output sent to a microSD card for further analysis. (Refer to Figure 3.3, page 38 for image of prototype)

The Sharp GP2D120 IR proximity sensor proved to be a useful tool to measure skin deformation remotely while the skin was under the applied negative pressure. An infrared opaque cap with a 1mm pinhole at the center was placed over the IR sensor LED emitter bulb to reduce the divergent beam width to ~5mm when the light contacted the skin at the probe's end. This beam occlusion reduced the amount of erroneous light reflection due to surfaces other than

the top peak of the skin dome resulting from the suction applied. The voltage output of the sensor's IR detector was only slightly reduced by the filtering cap.

A dual, low-pass signal filtering circuit was also applied to the Sharp GP2D120 IR proximity sensor to reduce the noise of the voltage output. (Refer to Figure 3.8, page 43) This pre-sensor and post-sensor RC filter system was optimized to stabilize the voltage output of the IR detector and to improve the 95% tolerance of the skin deformation measurement from $\pm 0.3\text{cm}$ to $\pm 0.139\text{cm}$. A calibration curve between the decimal from the 12-bit analog to digital conversion of the voltage output and the distance of the reflective surface was determined for the GP2D120 sensor to be most similar to a quadratic equation. This quadratic equation was used in the programming of the uM-FPU math co-processor to calculate the deformation of the skin.

The effect of dynamic surface deformation on the sensor output was explored using an automated precision stage to move a beam reflective surface within the probe. This setup was used to determine the overall tolerance of the distance or deformation measurement to be $\pm 0.139\text{cm}$ for surface velocities up to 1.875cm/sec and to provide a secondary validation of the skin deformation measurement. The tolerance in the deformation measurements did not significantly change for surface speeds between 0.24cm/sec to 1.875cm/sec . (Refer to Figures 3.27a, b and 3.28, page 62) During the dorsal hand skin testing, the fastest skin velocity recorded amongst the forty subjects was 0.68 cm/sec . Therefore, the sensor had the capability to detect the skin's surface when it was in motion without increasing measurement variability.

The impact of color variation on the Sharp GP2D120 IR proximity sensor was also observed. There was a correlation of sensor output and the lightness of the different represented skin hues tested, where darker samples yielded lower voltage outputs. This color effect on the IR detector was overcome by the addition of a beam reflector to the surface being tested. Makeup

concealer of a neutral shade was chosen as the reflector material, since it could be applied easily and uniformly to skin and the other materials tested in this project. The concealer was viscous cream that appeared to be easily adaptable to the shape changes of the surface it covered, allowing for a continued coverage during the material's movement within the Cutisfirm probe during operation. Initial testing on skin showed no apparent difference in the deformation results between pale skin and the concealer used. (See Figure 3.40) An added benefit to using the makeup concealer was that it has been designed for use on skin already and it would only have the minimal allergy risks of cosmetics. During the skin experiments, the use of the concealer was effective in normalizing the different hues of skin. Four subjects out of the forty tested with the concealer reflector had dark pigmented skin. The data components from the deformation-time curves (e.g., E,V,T,R) for each of the four people were compared with the average of the others tested using a Student's T-Test (paired, two-tailed) and no significance between the people with dark skin and pale skin was found. ($P>0.152$)

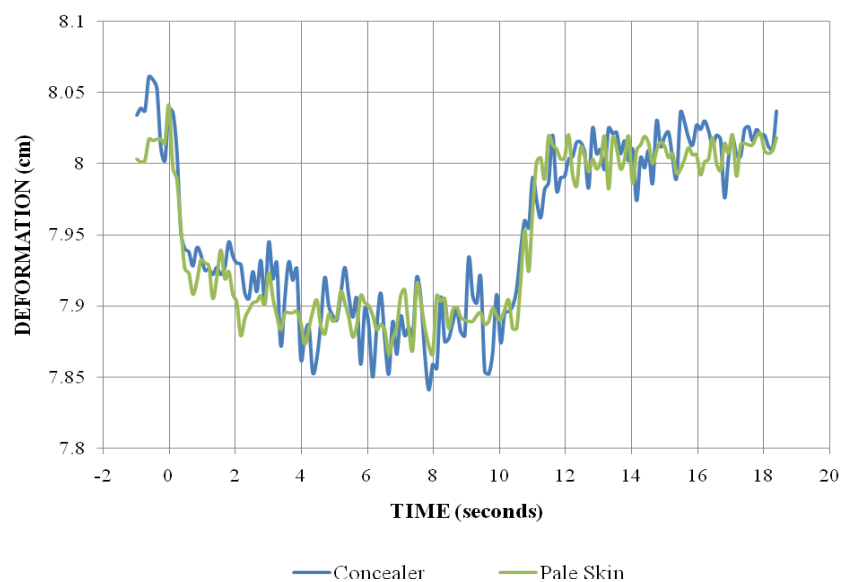


Figure 3.40: The non-significant effect of concealer application on the skin deformation measurement for a skin tone similar to the concealer.

Polyurethane elastomer (Sorbothane®) sheets of five different hardness levels were used as artificial skin models to test the overall function of the Cutisfirm device. Sorbothane® was designed for use in shock absorption or vibration damping and had been reported to have a longer fatigue life due to its low creep rate when compared to other polymers used for damping. (Sorbothane 2009) When the elastomer sheets were tested with the Cutisfirm device, a negative correlation ($r = -0.99$) of the material's hardness to the total amount of deformation during suction was observed. (Refer to Figure 3.32, page 68) This observation was expected based on the material property change with respect to hardness shown in Table 3.5. There was also an increase in the viscous deformation contribution for softer sheets of the Sorbothane® material. The increase in density shown in Table 3.5 gave evidence that more oily polymers residues of the material were used in the softer sheets which reduced the amount of trapped air compared to the more rigid sheets.

Table 3.5 Material Properties of Sorbothane®

Property	Durometer (Shore OO)			Units
	30	50	70	
Tensile Stress at 100% Strain	17.86	25.47	66.18	psi
Compressive Stress at 20% Strain	6.4	12.0	30.0	psi
Tear Strength	43.62	48.73	65.26	lb/in
Density	85.5	85.0	84.9	lb/ft ³
Specific Gravity	1.372	1.364	1.363	
Kinetic Coefficient of Friction	3.3	2.6	2.5	

The effect of tension on the 50 OO, polyurethane sheet was explored by hanging weights from the material. The results in Figure 3.33 (on page 69) were somewhat unexpected at first. Increased tension in the lateral plane was expected to decrease the deformation in the axial direction measured by the Cutisfirm device. The theory was true for only the addition of the 75N

lateral force with a decrease in the material deformation from 0.28cm to 0.22cm. However the material with the higher tensions added had similar deformation distances to its relaxed state. The reason for this observation was that the material was being thinned by the increased lateral tension, allowing for more flexibility in the axial direction. This idea was confirmed by comparing the simplified strain-energy densities (u) for the relaxed and high tension states. The strain-energy density, defined as the strain energy for a unit volume of a material, can be represented by the equation:

$$u = \frac{1}{2}(\sigma_x \epsilon_x + \sigma_y \epsilon_y + \sigma_z \epsilon_z) \quad (\text{Eqn 3 - 1})$$

for triaxial stresses. (See Figure 3.41a) For simplicity, the stress applied by the vacuum from the Cutisfirm device was assumed to be a normal stress and resolved into a point force. The comparison for the all of the tension applications has been shown in Figure 3.41b. Unlike the relationship between deformation and force, the deformation / strain-energy density relationship correlates well, with increasing strain-energy density exponentially for increasing tension.

The Cutisfirm skin tension measurement device was then tested on the dorsal hand skin of forty subjects with different ages, backgrounds, and gender to observe the performance of the device. The back of the hand was selected as the testing site since a difference in skin tension could be visually observed for changes in hand position. The dorsal hand was an easily accessible region of the body and was less likely to deter volunteers compared to the abdominal region originally targeted for the Cutisfirm design. The hand skin would also provide a very diverse data set based on the differences in hygiene practices (e.g., lotion use, hand-washing) and general health of the tested people.

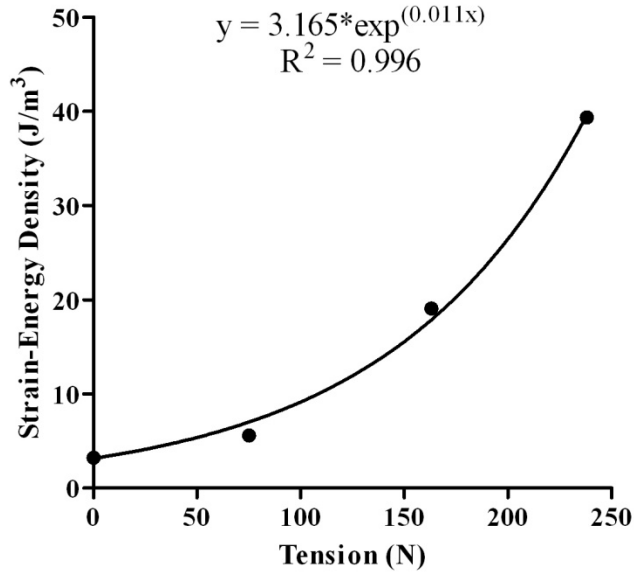
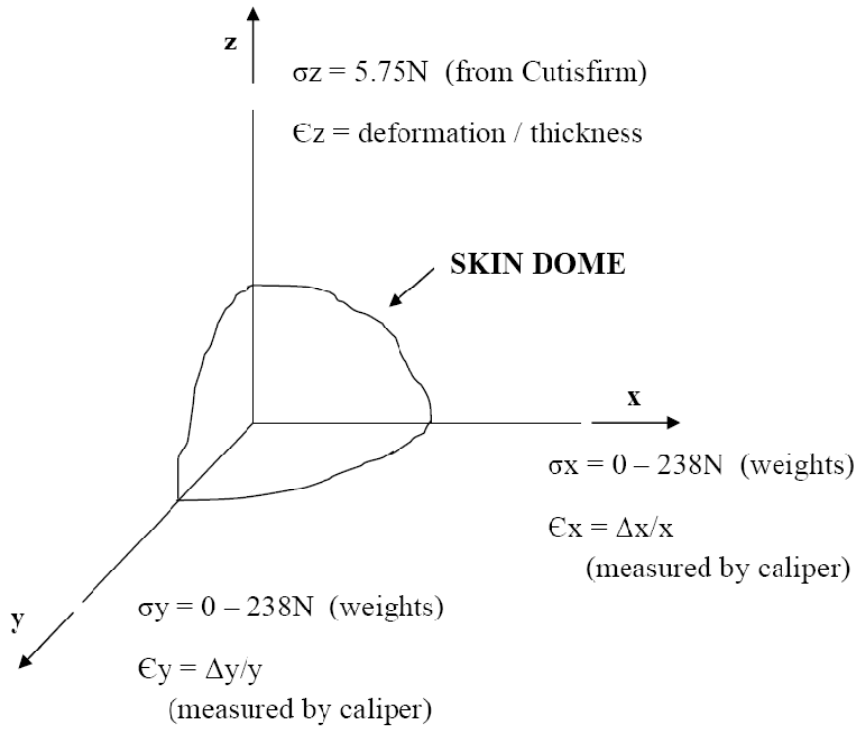


Figure 3.41: Strain-energy densities for 50 OO polyurethane elastomer in tension. (a) The parameters in Equation 3-1 described. (b) The comparison of the strain-energy densities (u) for the 0N, 75N, 163N, and 238N tension applications to the 50 OO polurethane sheet. Refer to Figure 3.33 for the original deformation/time curves.

The difference between relaxed and fisted hand positions was the main focus of the *in vivo* experiment. Significant differences were observed in the main curve components T, E, V, and R; along with the viscoelastic ratio (V/E) and the cumulative recoil distance (RD) using a paired, two-tailed Student's T-Test between the relaxed and fisted hand positions. (Refer to Table 3.3 and Figure 3.36, starting on page 73) The data curve component that was not significant was the time of recovery (ToR) and this was likely due to the large variability of the data. The ToR was determined using crude linear forecasting approximation near the end of the dataset as shown in an example, Figure 3.42. This type of rough approximation also may have increased the data variance, and thus increasing the P-value of the T-Test.

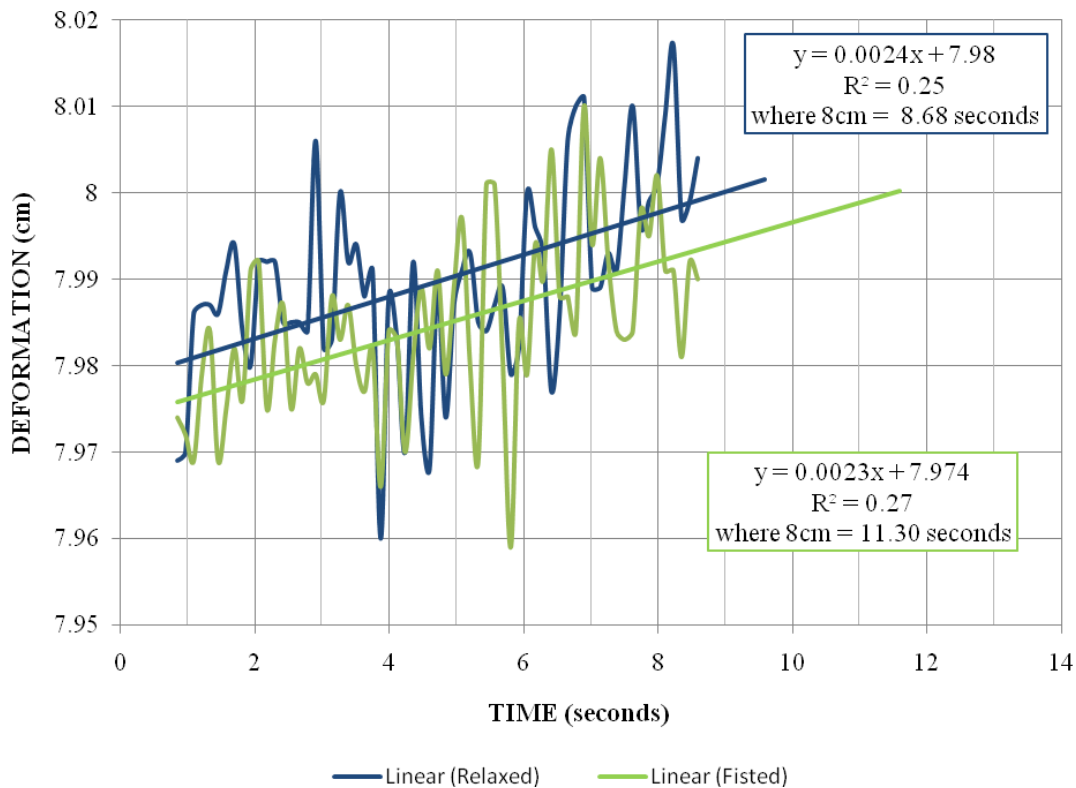


Figure 3.42: Time of recovery determination by the linear approximation for the dorsal hand skin experiments.

Two ratios of the data components also did not have significance when analyzed: the R/E and the R/T. The R/E ratio was considered to be a representation of the skin's elastic recovery, where the amount of recoil elastic response was compared to the original elastic response when the vacuum was initiated. The R/T ratio was considered the biological elasticity of the skin, where the general elastic return response of the skin can be observed. The data from the population subset was variable in these parameters which may contribute to the lack of significant difference between the hand positions. However, these ratios may also be not significantly different since the ratios were proportional comparisons of deformation components. These ratios then could be a result of the anatomical makeup of the skin, rather than position or tensioning.

The data components of the deformation/time curves were also compared to the biological parameters of age and gender to determine if population trends could be detected by the Cutisfirm device. The largest and only significant difference was seen with the +40 years male group in the total (T) and recoil (R) deformations. (Refer to Figures 3.37 and 3.38 on page 75) As to why the older female group did not show any difference from the younger females might be due to increased lotion use on their hands when compared to the older men group. The approximate lotion use per week of each gender-age group has been shown in Figure 3.43. There was a significant difference ($P < 0.01$, 2-way ANOVA) between the genders for both age groups in lotion application frequency. The increased lotion use by the female groups may lead to the slower decrease in total deformation and recoil response that was seen in the male population. The lotion use data was obtained through an informal questionnaire, and although the data provided an interesting idea to explain the differences between the +40 gender groups, a more controlled study on lotion application would need to be performed for theory validation.

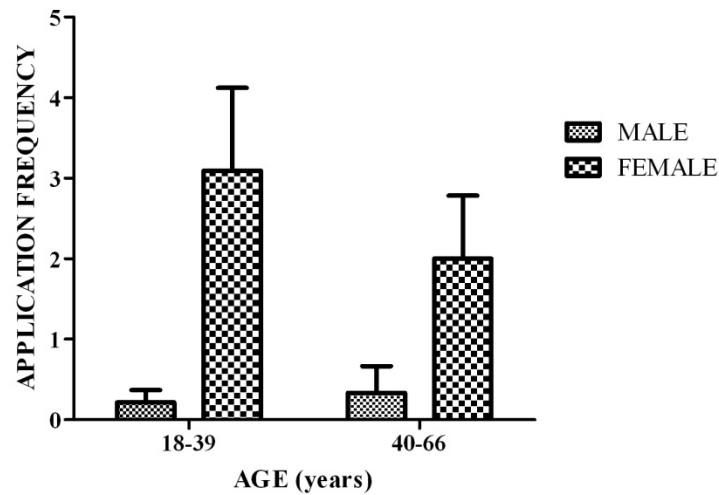


Figure 3.43: Age and gender comparison in lotion application frequency of the tested population.

A possible reason for the significant difference between the older men and women may be the difference in skin aging between the sexes. The dermis in male skin has been reported to demonstrate gradual thinning with increasing age (12-93), where the dermis in female skin remains a constant thickness up until 50 years. (Tur 1997) However, Tur also mentions that women start with thinner dermis layers than men. The rate of change in the dermis of the skin between men and women might contribute to the difference seen in the *in vivo* experiment; however the significant difference was more likely to be caused by environmental factors such as diet, water intake, lotion use, humidity, and temperature. (Hendriks, Brokken et al. 2004)

The results in this report have shown that the Cutisfirm skin tension measurement system can be an effective product for measuring dynamic mechanical response in skin. The Cutisfirm device was designed to be a suction device, which was the chosen type for its simple device mechanics along with the most informative data on the effects of full-thickness skin tension. The Cutisfirm device effectively measured deformation changes in the skin and artificial skin models within the 95% tolerance level of $\pm 0.139\text{cm}$ and up to 1.875cm/sec movement velocities.

Results showing changes in body position, gender, and age demonstrate that the Cutisfirm was able to detect changes in skin tension for a diverse population. Therefore, the Cutisfirm skin tension measurement system was proven to be a potential candidate for a mass produced, affordable device option for general clinical use.

The Cutisfirm device, if commercialized however, will not be the best skin tension device on the market for measurement accuracy and precision. The best commercial device for skin tension measurement may be the recently-unveiled BTC-2000TM Biomechanical Tissue Characterization System which incorporates a suction device with a high-resolution laser (μm) for deformation measurement. The BTC-2000TM also has a touchscreen interface that provides real-time data output and calculation results. (Smalls, Randall Wickett et al. 2006) The \$37,500 device samples data at 10Hz and concurrently monitors pressure profile and skin deformation to provide dynamic stress information. (Surgical Research Laboratory 2007) The Cutisfirm, however, is designed to be affordably mass produced due to its simple design and commercially available sensors. Therefore, the Cutisfirm could have its place in making skin tension measurement a more common practice in clinics and research.

CHAPTER 4: CONCLUSIONS AND FUTURE CONSIDERATIONS

4.1 Conclusions

Research and design efforts from this project provided feasibility data on a novel and cost-effective device to measure full-thickness skin tension. The Cutisfirm skin tension measurement system was designed, validated, tested on artificial skin models, and then an *in vivo* comparison of body position on skin was performed on diverse population of forty human subjects. The Cutisfirm device was designed to measure skin deformation under vacuum using a non-invasive, low power, reflective light sensor.

The Cutisfirm device effectively measured deformation changes in the skin and artificial skin models within the 95% tolerance level of $\pm 0.139\text{cm}$ and up to 1.875cm/sec movement velocities. The measurement capability of the device was acceptable to detect changes in polyurethane elastomers of different Shore OO hardness. The Cutisfirm skin tension measurement system also was able to detect differences in dorsal hand skin tension in open and closed fist positions. In summary, the prototype design of the Cutisfirm skin tension device was successful in employing the use of the semiconductor optical distance detector, the Sharp GP2D120 IR sensor.

4.2 Future Considerations

The future considerations of the Cutisfirm skin tension measurement system are categorized into two topics: instrumental design and suggested research. The instrumental design recommendations start with developing a second working prototype of the device. The next prototype design should incorporate the probe design made in Autodesk® Inventor TM Professional 2008. The new probe can be made from plastic casting or injection molding. The

design's integrity can then be tested (e.g., impact strength, vacuum effectiveness, and testing ergonomics).

The instrumentation electronics can also be improved for the next prototype. Switching from mechanical relays to solid-state relays is recommended to reduce current fluctuations observed in the rigid plastic experiments. Also, it is highly recommended that the pump and valve have an isolated power supply from the power of the main electronics. This isolation will also reduce the signal noise of the system.

The main electronic board in the first working prototype has been altered in redesigns throughout the project. The circuitry for the next prototype can be laid out more efficiently to improve space utilization and operation.

The suggested research studies start with a comparison of the Cutisfirm skin tension measurement device with a commercial skin tension device. The Cutisfirm device should be directly compared in its sensitivity, repeatability, and accuracy to that of the DermaLab (Cortex Technology, Denmark) The DermaLab suction cup consists of a short plastic probe and is affixed to the skin using double-sided sticky tape. Inside the probe, two beams of light travel across the probe center at different heights from the skin surface, which serve as elevation detectors. As vacuum is applied, the light beams are obstructed by the deforming skin and the pressure is noted at those points. (Grove, Damia et al. 2006) This device has been chosen over the Cutometer (Courage + Khazaka, Germany) or BTC-2000TM (Surgical Research Laboratory, Inc., Nashville, TN) since the DermaLab will be more of a direct competitor in terms of cost and functionality. The devices can be compared using artificial skin models and *in vivo*.

Other suggested research studies should be on the characterization of measurement errors which effect the skin tension measurement of the Cutisfirm device. For instance, the data should

be compared between handholding the probe or placing it in a brace. The effect of probe placement angle on the skin tension measurement (example seen in Figure 2.7, page 13) should also be explored.

And finally, future clinical tests will need to be done in a consistent temperature and humidity environment for the best probability of stable results. The human subjects should be in the testing room for at least fifteen minutes prior to testing, so that their skin is allowed to equate to the temperature and humidity. The testing should also be filmed or image with careful consideration of parallax viewing of the skin dome. The skin dome could be measured through image scaling and analysis, and then compared to the deformation measurements received from the instrument as a secondary validation of the device.

REFERENCES

- Arokoski, J. P., J. Surakka, T. Ojala, P. Kolari and J. S. Jurvelin (2005). "Feasibility of the use of a novel soft tissue stiffness meter." Physiological Measurement **26**(3): 215-28.
- ASAPS (2007). ASAPS Cosmetic Surgery National Data Bank Statistics, American Society for Aesthetic Plastic Surgery.
- ASAPS. (2008). "Tummy Tuck (Abdominoplasty)." Retrieved 8-2008, from http://www.surgery.org/public/procedures/tummy_tuck.
- ASMBS. (2007, 8/22/2007). "Bariatric Surgical Society Takes on New Name, New Mission and New Surgery: Metabolic Surgery Expected to Play Bigger Role in Treating Type 2 Diabetes." Retrieved 9/25/2008.
- Barbenel, J.C. (2006). Identification of Langer's Lines. Handbook of Non-Invasive Methods and the Skin. J. Serup. Boca Raton, CRC Press: 565 -569.
- Beaulax Co., Ltd. (2006). "Bio Skin." from <http://www.beulax.co.jp/BioSkinData.pdf>.
- Berndt, U. and P. Elsner (2002). Hardware and Measuring Principle: The Cutometer^(R) Bioengineering of the Skin: Skin Biomechanics. P. Elsner, E. Berardesca, K. Wilhelm and H. Maibach. Boca Raton, CRC Press: 91-97.
- Boyer, G., H. Zahouani, A. Le Bot and L. Laquieze (2007). "In vivo characterization of viscoelastic properties of human skin using dynamic micro-indentation." Conference Proceedings of IEEE Engineering in Medicine and Biology Society **1**: 4584-7.
- Daly, C. H. and G. F. Odland (1979). "Age-related changes in the mechanical properties of human skin." The Journal of Investigative Dermatology **73**(1): 84-7.
- Dawes-Higgs, E. K., M. V. Swain, R. J. Higgs, R. C. Appleyard and S. Kossard (2004). "Accuracy and reliability of a dynamic biomechanical skin measurement probe for the analysis of stiffness and viscoelasticity." Physiological Measurement **25**(1): 97-105.
- Diridollou, S., M. Berson, V. Vabre, D. Black, B. Karlsson, F. Auriol, J. M. Gregoire, C. Yvon, L. Vaillant, Y. Gall and F. Patat (1998). "An in vivo method for measuring the mechanical properties of the skin using ultrasound." Ultrasound in Medicine & Biology **24**(2): 215-24.
- Diridollou, S., J. de Rigal, B. Querleux, F. Leroy and V. Holloway Barbosa (2007). "Comparative study of the hydration of the stratum corneum between four ethnic groups: influence of age." International Journal of Dermatology **46 Suppl 1**: 11-4.

Diridollou, S., F. Patat, F. Gens, L. Vaillant, D. Black, J. M. Lagarde, Y. Gall and M. Berson (2000). "In vivo model of the mechanical properties of the human skin under suction." Skin Research & Technology **6**(4): 214-221.

Edwards, C. and R. Marks (1995). "Evaluation of biomechanical properties of human skin." Clinics in dermatology **13**(4): 375-80.

Elling, S. V. and F. C. Powell (1997). "Physiological changes in the skin during pregnancy." Clinics in dermatology **15**(1): 35-43.

Fox, SI (1999). Human Physiology. 6th ed. Boston, McGraw-Hill.

Graves, C.J. and C. Edwards (2002). Hardware and Measuring Principles: The Microindentometer. Bioengineering of the Skin: Skin Biomechanics. P. Elsner, E. Berardesca, K. Wilhelm and H. Maibach. Boca Raton, CRC Press: 161-178.

Grove, G.L., J. Damia, M.J. Grove and C. Zerwick (2006). Suction Chamber Method for Measurement of Skin Mechanics: The DermaLab. Handbook of Non-Invasive Methods and the Skin, Second Edition. J. G. Serup J, Grove GL. Boca Raton, FL, CRC Press: 593 - 599.

Harrison, S. M., M. B. Bush and P. E. Petros (2007). "A pinch elastometer for soft tissue." Medical Engineering & Physics **29**(3): 307-15.

Hendriks, F. M., D. Brokken, C. W. Oomens and F. P. Baaijens (2004). "Influence of hydration and experimental length scale on the mechanical response of human skin in vivo, using optical coherence tomography." Skin Research & Technology **10**(4): 231-41.

Hendriks, F. M., D. Brokken, J. T. van Eemeren, C. W. Oomens, F. P. Baaijens and J. B. Horsten (2003). "A numerical-experimental method to characterize the non-linear mechanical behaviour of human skin." Skin Research & Technology **9**(3): 274-83.

Hendriks, FM (2001). Mechanical Behavior of Human Skin in Vivo. National Lab Unclassified Report 2001/820, Koninklijke Phillips Electronics N. V.: 1-46.

Henry, F., R. VanLook, V. Goffin, J. Fissette and G. E. Pierard (1996). "Mechanical properties of skin and liposuction." Dermatologic Surgery **22**(6): 566-568.

Hull, M. T. and K. A. Warfel (1983). "Age-related changes in the cutaneous basal lamina: scanning electron microscopic study." The Journal of Investigative Dermatology **81**(4): 378-80.

Jachowicz, J., R. McMullen and D. Prettypaul (2007). "Indentometric analysis of in vivo skin and comparison with artificial skin models." Skin Research & Technology **13**(3): 299-309.

Jemec, G. B., E. Selvaag, M. Agren and H. C. Wulf (2001). "Measurement of the mechanical properties of skin with ballistometer and suction cup." Skin Research & Technology **7**(2): 122-6.

Khatyr, F., C. Imberdis, D. Varchon, J. M. Lagarde and G. Josse (2006). "Measurement of the mechanical properties of the skin using the suction test." *Skin Research & Technology* **12**(1): 24-31.

Kissin, E. Y., A. M. Schiller, R. B. Gelbard, J. J. Anderson, V. Falanga, R. W. Simms, J. H. Korn and P. A. Merkel (2006). "Durometry for the assessment of skin disease in systemic sclerosis." *Arthritis & Rheumatism* **55**(4): 603-9.

Kollias, N. (1995). "The physical basis of skin color and its evaluation." *Clinics in dermatology* **13**(4): 361-7.

Korhonen, R. K., S. Saarakkala, J. Toyras, M. S. Laasanen, I. Kiviranta and J. S. Jurvelin (2003). "Experimental and numerical validation for the novel configuration of an arthroscopic indentation instrument." *Physics in Medicine and Biology* **48**(11): 1565-76.

Larrabee, W. F., Jr. (1986). "A finite element model of skin deformation. I. Biomechanics of skin and soft tissue: a review." *Laryngoscope* **96**(4): 399-405.

Larrabee, W. F., Jr. and J. A. Galt (1986). "A finite element model of skin deformation. III. The finite element model." *Laryngoscope* **96**(4): 413-9.

Larrabee, W. F., Jr. and D. Sutton (1986). "A finite element model of skin deformation. II. An experimental model of skin deformation." *Laryngoscope* **96**(4): 406-12.

Leveque, J. L., J. de Rigal, P. G. Agache and C. Monneur (1980). "Influence of ageing on the in vivo extensibility of human skin at a low stress." *Archives of Dermatological Research* **269**(2): 127-35.

Mann, M. W., M. D. Palm and R. D. Sengelmann (2008). "New advances in liposuction technology." *Seminars in Cutaneous Medicine and Surgery* **27**(1): 72-82.

Niemz, M.H. (2007). *Laser-Tissue Interactions: Fundamentals and Applications*. Berlin, Springer.

Oikarinen, A. and A. Knuutinen (2002). Mechanical Properties of Human Skin: Biochemical Aspects. *Bioengineering of the Skin: Skin Biomechanics*. P. Elsner, E. Berardesca, K. Wilhelm and H. Maibach. Boca Raton, CRC Press: 3-16.

Pedersen, L., B. Hansen and G. B. Jemec (2003). "Mechanical properties of the skin: a comparison between two suction cup methods." *Skin Research & Technology* **9**(2): 111-5.

Pierard, G. E. (1999). "EEMCO guidance to the in vivo assessment of tensile functional properties of the skin. Part 1: relevance to the structures and ageing of the skin and subcutaneous tissues." *Skin Pharmacol Appl Skin Physiol* **12**(6): 352-62.

Pugliese, P.T. and J.R. Potts (2002). Hardware and Measuring Principles: The Ballistometer. Bioengineering of the Skin: Skin Biomechanics. P. Elsner, E. Berardesca, K. Wilhelm and H. Maibach. Boca Raton, CRC Press: 147 - 160.

Rigal, J. (2002). Hardware and Basic Principles of the Dermal Torque Meter. Bioengineering of the Skin: Skin Biomechanics. P. Elsner, E. Berardesca, K. Wilhelm and H. Maibach. Boca Raton, CRC Press: 63-76.

Romanelli, M. and V. Falanga (2002). Hardware and Measuring Principles: The Durometer. Bioengineering of the Skin: Skin Biomechanics. P. Elsner, E. Berardesca, K. Wilhelm and H. Maibach. Boca Raton, CRC Press: 139-145.

Schmidt, F.E.W. (1999). Development of a Time-Resolved Optical Tomography System for Neonatal Brain Imaging. Dept. of Medical Physics and Bioengineering. London, University College London. **Ph.D.:** 207.

Serup, J. (2002). Hardware and Measuring Principles: The DermaLab. Bioengineering of the Skin: Skin Biomechanics. P. Elsner, E. Berardesca, K. Wilhelm and H. Maibach. Boca Raton, CRC Press: 117-122.

Serup, J. (2002). Mechanical Properties of Human Skin: Elasticity Parameters and Their Relevance. Bioengineering of the Skin: Skin Biomechanics. P. Elsner, E. Berardesca, K. Wilhelm and H. Maibach. Boca Raton, CRC Press: 41-47.

Smalls, L. K., R. Randall Wickett and M. O. Visscher (2006). "Effect of dermal thickness, tissue composition, and body site on skin biomechanical properties." Skin Research & Technology **12**(1): 43-9.

Sorbothane, Inc. (2009). "About Sorbothane Materials Properties." Retrieved July 7, 2009, from <http://www.sorbothane.com/material-properties.php>.

Sumino, H., S. Ichikawa, M. Abe, Y. Endo, O. Ishikawa and M. Kurabayashi (2004). "Effects of aging, menopause, and hormone replacement therapy on forearm skin elasticity in women." Journal of the American Geriatrics Society **52**(6): 945-9.

Surgical Research Laboratory, Inc. (2007). "SRLI Technologies BTC-2000™." Retrieved July, 2009, from <http://www.srli.com/technologies/BTC2000.html>.

Tur, E. (1997). "Physiology of the skin--differences between women and men." Clinics in dermatology **15**(1): 5-16.

Vangemert, M. J. C., S. L. Jacques, H. J. C. M. Sterenborg and W. M. Star (1989). "Skin Optics." Ieee Transactions on Biomedical Engineering **36**(12): 1146-1154.

Vescovo, P., D. Varchon and P. Humbert (2002). *In Vivo* Tensile Tests on Human Skin: The Extensometers. Bioengineering of the Skin: Skin Biomechanics. P. Elsner, E. Berardesca, K. Wilhelm and H. Maibach. Boca Raton, CRC Press: 77-90.

Vexler, A., I. Polyansky and R. Gorodetsky (1999). "Evaluation of skin viscoelasticity and anisotropy by measurement of speed of shear wave propagation with viscoelasticity skin analyzer." Journal of Investigative Dermatology **113**(5): 732-9.

Viac, J., D. Schmitt and A. Claudy (1994). "[Adhesion molecules and inflammatory dermatoses]." Allergie et immunologie **26**(8): 274-7.


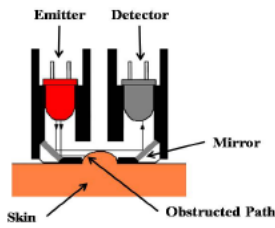
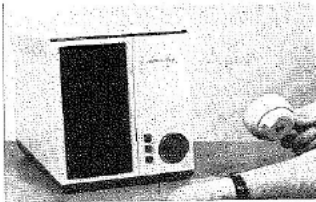

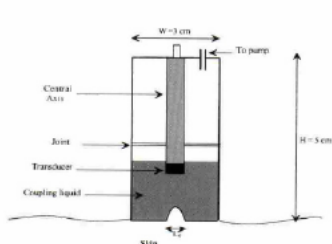

Waller, J. M. and H. I. Maibach (2005). "Age and skin structure and function, a quantitative approach (I): blood flow, pH, thickness, and ultrasound echogenicity." Skin Research & Technology **11**(4): 221-35.

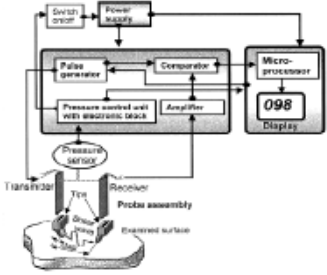
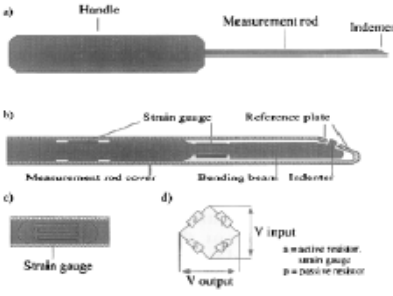

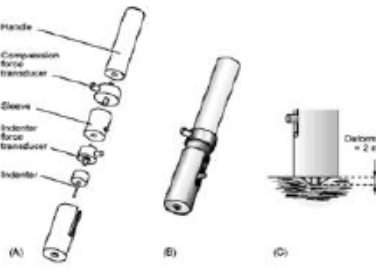
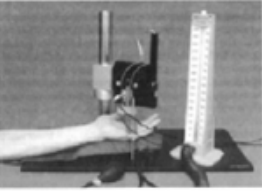
Waller, J. M. and H. I. Maibach (2006). "Age and skin structure and function, a quantitative approach (II): protein, glycosaminoglycan, water, and lipid content and structure." Skin Research & Technology **12**(3): 145-54.

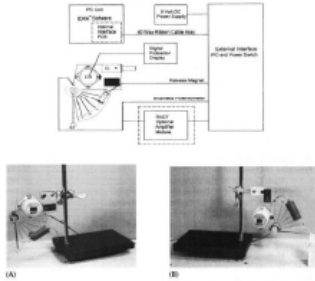
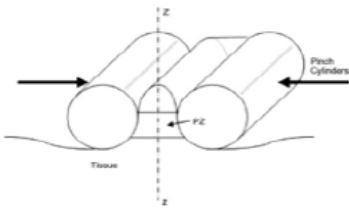
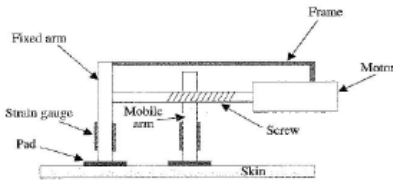
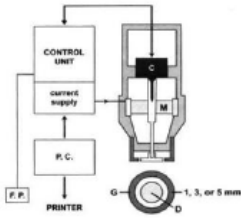
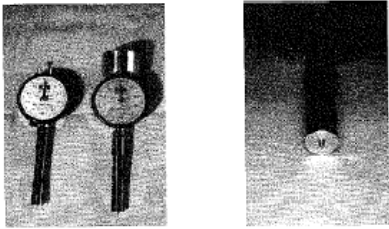
Wilson, B. C. and S. L. Jacques (1990). "Optical Reflectance and Transmittance of Tissues - Principles and Applications." Ieee Journal of Quantum Electronics **26**(12): 2186-2199.

Wu, J. Z., R. G. Cutlip, D. Welcome and R. G. Dong (2006). "Estimation of the viscous properties of skin and subcutaneous tissue in uniaxial stress relaxation tests." Bio-medical Materials and Engineering **16**(1): 53-66.

APPENDIX A: COMMERCIAL DEVICES FOR SKIN TENSION MEASUREMENT

Style of Device	Device Name	Description	Papers
Suction	Cutometer MPA 580 or SEM 474, 575	 <p style="font-size: small;">Fig. 2. SEM 474 cutometer system consists of measurement unit containing a vacuum pump, a measurement probe with a fixed opening (2 to 10 mm), and a personal computer.</p> 	<p>Henry et al 1996 Amer Soc Derma Surg 22: 566-568 - monitoring liposuction results</p> <p>Enomoto et al 1996 J Amer Acad Derma 35: 381-387 - 2 and 8mm probe, scleroderma</p> <p>Dobrev et al 1999 J Amer Acad Derma 40: 436-442 - 2 and 8mm probe, scleroderma</p> <p>Pierard et al 1999 J Med Eng Tech 23: 69-72 - 2 and 4mm probe, excised breast tissue</p> <p>Koch et al 1999 Arch Facial Plast Surg 1: 272-275 - 2mm probe, facial tissue</p> <p>Tsukahara et al 2001 Brit J Derma 145(4): 590-596 - face, upper arm and forearm</p> <p>Bioengineering of the Skin: Skin Biomechanics 2002 - Chap 7</p> <p>Sclangen et al 2003 Skin Res Tech 9: 122-130 - 2mm probe, facial tissue</p> <p>Draaijers et al 2004 Burns 30: 109-114 - 6mm probe, on scars</p> <p>Dobrev et al 2005 Skin Res Tech 11: 120-122 - 2mm probe, temples and forearms</p> <p>Khatyr et al 2006 Skin Res Tech - modelling example</p> <p>Smalls et al 2006 Skin Res Tech - 6mm probe, manual ultrasound for thickness</p> <p>Handbook of Non-invasive Methods and the Skin, 2nd ed. 2006 - Chap. 66,67</p> <p>Ryu et al 2008 Skin Res Tech 14: 354-358</p>
	Dermaflex		<p>Bioengineering of the Skin: Skin Biomechanics 2002 - Chap 9</p> <p>Pederson et al 2003 Skin Res Tech 9: 111-115 - compared against Dermaflex and slightly more</p> <p>Handbook of Non-invasive Methods and the Skin, 2nd ed. 2006 - Chap. 65</p> <p>Khatyr et al 2006 Skin Res Tech 12: 24-31 - modelling example</p> <p>10sqmm aperture</p>
	Dermalab		<p>Bioengineering of the Skin: Skin Biomechanics 2002- Chap 10</p> <p>Pederson et al 2003 Skin Res Tech 9: 111-115 - compared against Dermaflex - fixed distention</p> <p>Handbook of Non-invasive Methods and the Skin, 2nd ed. 2006- Chap. 68</p>
	Echorheometer	 <p style="font-size: x-small;">Fig. 1. View of the cylinder (Echorheometer).</p>	<p>Diridollou et al 1998 Ultrasound in Med. & Bio. 24(2): 215-224</p> <p>Diridollou et al 2000 Skin Res Tech 6: 214-221 - skin displacement measured by ultrasound transducer</p> <p>Tsukahara et al 2001 Brit J Derma 145(4): 590-596</p> <p>Dahan et al 2004 Amer Soc Derma Surg 30: 872-880</p> <p>Waller et al 2005 SRT</p>
	BTC-2000		<p>http://www.srli.com/technologies/BTC2000.html</p> <p>Babir-Gurman et al 2002 Ann Rheum Dis 61: 237-241 - systemic sclerosis</p> <p>Smalls et al 2006 Skin Res & Tech 12:43-49</p>

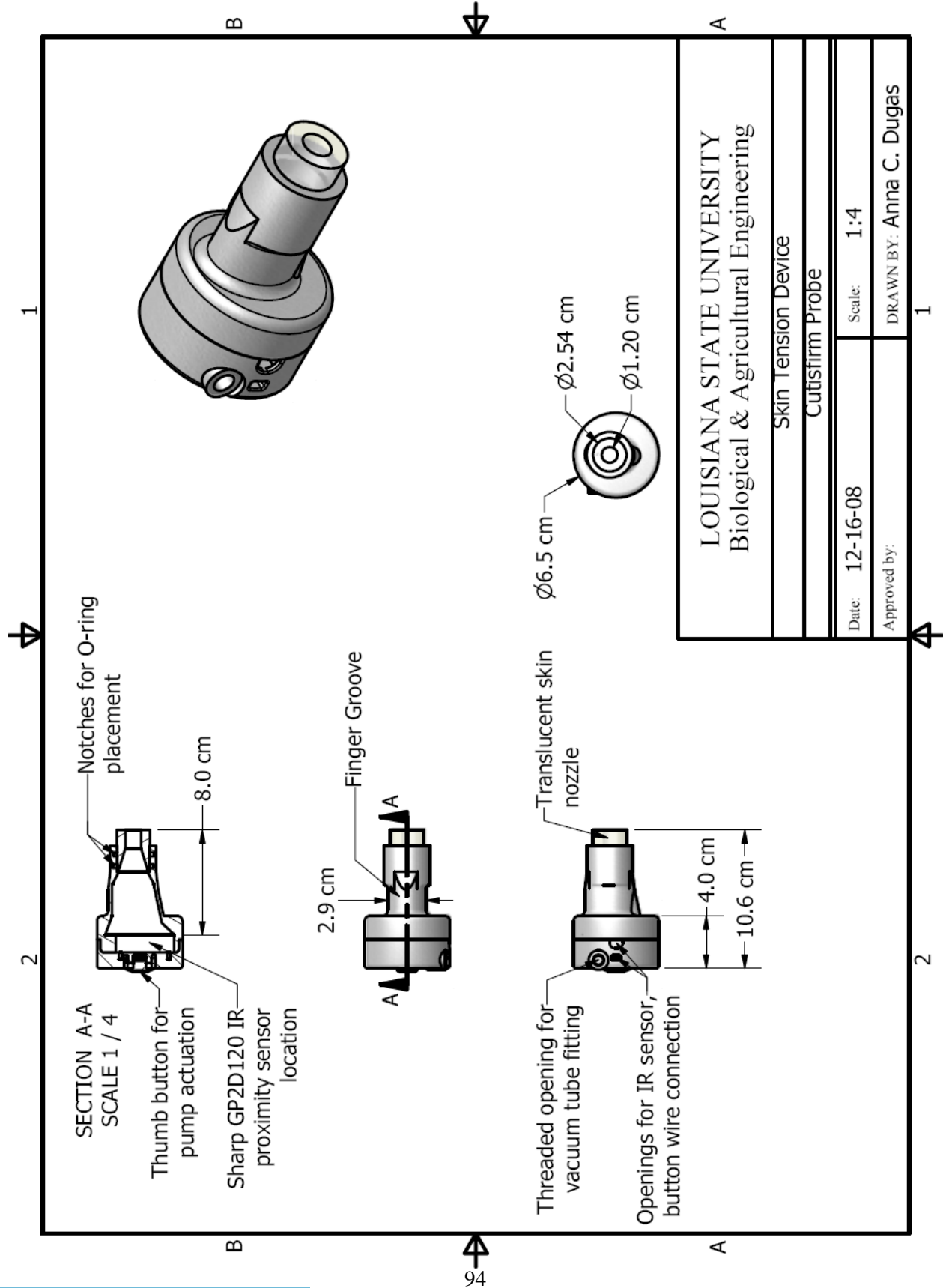
<p>Elastic Shear Propagation uses pulsed waves of pressure to measure firmness - difficult to characterize</p>	<p>VESA</p> 	<p>Vexler et al 1999 J Invest Derma 113(5): 732-739 - measures anisotropy as well, forearm</p>
	<p>Artscan 200</p> 	<p>http://www.kshproductor.fi/artscan/pages/as/arts1000.htm Lyyra et al 1995 Med Eng Phys 17(5): 395-399 - device designed Korhonen et al 2003 Phys Med Biol 48(11): 1565-1576 - actually measures cartilage</p>
<p>Indentation</p>	<p>DBSM</p>  <p>Figure 1. The dynamic biomechanical skin measurement probe.</p>	<p>Dawes-Higgs et al 2004 Physiol Meas 25(1): 97-105 - oscillating beam held perpendicular to skin in a cantilever configuration with strain gauges attached to fixed end</p>
	<p>STSM</p> 	<p>Arokoski et al 2005 Physiol Meas 26(3): 215-228 - soft tissue stiffness meter, forearm, principle based off of cartilage testers</p>
	<p>Micro-indentometer</p> 	<p>Bioengineering of the Skin: Skin Biomechanics 2002 - Chap 14</p>

<p>Indentation cont...</p>	<p>Ballistometer</p> 	<p>Bioengineering of the Skin: Skin Biomechanics 2002 - Chap 13</p>
<p>Pinching devices</p>	<p>Pinch Elastomer</p> 	<p>Harrison et al 2007 Med Eng Phys 29(3): 307-315 - for vaginal tissue pinches the tissue with cylinders</p>
<p>Pulling devices used for more superficial skin measurements than what we want.</p>	<p>Extensometer</p> 	<p>Bioengineering of the Skin: Skin Biomechanics 2002 - Chap 6</p>
<p>Torsionmeter used for more superficial skin measurements than what we want.</p>	<p>Twistometer Dermal Torque Meter</p> 	<p>Leveque et al 1980 Arch Dermatol Res 269, 127-135 Bioengineering of the Skin: Skin Biomechanics 2002 - Chap 5</p>
<p>Durometers used for more superficial skin measurements than what we want.</p>	<p>Durometer</p> 	<p>Seyger et al 1997 J Amer Acad of Dermatology 37(5): Pt.1 793-796 Bioengineering of the Skin: Skin Biomechanics 2002 - Chap 12 Kissin et al 2006 Arth & Rheum 55(4): 603-609 monitoring systemic sclerosis</p>

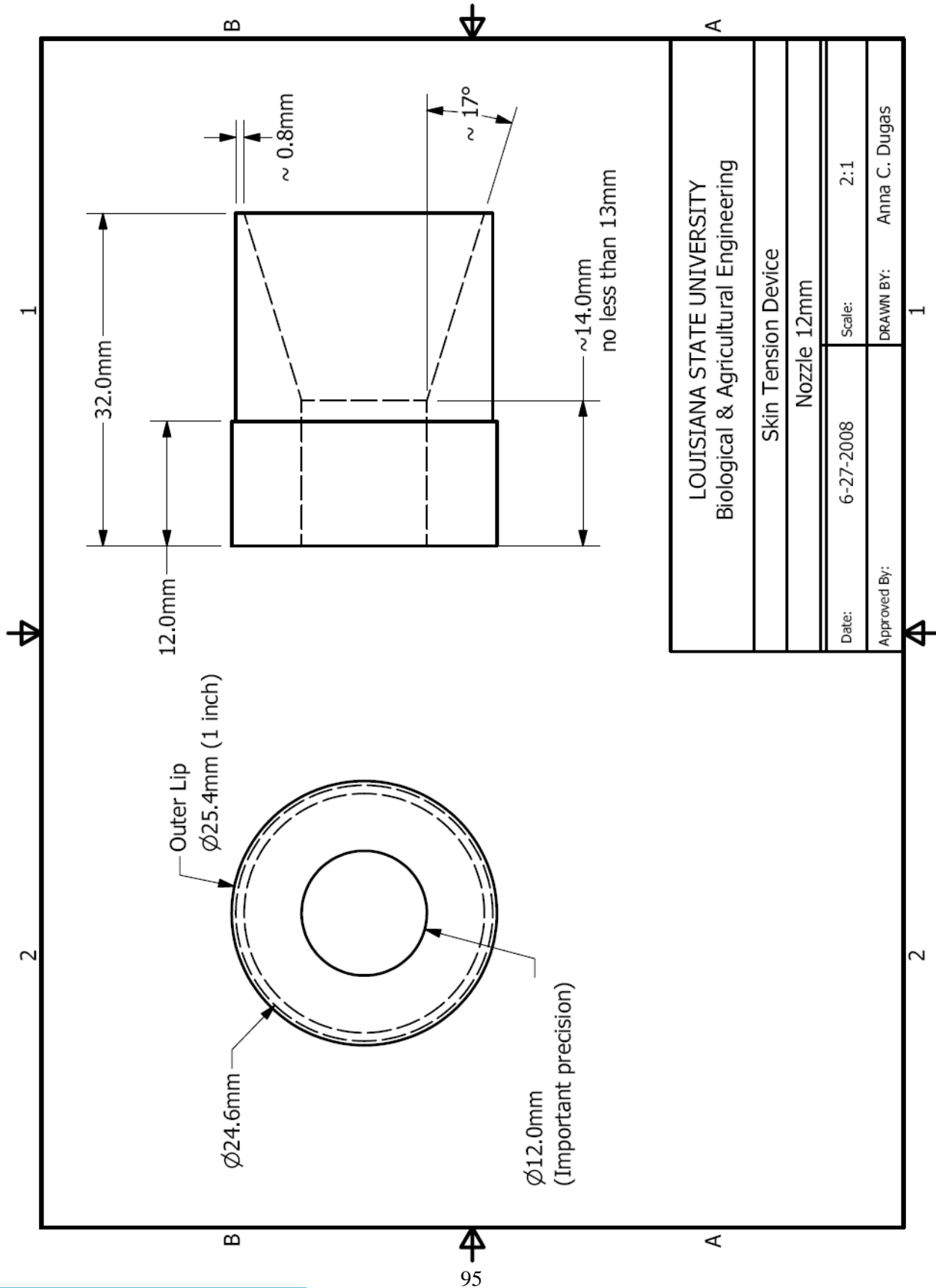
A compilation of the skin tension measurement devices reported in recent literature. The different devices can be categorized by their function as the following: suction, shear propagation, indentation, torsion, and durometry. Images are taken from papers and book chapters mentioned in right column.

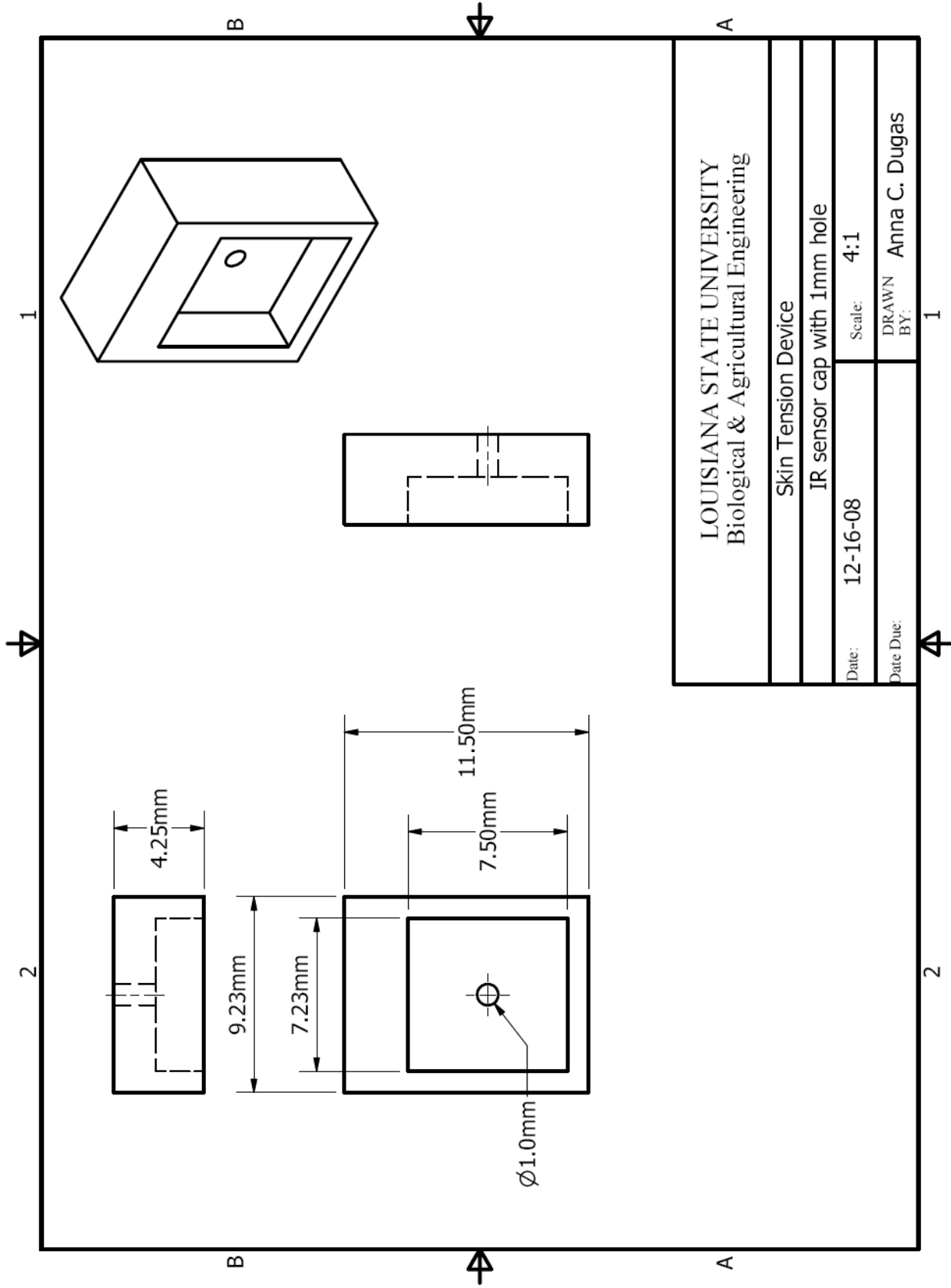
APPENDIX B: DRAWINGS OF THE CUTISFIRM DEVICE

		PAGE
<u>Drawing 1:</u>	Skin Tension Device: Cutisfirm Probe	94
<u>Drawing 2:</u>	Skin Tension Device: Nozzle 12mm	95
<u>Drawing 3:</u>	Skin Tension Device: IR Sensor Cap with 1mm Hole	96



LOUISIANA STATE UNIVERSITY Biological & Agricultural Engineering	
Skin Tension Device	
Cutisfirm Probe	
Date: 12-16-08	Scale: 1:4
Approved by: Anna C. Dugas	

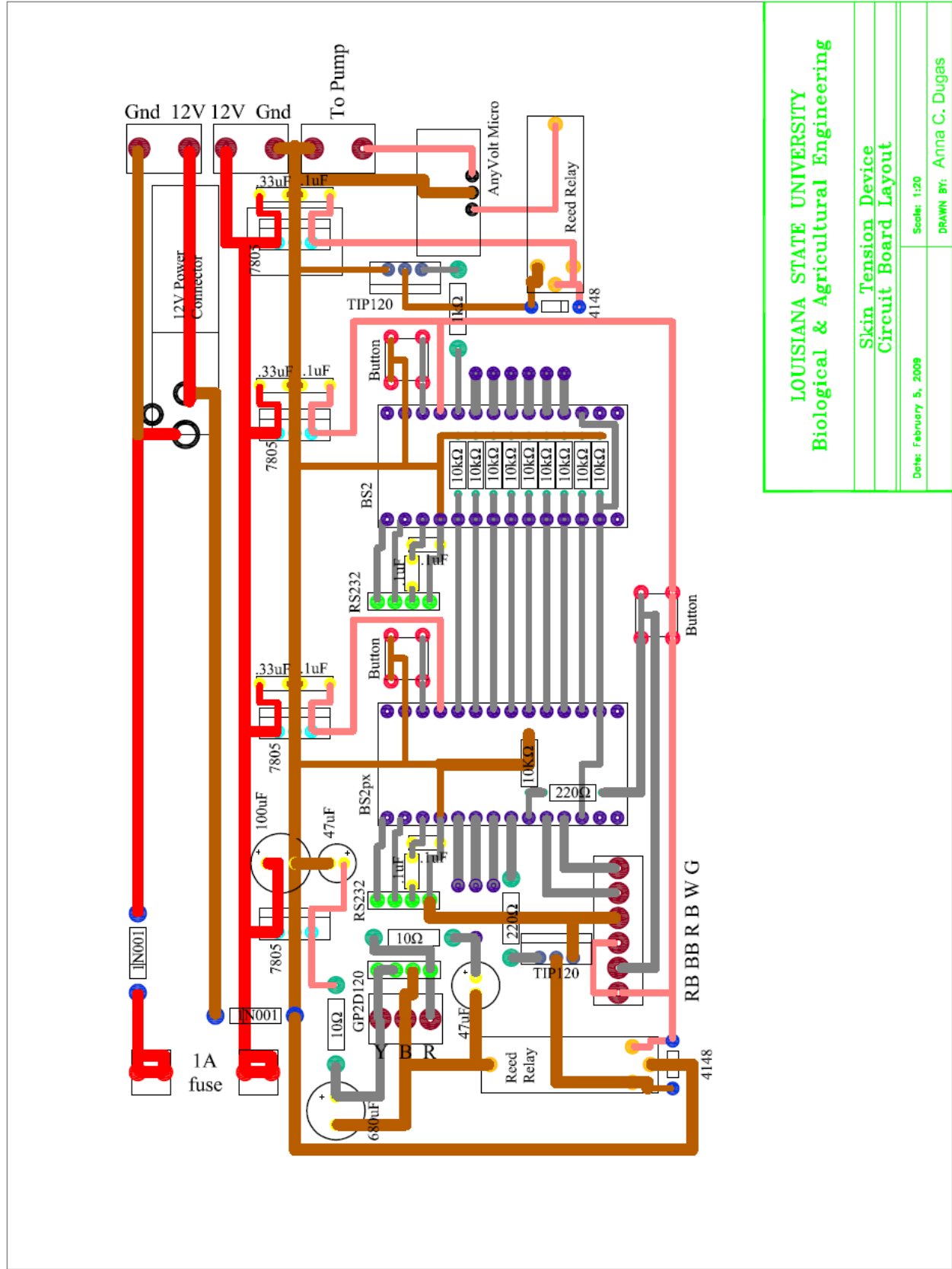




LOUISIANA STATE UNIVERSITY Biological & Agricultural Engineering	
Skin Tension Device	
IR sensor cap with 1mm hole	
Date: 12-16-08	Scale: 4:1
Date Due:	DRAWN BY: Anna C. Dugas

APPENDIX C: WIRING DIAGRAMS AND PART INFORMATION

		PAGE
<u>Layout 1:</u>	Cutisfirm Circuit Diagram of Prototype 1	98
<u>Layout 2:</u>	Circuit Board Layout	99
<u>Table 1:</u>	Electronic Parts List Including Recommended Changes	100
<u>Part 1:</u>	Sharp GP2D120 Optoelectronic Device	101
<u>Part 2:</u>	Hargraves C103E-12 BTC Diaphragm Pump	104
<u>Part 3:</u>	Clippard EVO-3-6-H Three-way Solenoid Valve	105
<u>Part 4:</u>	The V-800 Miniature Precision Vacuum Regulator	106
<u>Part 5:</u>	The BASIC Stamp BS2px and BS2 Microcontrollers	108
<u>Part 6:</u>	The uM-FPU V3.1 Floating Point Co-processor	109
<u>Part 7:</u>	MPXV6115VC6U Integrated Pressure Sensor	111
<u>Part 8:</u>	uDRIVE-uSD-G1 Embedded DOS micro-Drive	113



LOUISIANA STATE UNIVERSITY
 Biological & Agricultural Engineering

Skin Tension Device
 Circuit Board Layout

Date: February 5, 2009 Scale: 1:20
 DRAWN BY: Anna C. Dugas

Electronic Parts List Including Recommended Changes

Part Description	Quantity	Model Number	Company Purchased From	Units/Price	Price (tax excluded)	Use in Design	Recommended changes
Sharp GP2D120 IR Proximity Sensor	1	425-1162-ND	Digi-Key Corporation	\$12.18 / each	\$12.18	Scan height measurement	Newer model Sharp GP2D120X00F, same features
BTC Diaphragm Pump, Brush Motor	1	C103E-12	Hargaves Technology Corporation	\$85.00 / each	\$85.00	Synthesizes vacuum in probe	Include 5 micron filter to pump intake for dust
3-way Normally Closed Solenoid Valve	1	EVO-3-6-H	Clippard Instrument Laboratory	\$23.20 / each	\$23.20	Releases vacuum in probe	Use EVO-3-12-H, the 12V version which can use the same isolated power supply as the pump
Miniature Precision Vacuum Regulator	1	V-800-30-W/K	Automation Engineering, Baton Rouge	\$41.00 / each	\$41.00	To control vacuum pressure	Supply a extra pressure readout gauge to verify vacuum setting of the regulator
BASIC Stamp BS2px Module	1	BS2PX24	Parallax, Inc	\$79.00 / each	\$79.00	Microcontroller computer to operate system	
BASIC Stamp BS2 Module	1	BS2-IC	Parallax, Inc	\$49.00 / each	\$49.00	Microcontroller to operate pump and valve timing	
32-bit Floating Point Coprocessor V3.1	1	604-00050	Parallax, Inc	\$19.00 / each	\$19.00	Analog-to-Digital convertor, math processing chip	
Freescal Semiconductor Integrated Silicon Pressure Sensor	1	MPXV6115VC6L-ND	Digi-Key Corporation	\$9.29 / each	\$9.29	Measure vacuum pressure at probe during testing	Consider signal conditioning using RC low-pass filter circuit. (See Freescale Application Note: AN1646)
4D Systems Embedded DOS micro-Drive	1	DEV-08567	Sparkfun Electronics	\$34.95 / each	\$34.95	Writes data to micro-SD card	
3.8" Amulet OnBoard™ Module	1	681-1003-ND	Digi-Key Corporation	\$239.00 / each	\$239.00	LCD touchscreen for user-friendly device operation	The 3.8" screen could be mounted directly onto the electronics box
AnyVolt Micro Universal DC-DC Converter and Voltage Stabilizer	1	52011	All-Battery.com	\$21.99 / each	\$21.99	Increases 5V to 6V for valve	If 12V Clippard solenoid valve is used, this item could be removed from design
5VDC/1A SPDT Micro Relay	1	275-240	RadioShack Corporation	\$4.69 / each	\$4.69	Relay switch to assist in control of the pump turn on	Replace with SPST solid state relay, suggested Catalog #: CC1060-ND from Digikey, Corp., \$10.78
Compact 5VDC/1A SPST Reed Relay	2	275-232	RadioShack Corporation	\$2.99 / each	\$5.98	Relay switches to assist in control of IR sensor and valve	Replace with SPST solid state relay, suggested Catalog #: CC1060-ND from Digikey, Corp., \$10.78
Clare CPCI218Y 4-Pin SIP OptoMOS Relay	1	CLA274-ND	Digi-Key Corporation	\$2.15 / each	\$2.15	Relay switch used in BS2 reset circuit	
Silicon Switching Diodes (1N914/1N414)	4	276-1620	RadioShack Corporation	\$2.59 / 50 pack	\$0.21	Controls current directional flow for relay coils	If using the solid state relays recommended, not necessary to include
1N4001 Micro 1A Diodes	2	276-1101	RadioShack Corporation	\$0.99 / each	\$1.98	Controls current directional flow for power supply and fuse	
+5V Fixed-Voltage Regulator 7805 1A	4	497-1441-5-ND	Digi-Key Corporation	\$0.72 / each	\$2.88	Voltage regulator to convert 12V battery input into 5VDC	Use 2A, 5V voltage regulator (Digi-Key 497-1468-5-ND) to consolidate power supply with enough current
+12V Fixed-Voltage Regulator 7812 1A	1	276-1771	RadioShack Corporation	\$1.59 / each	\$1.59	Voltage regulator to confirm 12V battery input for 12VDC	
Heat Sink	5	HS115-ND	Digi-Key Corporation	\$0.28 / each	\$0.28	For temperature regulation of voltage regulators	
12V 7.2AH Sealed Lead Acid Battery	2	23-275	RadioShack Corporation	\$34.99 / each	\$69.98	Battery supply	Separate batteries are used to isolate the pump circuit from the IR sensor circuit
TIP120 NPN-D Transistor	4	276-2068	RadioShack Corporation	\$1.59 / each	\$1.59	Power switching for various circuits	
Capacitor 680uF 10V Electrolytic	1	P10222-ND	Digi-Key Corporation	\$0.48 / each	\$0.48	in signal conditioning for IR proximity sensor	
Capacitor 100uF 10V Electrolytic	1	P10294-ND	Digi-Key Corporation	\$0.38 / each	\$0.38	in signal conditioning for IR proximity sensor	
Capacitor 47uF 10V Electrolytic	2	P907-ND	Digi-Key Corporation	\$0.21 / each	\$0.21	in signal conditioning for IR proximity sensor	
Capacitor 0.33uF Tantulum	3	399-3538-ND	Digi-Key Corporation	\$0.54 / each	\$0.54	Capacitor	
Capacitor 0.1uF Tantulum	7	399-3527-ND	Digi-Key Corporation	\$0.59 / each	\$0.59	Capacitor	
Resistor 10K ohm	9	271-1335	RadioShack Corporation	\$0.99 / 5pk	\$1.98	Resistor	
Resistor 1Kohm	5	271-1321	RadioShack Corporation	\$0.99 / 5pk	\$0.99	Resistor	
Resistor 220ohm	2	271-1313	RadioShack Corporation	\$0.99 / 5pk	\$0.99	Resistor	
Resistor 10ohm	2	271-1301	RadioShack Corporation	\$0.99 / 5pk	\$0.99	Resistor	
Push Button	3	B0050	Basie Micro, Inc.	\$0.40 / each	\$1.20	Reset buttons	Move them to be more accessible during diagnostic operation

FEATURES

- Analog output
- Effective range: 4 to 30 cm
- Typical response time: 39 ms
- Typical start up delay: 44 ms
- Average Current Consumption: 33 mA

DESCRIPTION

The GP2D120 is a distance measuring sensor with integrated signal processing and analog voltage output.

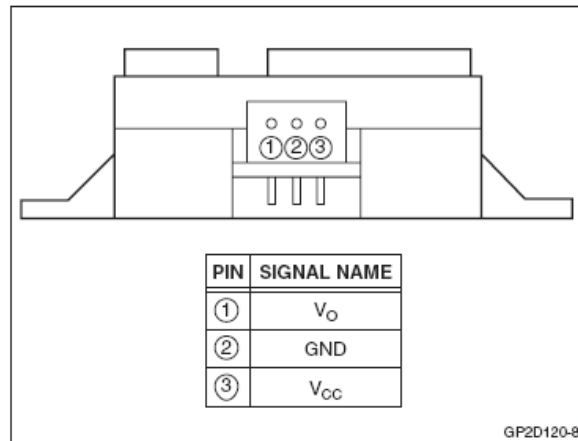


Figure 1. Pinout

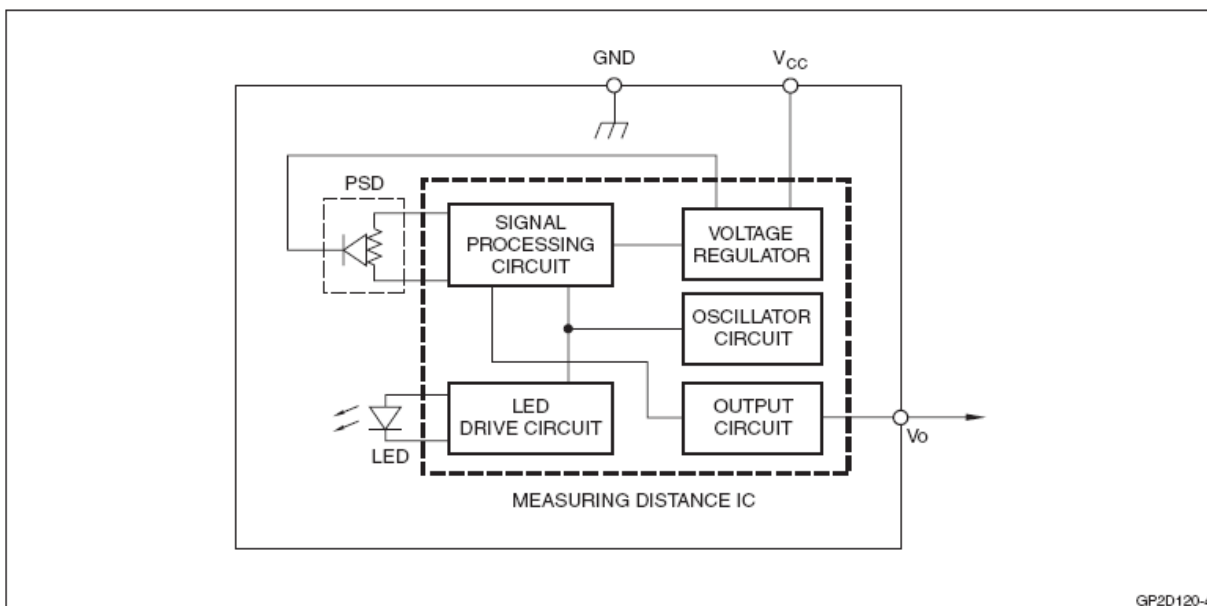


Figure 2. Block Diagram

ELECTRICAL SPECIFICATIONS

Absolute Maximum Ratings

Ta = 25°C, V_{CC} = 5 VDC

PARAMETER	SYMBOL	RATING	UNIT
Supply Voltage	V _{CC}	-0.3 to +7	V
Output Terminal Voltage	V _O	-0.3 to (V _{CC} +0.3)	V
Operating Temperature	T _{opr}	-10 to +60	°C
Storage Temperature	T _{stg}	-40 to +70	°C

Operating Supply Voltage

PARAMETER	SYMBOL	RATING	UNIT
Operating Supply Voltage	V _{CC}	4.5 to 5.5	V

Electro-optical Characteristics

Ta = 25°C, V_{CC} = 5 VDC

PARAMETER	SYMBOL	CONDITIONS	MIN.	TYP.	MAX.	UNIT	NOTES
Measuring Distance Range	ΔL		4	—	30	cm	1, 2
Output Terminal Voltage	V _O	L = 30 cm	0.25	0.4	0.55	V	1, 2
Output Voltage Difference	ΔV _O	Output change at ΔL (30 cm – 4 cm)	1.95	2.25	2.55	V	1, 2
Average Supply Current	I _{CC}	L = 30 cm	—	33	50	mA	1, 2

NOTES:

1. Measurements made with Kodak R-27 Gray Card, using the white side, (90% reflectivity).
2. L = Distance to reflective object.

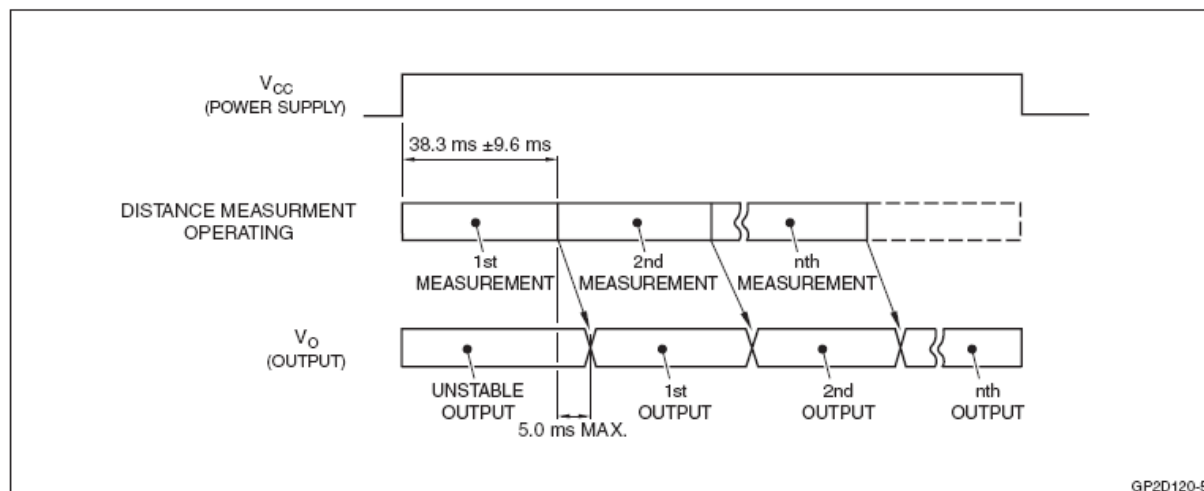


Figure 3. Timing Diagram

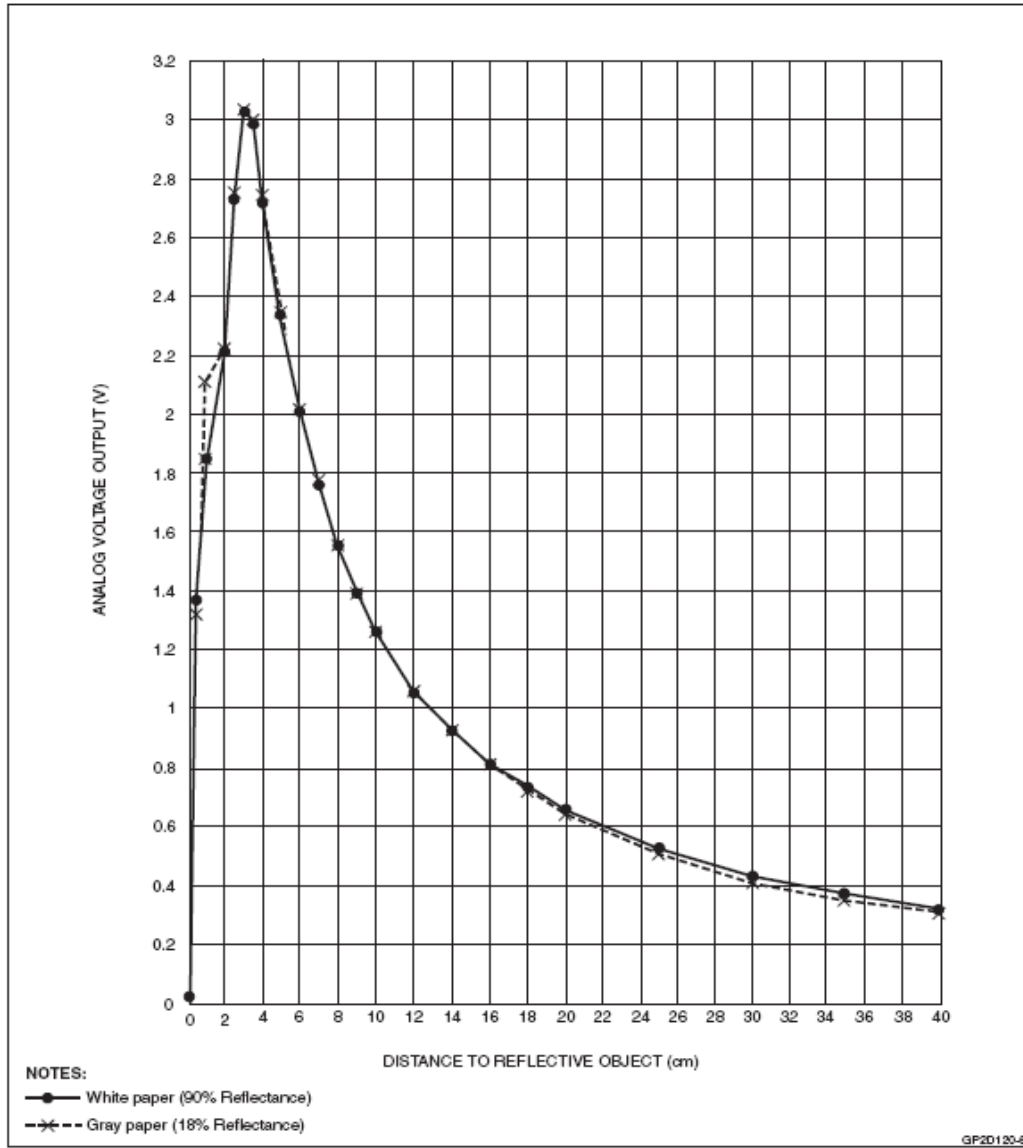


Figure 4. GP2D120 Example of Output Distance Characteristics

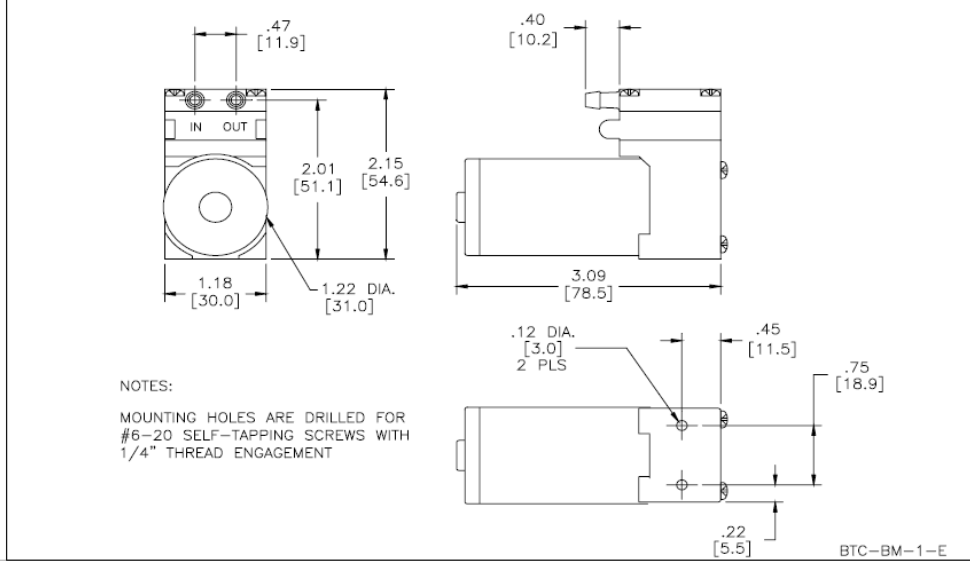


HARGRAVES

Moorestville, North Carolina 28117
 T: 704-662-3500 F: 704-662-8744
 www.hargravesfluidics.com

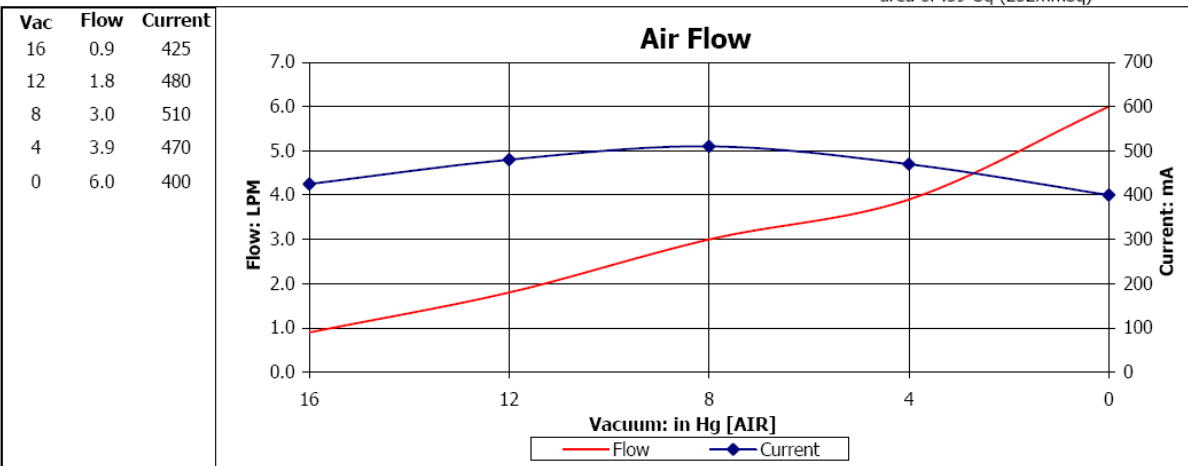
Part No.: **C103E-12**
 Model No.: **B.1C60E1.B12VDC**
 Description: **BTC Diaphragm Pump, Brush Motor**

Dimensional Layout:



Specifications:

- | | | | | | |
|-----------------------------|-----------------------|-----------------|-----------------------------------|---|---------------------------------------|
| 1. Wetted Materials: | Pump Head: | Vectra [LCP] | 3. Electrical: | Motor: | Brush Dual Bearing |
| | Retainer Washer: | 2024 Alum [700] | | Operating Voltage: | 12.0 VDC |
| | Retainer Screw: | 316 Stainless | | In-rush Current: | 5 x Operating Current for up to 50 ms |
| | Valves: | AEPDM [80] | | Recommended Fusing: | Slow Blow @ 2 x Operating Current |
| | Diaphragm: | AEPDM [T80] | | Temperature Range: | 5 - 50° C |
| | Gasket: | EPDM [65] | | Free Flow RPM: | 4400 |
| | | | | Eccentric: | C900 |
| 2. Performance: | <u>Continuous</u> | <u>Maximum</u> | 4. Other: | | |
| | - Vacuum: in Hg [AIR] | 20.0 | | 20.0 | 5. Operating Limitations: |
| | | | 6. Recommended Filtration: | 40 Micron media w/ a minimum surface area of .39"sq (252mmSq) | |



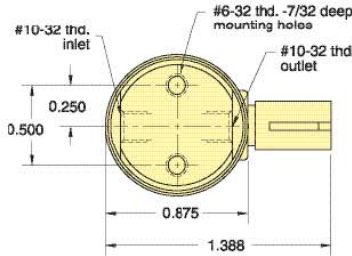
The above graph denotes nominal performance at 800' above sea level, 24°C, and at the specified voltage.

ST

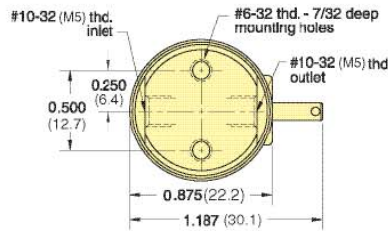


EV, ET, EC SERIES 3-WAY NORMALLY CLOSED VALVES IN-LINE MOUNT

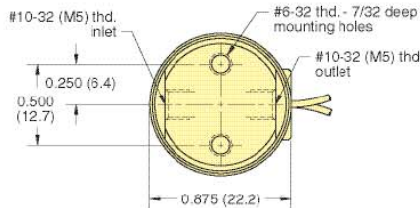
EC - 3 - □ - □



ET - 3 - □ - □



EV - 3 - □ - □



Type: Normally Closed 3-Way

Medium: Air (40 micron filtration)

Temperature Range: 30° to 180°

Power Consumption: 0.67 watt

Response: 5 - 10 milliseconds

Mounting: In-line

Ports: #10-32 (M5)

Operating Range: 90% to 150% of rated voltage

Air Flow: 0.6 scfm @ 100 psig
15 l/min @ 7 bar

“L” option - 0.5 scfm @ 50 psig;
15 l/min @ 3.5 bar

“H” option - 0.45 scfm @ 25 psig;
14 l/min @ 1.8 bar

Pressure Range:

28" Hg Vac. to 105 psig;
0-7 bar max

“L” option:

28" Hg Vac. to 50 psig;
0-3.5 bar max

“H” option:

28" Hg Vac. to 25 psig;
0-1.8 bar max



For Cable and Connectors,
see Page 184.



NUMBERING SYSTEM

E □ - 3 - □ - □ - □

C - Connector
T - Terminal Spades
V - Wire Leads

Voltages: *
6 - 6 Volts
12 - 12 Volts
24 - 24 Volts

Standard Options:
Blank - Standard orifice 0.025
L - 0.040 orifice
H - 0.060 orifice
V - Viton® seals
Non-Standard Options:
E - EPR seals
S - Silicon seals
D - Diode

M5 - Metric

* Consult factory for availability of non-standard voltages and other options



Introduction

Table of Contents

Contact Factory

Contact Local Distributor

V-800 SERIES

Miniature Precision Vacuum Regulator
1/8" NPT ports

U.S. Patent No. 5,358,004

The V-800 Series vacuum regulators are designed for applications requiring high precision in a miniature package. Hysteresis free adjustments are made through a non-rising stem. Available with an attractive knob, or plain, allowing installation of OEM knobs. Also available is a flush adjusting shaft, and factory pre-set tamper-resistant models. Units may be base mounted or panel mounted.

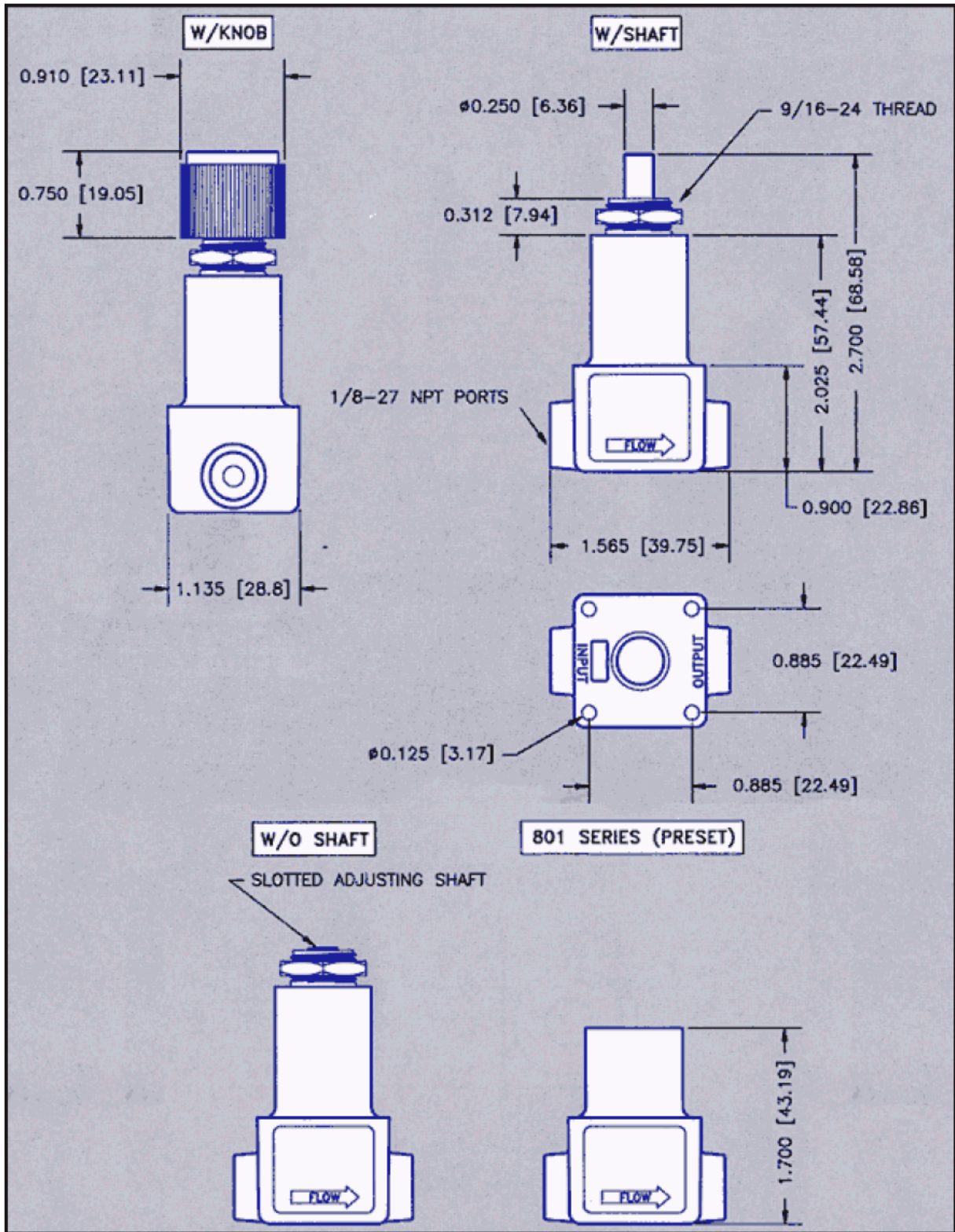


APPLICATIONS:

- Medical Equipment
- Pick 'n Place
- Laboratory Instruments
- Process Control

SPECIFICATIONS

REGULATOR TYPE	Constant Bleed, Relieving
WETTED MATERIALS	Polysulfone, Buna-N, EPDM, Acetal, Polyurethane, Stainless steel
SUPPLY CONSUMPTION	< 16 SCIM (260 cc/min) @ 30" (760 mm) Hg supply
MAX SUPPLY	30" [760 mm] Hg
TEMPERATURE RANGE	40° - 150° F (4° - 66° C)
EFFECT OF SUPPLY VARIATION	< 0.03" (.76 mm) per 5" (127 mm) Hg supply change when dead-ended
REPEATABILITY	< +/- 0.05" (1.25 mm) Hg when supply is removed and re-applied
SENSITIVITY	1" (25.4 mm) H ₂ O
MAXIMUM FLOW	1.0 cu.ft./min. (28 LPM)
RECOMMENDED FILTRATION	5 micron



BASIC Stamp BS2px and BS2 Information:



The BASIC Stamp 2 and 2px serve as the brains inside of electronics projects and applications that require a programmable microcontroller. They are able to control and monitor timers, keypads, motors, sensors, switches, relays, lights, and more. Programming is performed in an easy-to-learn language called PBASIC.

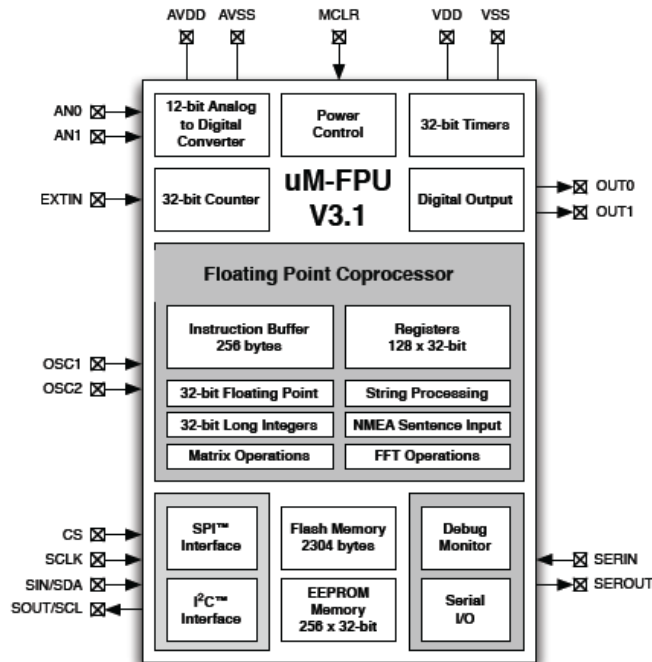
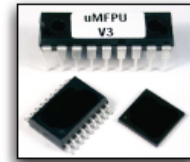
BASIC Stamp Model Comparison Table

Products	BS1	BS2	BS2px
Environment	0° - 70° C (32° - 158° F)	0° - 70° C (32° - 158° F)	0° - 70° C (32° - 158° F)
Microcontroller	Microchip PIC16C56a	Microchip PIC16C57c	Ubicom SX48AC
Processor Speed	4 MHz	20 MHz	32 MHz Turbo
Program Execution Speed	~2,000 instructions/sec.	~4,000 instructions/sec	~19,000 instructions/sec.
RAM Size	16 Bytes (2 I/O, 14 Variable)	32 Bytes (6 I/O, 26 Variable)	38 Bytes (12 I/O, 26 Variable)
Scratch Pad Ram	N/A	N/A	128 Bytes
EEPROM (Program) Size	256 Bytes, ~80 instructions	2K Bytes, ~500 instructions	8 x 2K Bytes, ~4,000 inst.
Number of I/O Pins	8	16 + 2 Dedicated Serial	16 + 2 Dedicated Serial
Voltage Requirements	5 - 15 vdc	5 - 15 vdc	5 - 12 vdc
Current Draw @ 5 volts	1 mA Run, 25 µA Sleep	3 mA Run, 50 µA Sleep	55 mA Run, 450 µA Sleep
Source/Sink Current per I/O	20 mA / 25 mA	20 mA / 25 mA	30 mA / 30 mA
Source/Sink Current per unit	40 mA / 50 mA	40 mA / 50 mA per 8 I/O pins	60 mA / 60 mA per 8 I/O pins
PBASIC Commands*	32	42	63
PC Interface	Serial (w/BS1 Serial Adapter)	Serial (9600 baud)	Serial (19200 baud)
Windows Text Editor Version	Stampw.exe (v2.1 and up)	Stampw.exe (v1.04 and up)	Stampw.exe (v2.2 and up)

* PBASIC Command count totals include PBASIC 2.5 commands on all BS2 models.

uM-FPU V3.1

32-bit Floating Point Coprocessor



Applications

- sensor data processing
- GPS data input and processing
- robotic control
- data transformations
- embedded systems

Features

- 32-bit IEEE 754 floating point
- 32-bit integer operations
- GPS serial input
- NMEA sentence parsing
- FFT operations
- 12-bit A/D Converters
- Serial input/output
- String handling
- Matrix operations
- SPI™ or I²C™ interface
- 2.7V, 3.3V, 5V supply
- low power modes
- 18-pin DIP, SOIC-18, QFN-44
- RoHS compliant

The uM-FPU V3.1 chip easily interfaces to virtually any microcontroller using an SPI™ or I²C™ interface.

Many microcontrollers used in embedded systems lack floating point support, but the wide range of sensors available today often require additional computations or data transformations to provide accurate results.

Advanced operations and fast execution allows the uM-FPU V3.1 chip to outperform comparable software math libraries. It also provides Flash memory and EEPROM for storing user-defined functions and data, and 128 32-bit registers for floating point and integer data.

Software math libraries often use large amounts of memory on microcontrollers, particularly as more complex library functions are used. The uM-FPU V3.1 chip offloads this overhead, and provides a comprehensive set of floating point operations, including advanced functions such as FFT, matrix operations and NMEA sentence parsing.

Development support is provided by the uM-FPU V3 IDE which takes traditional math expressions and automatically produces uM-FPU code targeted for one of the many microcontrollers and compilers supported. The IDE also interacts with the built-in debugger on the uM-FPU V3.1 chip to assist in debugging and testing the uM-FPU code.

The single unit price is \$19.95 with volume discounts available.



Micromega Corporation
www.micromegacorp.com

32-bit Floating Point and 32-bit Integer

A comprehensive set of 32-bit floating point and 32-bit integer operations are provided. See the uM-FPU V3.1 datasheet for details.

User-defined Functions

User-defined functions can be stored in Flash and EEPROM. Flash functions are programmed through the SERIN/SEROUT pins using the uM-FPU V3 IDE. The EEPROM functions can be programmed at run-time. Conditional execution is supported using conditional branch and jump instructions.

Matrix Operations

A matrix can be defined as any set of sequential registers. The MOP instruction provides scalar operations, element-wise operations, matrix multiply, inverse, determinant, count, sum, average, min, max, copy and set operations.

FFT Instruction

Provides support for Fast Fourier Transforms. Used as a single instruction for data sets that fit in the available registers, or as a multi-pass instruction for working with larger data sets.

Serial Input / Output

When not used for debugging, the SERIN and SEROUT pins can be used for serial I/O. For example, SERIN can be used to read data from a GPS, and SEROUT can be used to drive an LCD.

NMEA Sentence Parsing

The serial input can be set to scan for valid NMEA sentences with optional checksum. Multiple sentences can be buffered for further processing.

String Handling

String instructions are provided to insert and append substrings, search for fields and substrings, convert from floating point or long integer to a substring, or convert from a substring to floating point or long integer. For example, the string instructions could be used to parse a GPS NMEA sentence, or format multiple numbers in an output string.

Table Lookup Instructions

Instructions are provided to load 32-bit values from a table or find the index of a floating point or long integer table entry that matches a specified condition.

MAC Instructions

Instructions are provided to support multiply and accumulate and multiply and subtract operations.

A/D Conversion

Two 12-bit A/D channels are provided. The A/D conversion can be triggered manually, through an external input, or from a built-in timer. The A/D values can be read as raw values or automatically scaled to a floating point value. Data rates of up to 10,000 samples per second are supported.

Timers

Timers can be used to trigger the A/D conversion, or to track elapsed time. A microsecond and second timer are provided.

External Input

An external input can be used to trigger an A/D conversion, or to count external events.

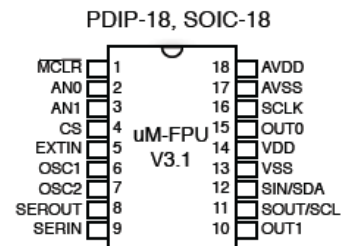
Low Power Modes

When the uM-FPU V3 chip is not busy it automatically enters a power saving mode. It can also be configured to enter a sleep mode which turns the device off while preserving register contents. In sleep mode the uM-FPU V3 chip consumes negligible power.

Internal Oscillator

Operates at full speed from internal oscillator. No external components required.

Pin Diagram and Pin Descriptions



Pin	Name	Type	Description
1	/MCLR	Input	Master Clear (Reset)
2	AN0	Input	Analog Input 0
3	AN1	Input	Analog Input 1
4	CS	Input	Chip Select / Interface Select
5	EXTIN	Input	External Input
6	OSC1	Input	Oscillator Crystal (optional)
7	OSC2	Output	Oscillator Crystal (optional)
8	SEROUT	Output	Serial Output, Debug Monitor - Tx
9	SERIN	Input	Serial Input, Debug Monitor - Rx
10	OUT1	Output	Digital Output 1
11	SOUT	Output	SPI Output, Busy/Ready Status
	SCL	Input	I ² C Clock
12	SIN	Input	SPI Input
	SDA	In/Out	I ² C Data
13	VSS	Power	Digital Ground
14	VDD	Power	Digital Supply Voltage
15	OUT0	Output	Digital Output 0, Busy/Ready Status
16	SCLK	Input	SPI Clock
17	AVSS	Power	Analog Ground
18	AVDD	Power	Analog Supply Voltage

High Temperature Accuracy Integrated Silicon Pressure Sensor On-Chip Signal Conditioned, Temperature Compensated and Calibrated

The MPXV6115VC6U sensor integrates on-chip, bipolar op amp circuitry and thin film resistor networks to provide a high output signal and temperature compensation. The small form factor and high reliability of on-chip integration make the Freescale Semiconductor, Inc. pressure sensor a logical and economical choice for the system designer.

The MPXV6115VC6U piezoresistive transducer is a state-of-the-art, monolithic, signal conditioned, silicon pressure sensor. This sensor combines advanced micromachining techniques, thin film metallization, and bipolar semiconductor processing to provide an accurate, high level analog output signal that is proportional to applied pressure.

Figure 1 shows a block diagram of the internal circuitry integrated on a pressure sensor chip.

Features

- Improved Accuracy at High Temperature
- 1.5% Maximum Error over 0° to 85°C
- Ideally suited for Microprocessor or Microcontroller-Based Systems
- Temperature Compensated from -40° to +125°C
- Durable Thermoplastic (PPS) Surface Mount Package

Typical Applications

- Vacuum Pump Monitoring
- Brake Booster Monitoring

ORDERING INFORMATION					
Device Type	Options	Case No.	MPX Series Order No.	Packing Options	Device Marking
Ported Element	Vacuum, Axial Port	482A	MPXV6115VC6U	Rails	MPXV6115V

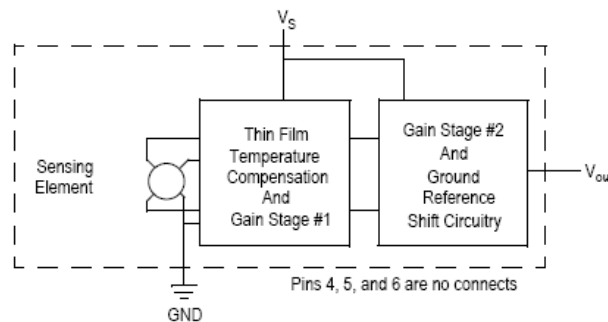
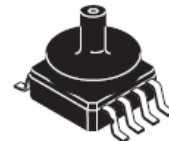


Figure 1. Fully Integrated Pressure Sensor Schematic

MPXV6115VC6U

**INTEGRATED
PRESSURE SENSOR**
-115 TO 0 kPa (-16.7 TO 2.2 psi)
0.2 TO 4.6 VOLTS OUTPUT

SMALL OUTLINE PACKAGE



MPXV6115VC6U
CASE 482A-01

PIN NUMBER⁽¹⁾

1	N/C	5	N/C
2	V _S	6	N/C
3	GND	7	N/C
4	V _{OUT}	8	N/C

1. Pins 1, 5, 6, and 8 are internal device connections. Do not connect to external circuitry or ground. Pin 1 is denoted by the notch in the lead.

Table 1. Maximum Ratings⁽¹⁾

Rating	Symbol	Value	Units
Maximum Pressure (P1 > P2)	P _{max}	400	kPa
Storage Temperature	T _{stg}	-40° to +125°	°C
Operating Temperature	T _A	-40° to +125°	°C
Output Source Current @ Full Scale Output ⁽²⁾	I _{o+}	0.5	mAdc
Output Sink Current @ Minimum Pressure Offset ⁽²⁾	I _{o-}	-0.5	mAdc

1. Exposure beyond the specified limits may cause permanent damage or degradation to the device.
2. Maximum Output Current is controlled by effective impedance from V_{out} to Gnd or V_{out} to V_S in the application circuit.

Table 2. Operating Characteristics (V_S = 5.0 Vdc, T_A = 25°C unless otherwise noted, P1 > P2)

Characteristic	Symbol	Min	Typ	Max	Unit
Pressure Range	P _{OP}	-115	—	0	kPa
Supply Voltage ⁽¹⁾	V _S	4.75	5.0	5.25	Vdc
Supply Current	I _o	—	6.0	10	mAdc
Full Scale Output ⁽²⁾ @ V _S = 5.0 Volts	V _{F_{SO}}	4.534	4.6	4.665	Vdc
		(0 to 85°C) (P _{diff} = 0 kPa)			
Full Scale Span ⁽³⁾ @ V _S = 5.0 Volts	V _{F_{SS}}	—	4.4	—	Vdc
		(0 to 85°C)			
Accuracy ⁽⁴⁾	—	—	—	±1.5	%V _{F_{SS}}
		(0 to 85°C)			
Sensitivity	V/P	—	38.26	—	mV/kPa
Response Time ⁽⁵⁾	t _R	—	1.0	—	ms
Warm-Up Time ⁽⁶⁾	—	—	20	—	ms
Offset Stability ⁽⁷⁾	—	—	±0.5	—	%V _{F_{SS}}

1. Device is ratiometric within this specified excitation range.
2. Full Scale Output (V_{F_{SO}}) is defined as the output voltage at the maximum or full rated pressure.
3. Full Scale Span (V_{F_{SS}}) is defined as the algebraic difference between the output voltage at full rated pressure and the output voltage at the minimum rated pressure.
4. Accuracy is the deviation in actual output from nominal output over the entire pressure range and temperature range as a percent of span at 25°C due to all sources of error including the following:
 - Linearity: Output deviation from a straight line relationship with pressure over the specified pressure range.
 - Temperature Hysteresis: Output deviation at any temperature within the operating temperature range, after the temperature is cycled to and from the minimum or maximum operating temperature points, with zero differential pressure applied.
 - Pressure Hysteresis: Output deviation at any pressure within the specified range, when this pressure is cycled to and from minimum or maximum rated pressure at 25°C.
 - TcSpan: Output deviation over the temperature range of 0° to 85°C, relative to 25°C.
 - TcOffset: Output deviation with minimum pressure applied, over the temperature range of 0° to 85°C, relative to 25°C.
5. Response Time is defined as the time for the incremental change in the output to go from 10% to 90% of its final value when subjected to a specified step change in pressure.
6. Warm-up Time is defined as the time required for the product to meet the specified output voltage after the pressure has been stabilized.
7. Offset Stability is the product's output deviation when subjected to 1000 cycles of Pulsed Pressure, Temperature Cycling with Bias Test.



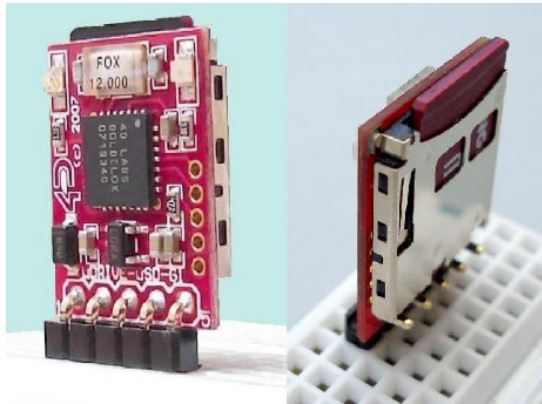
4D SYSTEMS

uDRIVE-uSD-G1 Embedded DOS micro-Drive

Data Sheet

Description

The micro-DRIVE (uDRIVE-uSD-G1) is an extremely compact high performance "Embedded Disk Drive" module that can be easily added to any micro-controller design that requires a DOS compatible file and data storage system. Most micro-controllers have small and limited on-chip memory. For those applications that require large volumes of data, the micro-DRIVE integrates the **GOLDELOX-DOS** chip onto a tiny 'drop-in-module'. A simple serial interface is all that is required to take away the burden of low level design that would otherwise be required for the host controller.



The micro-DRIVE module utilises off the shelf removable microSD memory cards of upto 2GB of capacity as its medium. A handful of straightforward commands provide direct access to the onboard memory card for storing and retrieving any size or type of data. Access to the card can be at (FAT based) file levels or at raw disk byte levels. Applications can range from data logging, program storage, music files, image and video files or any type of general purpose data storage. So next time your host micro-controller application requires a file/data storage, the micro-DRIVE maybe the ideal solution.

Features

- General purpose data storage device with a simple serial interface that can be added to any design in a wide range of embedded applications.
- DOS compatible file access (FAT16 format) as well as low level access to card memory.
- On board microSD memory card interace and adaptor.
- Accomodates off the shelf microSD removable memory cards upto 2GB capacity.
- Simple serial commands provide full read-write access to the card.
- Easy 5 pin interface to any host device: VCC, TX, RX, GND, RESET.
- Serial interface (TTL levels) with auto-baud feature from 300 to 256K baud rates.
- Onboard Status LEDs:
 - **GREEN:** Power and Memory Card detect indicator
 - **RED:** Drive data access indicator
- 3.6V to 5.5V range operation.
- Tiny footprint: 14.9 x 18.9 x 3.5mm.
- RoHS Compliant.

Applications

- General purpose embedded data logging
- Embedded program, data or configuration storage for processors and FPGAs
- Audio, Video and Image file storage
- GPS type data base storage
- Industrial, medical, automotive, security and gaming equipment
- Test, measurement and general purpose instrumentation

APPENDIX D: DATA TABLE FROM DORSAL HAND SKIN STUDY

Person	Gender	Max Age	FISTED HAND										RELAXED HAND									
			E	V	T	R	ToR	V/E	R/E	R/T	RD	E	V	T	R	ToR	V/E	R/E	R/T	RD		
1	M	29	0.08	0.00	0.09	0.01	13.95	-0.03	0.11	0.10	0.49	0.08	0.01	0.09	9.00	0.08	0.60	0.56	0.16			
2	F	29	0.13	0.01	0.13	0.11	11.30	0.04	0.81	0.19	0.80	0.19	0.03	0.22	0.15	0.98	0.14	0.86	0.22			
3	M	29	0.12	-0.01	0.13	0.08	9.94	-0.06	0.63	0.60	0.60	0.17	0.01	0.20	0.14	0.18	0.07	0.74	0.24			
4	F	49	0.05	-0.02	0.05	0.04	12.20	-0.34	0.79	0.82	0.82	0.10	0.03	0.07	0.04	16.33	0.79	1.03	0.57			
5	F	39	0.10	0.02	0.09	0.04	8.11	0.18	0.45	0.52	0.15	0.15	0.00	0.14	0.07	62.91	0.04	0.53	0.51			
6	F	44	0.14	-0.03	0.13	0.11	4.04	-0.19	0.77	0.86	0.10	0.16	0.04	0.21	0.11	8.67	0.26	0.97	0.78			
7	M	39	0.12	-0.01	0.13	0.03	13.41	-0.09	0.21	0.19	0.57	0.20	0.01	0.11	11.34	0.03	0.52	0.51	0.36			
8	M	24	0.01	0.01	0.02	0.04	10.85	1.80	7.40	1.54	0.12	0.08	0.00	0.08	0.02	7.51	0.01	0.24	0.17			
9	M	54	0.09	0.01	0.07	0.02	23.71	0.12	0.26	0.34	0.40	0.03	0.02	0.05	3.88	0.81	2.04	1.12	0.05			
10	M	24	0.13	0.06	0.08	0.07	7.79	0.44	0.56	0.91	0.46	0.13	0.03	0.15	0.08	57.27	0.20	0.61	0.51			
11	M	24	0.12	0.00	0.13	0.12	3.00	-0.02	1.00	0.94	0.08	0.20	0.03	0.23	0.14	5.41	0.13	0.72	0.63			
12	M	24	0.03	-0.01	0.04	0.01	19.67	-0.22	0.37	0.27	0.24	0.04	0.05	0.09	0.04	20.63	1.50	1.03	0.41			
13	F	49	0.10	-0.01	0.10	0.10	14.13	-0.06	0.12	0.12	0.48	0.16	0.00	0.17	0.11	25.50	0.01	0.69	0.68			
14	M	29	0.08	-0.02	0.07	0.04	13.34	-0.22	0.55	0.58	0.23	0.15	0.06	0.22	0.07	11.22	0.43	0.45	0.32			
15	F	24	0.20	0.00	0.20	0.15	9.29	0.01	0.76	0.78	0.23	0.24	0.05	0.29	0.23	9.18	0.19	0.95	0.80			
16	M	44	0.02	-0.01	0.06	0.04	3.76	-0.43	1.61	0.66	0.08	0.10	0.00	0.10	0.06	9.95	0.02	0.61	0.60			
17	M	54	0.15	0.00	0.19	0.18	8.67	-0.02	1.21	0.95	0.16	0.14	0.01	0.10	0.09	11.98	0.10	0.70	0.64			
18	M	24	0.20	-0.02	0.22	0.18	4.00	-0.10	0.89	0.80	0.26	0.26	0.00	0.26	0.23	5.13	0.02	0.86	0.88			
19	M	39	0.03	0.01	0.06	0.06	4.26	0.24	2.36	1.05	0.05	0.24	0.01	0.23	0.24	5.15	0.02	0.99	1.01			
20	F	24	0.09	0.00	0.09	0.05	4.80	0.04	0.60	0.64	0.10	0.12	0.03	0.14	0.13	2.93	0.22	1.12	0.92			
21	F	24	0.11	-0.01	0.11	0.04	9.85	-0.05	0.37	0.36	0.38	0.20	0.00	0.19	0.13	10.23	0.02	0.63	0.69			
22	M	24	0.15	-0.01	0.17	0.17	7.67	-0.06	1.11	0.98	0.13	0.28	0.02	0.30	0.30	1.16	0.08	1.07	0.99			
23	M	29	0.19	-0.01	0.23	0.17	6.53	-0.05	0.87	0.74	0.26	0.14	0.02	0.31	0.12	5.31	0.16	1.11	0.95			
24	M	44	0.08	-0.03	0.12	0.13	0.98	-0.37	1.56	1.02	0.09	0.11	0.02	0.13	0.11	13.00	0.17	1.00	0.85			
25	M	64	0.11	-0.01	0.12	0.09	3.11	-0.06	0.80	0.72	0.12	0.11	0.02	0.12	0.06	12.89	0.17	0.53	0.46			
26	M	66	0.11	0.02	0.13	0.16	0.81	0.15	1.47	1.24	0.09	0.11	0.01	0.12	0.06	7.57	0.09	0.53	0.48			
27	F	24	0.07	0.00	0.08	0.07	5.37	-0.03	0.90	0.79	0.11	0.22	0.00	0.21	0.21	5.58	0.01	0.95	1.01			
28	F	29	0.11	0.00	0.12	0.12	1.09	-0.02	1.13	1.07	0.08	0.07	0.03	0.09	0.07	6.52	0.40	1.03	0.74			
29	M	34	0.05	-0.01	0.05	0.02	3.59	-0.23	0.44	0.48	0.08	0.03	0.03	0.06	0.04	17.80	0.88	1.36	0.73			
30	F	44	0.11	-0.01	0.13	0.12	0.91	-0.06	1.12	0.94	0.10	0.13	0.02	0.13	0.07	13.40	0.15	0.51	0.37			
31	M	29	0.20	-0.03	0.23	0.20	1.75	-0.12	1.00	0.88	0.13	0.21	0.03	0.24	0.22	4.75	0.12	1.04	0.93			
32	F	19	0.07	-0.01	0.10	0.09	7.18	-0.11	1.33	0.89	0.10	0.14	0.03	0.17	0.08	3.35	0.20	0.56	0.46			
33	F	24	0.20	-0.03	0.16	0.16	1.11	-0.16	0.82	1.03	0.10	0.28	0.01	0.27	0.23	2.17	0.02	0.84	0.86			
34	F	49	0.05	0.01	0.07	0.05	29.78	0.13	1.04	0.75	0.21	0.09	0.04	0.13	0.03	8.64	0.41	0.35	0.25			
35	F	60	0.10	-0.02	0.10	0.05	6.13	-0.18	0.56	0.55	0.19	0.19	0.00	0.19	0.20	0.99	0.02	1.06	1.04			
36	F	49	0.06	-0.01	0.08	0.06	8.22	-0.18	1.02	0.76	0.17	0.19	0.06	0.24	0.27	1.00	0.30	1.47	1.12			
37	F	44	0.09	-0.01	0.10	0.06	4.38	-0.15	0.71	0.63	0.11	0.15	0.02	0.17	0.10	3.05	0.14	0.68	0.59			
38	F	39	0.03	0.00	0.07	0.02	11.44	-0.13	0.70	0.30	0.08	0.19	0.01	0.17	0.18	2.01	0.05	0.92	1.03			
39	F	24	0.09	0.00	0.12	0.07	5.21	0.01	0.80	0.59	0.15	0.17	0.01	0.18	0.09	14.19	0.04	0.54	0.52			
40	F	44	0.14	0.01	0.16	0.07	7.11	0.04	0.50	0.44	0.27	0.18	0.01	0.19	0.11	20.67	0.04	0.60	0.58			
AVERAGE			0.103	-0.005	0.113	0.083	8.07	-0.113	0.992	0.716	0.188	0.150	0.020	0.167	0.123	11.33	0.214	0.829	0.701	0.284		
STDEV			0.051	0.015	0.051	0.055	6.22	0.336	1.129	0.307	0.132	0.066	0.016	0.064	0.074	12.72	0.301	0.335	0.238	0.175		
STDEVR			0.008	0.002	0.008	0.009	0.98	0.053	0.178	0.049	0.021	0.011	0.003	0.010	0.012	2.01	0.048	0.053	0.038	0.028		

	Population Averages for Different Hand Positions										
	E	V	T	R	ToR	R/E	R/T	RD	R/E	R/T	RD
Relaxed	0.15 ± 0.011	0.02 ± 0.003	0.17 ± 0.01	0.12 ± 0.012	11.33 ± 2.01	0.83 ± 0.033	0.70 ± 0.038	0.28 ± 0.028	0.83 ± 0.033	0.70 ± 0.038	0.28 ± 0.028
Fisted	0.10 ± 0.008	-0.005 ± 0.002	0.11 ± 0.008	0.08 ± 0.009	8.07 ± 0.98	0.99 ± 0.178	0.72 ± 0.049	0.19 ± 0.021	0.99 ± 0.178	0.72 ± 0.049	0.19 ± 0.021

(E,V,T,R in cm, ToR in sec)			DIFFERENCE (Relaxed - Fisted)								
Person	Gender	Max Age	E	V	T	R	ToR	V/E	R/E	R/T	RD
1	M	29	0.00	0.01	0.00	0.04	-4.95	0.10	0.49	0.45	-0.34
2	F	29	0.06	0.02	0.08	0.08	-2.62	0.11	0.17	0.06	0.02
3	M	29	0.06	0.02	0.07	0.06	-3.76	0.13	0.11	0.09	0.07
4	F	49	-0.02	0.05	0.02	0.00	4.13	1.13	0.23	-0.25	0.14
5	F	39	0.04	-0.01	0.05	0.03	54.80	-0.15	0.08	-0.01	0.46
6	F	44	0.02	0.07	0.08	0.05	4.63	0.44	0.21	-0.08	0.15
7	M	39	0.08	0.02	0.07	0.08	-2.07	0.12	0.32	0.32	-0.21
8	M	24	0.07	-0.01	0.05	-0.02	-3.34	-1.79	-7.16	-1.30	0.05
9	M	54	-0.07	0.01	-0.02	0.03	-19.83	0.70	1.78	0.78	-0.35
10	M	24	0.00	-0.03	0.07	0.00	49.49	-0.24	0.05	-0.40	0.05
11	M	24	0.08	0.03	0.10	0.03	2.41	0.15	-0.28	-0.30	0.15
12	M	24	0.00	0.06	0.05	0.03	0.96	1.72	0.65	0.14	0.11
13	F	49	0.07	0.01	0.06	0.10	11.37	0.07	0.56	0.56	-0.10
14	M	29	0.07	0.08	0.14	0.02	-2.12	0.65	-0.10	-0.26	0.68
15	F	24	0.04	0.04	0.09	0.08	-0.11	0.18	0.19	0.02	0.21
16	M	44	0.07	0.01	0.04	0.02	6.18	0.46	-0.99	-0.06	0.07
17	M	54	-0.02	0.02	-0.04	-0.09	3.31	0.12	-0.51	-0.31	0.23
18	M	24	0.07	0.02	0.04	0.05	1.13	0.12	-0.03	0.08	0.05
19	M	39	0.21	0.00	0.18	0.18	0.89	-0.22	-1.37	-0.04	0.13
20	F	24	0.03	0.02	0.06	0.08	-1.87	0.18	0.52	0.28	0.00
21	F	24	0.09	0.01	0.07	0.09	0.41	0.08	0.27	0.32	0.02
22	M	24	0.13	0.03	0.13	0.13	-6.50	0.14	-0.04	0.02	0.07
23	M	29	-0.08	0.03	-0.10	-0.05	-1.22	0.22	0.24	0.21	-0.17
24	M	44	0.03	0.05	0.01	-0.01	12.02	0.54	-0.56	-0.16	0.09
25	M	64	0.00	0.02	0.01	-0.03	9.78	0.23	-0.27	-0.26	0.32
26	M	66	0.00	-0.01	-0.01	-0.10	6.76	-0.06	-0.94	-0.76	0.24
27	F	24	0.15	0.00	0.12	0.14	0.21	0.04	0.05	0.22	0.03
28	F	29	-0.04	0.03	-0.02	-0.05	5.43	0.42	-0.10	-0.33	0.03
29	M	34	-0.02	0.04	0.01	0.02	14.21	1.11	0.92	0.25	0.11
30	F	44	0.03	0.03	0.00	-0.05	12.50	0.21	-0.61	-0.44	0.27
31	M	29	0.01	0.05	0.01	0.02	3.00	0.25	0.05	0.05	0.10
32	F	19	0.07	0.04	0.07	-0.01	-3.83	0.31	-0.77	-0.43	0.12
33	F	24	0.08	0.04	0.11	0.07	1.06	0.18	0.03	-0.18	0.13
34	F	49	0.04	0.03	0.06	-0.02	-21.14	0.27	-0.68	-0.50	0.28
35	F	60	0.09	0.02	0.09	0.15	-5.14	0.19	0.50	0.50	-0.06
36	F	49	0.13	0.07	0.16	0.21	-7.22	0.49	0.45	0.37	-0.01
37	F	44	0.06	0.03	0.07	0.04	-1.53	0.29	-0.03	-0.03	0.04
38	F	39	0.16	0.01	0.10	0.16	-9.43	0.19	0.22	0.73	0.03
39	F	24	0.08	0.00	0.06	0.02	8.98	0.02	-0.26	-0.07	0.30
40	F	44	0.04	0.00	0.03	0.04	13.56	0.00	0.10	0.14	0.31
		>0	31	35	34	29	23	35	23	20	32
		<0	7	5	5	11	17	5	17	20	8
		=0	2	0	1	0	0	0	0	0	0
		SUM	40	40	40	40	40	40	40	40	40
		% >0	77.5%	87.5%	85.0%	72.5%	57.5%	87.5%	57.5%	50.0%	80.0%
		% <0	17.5%	12.5%	12.5%	27.5%	42.5%	12.5%	42.5%	50.0%	20.0%
		% =0	5.0%	0.0%	2.5%	0.0%	0.0%	0.0%	0.0%	0.0%	0.0%
		%SUM	100%	100%	100%	100%	100%	100%	100%	100%	100%

Difference between Positions (Relaxed Hand - Fisted Hand)									
	E	V	T	R	ToR	V/E	R/E	R/T	RD
Difference	0.05 ± 0.009	0.02 ± 0.004	0.05 ± 0.009	0.04 ± 0.011	3.26 ± 2.17	0.23 ± 0.078	-0.16 ± 0.2	-0.01 ± 0.063	0.10 ± 0.030
Paired T-test	<0.0001	<0.0001	<0.0001	0.0007	0.1405	0.006	0.4108	0.8125	0.0025
Significance (P < 0.01)	Yes	Yes	Yes	Yes	No	Yes	No	No	Yes

APPENDIX E: BASIC STAMP 2px OPERATIONAL PROGRAM

```

'Cutisfirm0-072409-FPUMaxLCD.bpx      'Program Page 0
{$STAMP BS2px, Cutisfirm0-072409-FPUMax-LCD.bpx, Cutisfirm0-072409-FPUMax-LCD.bpx}
{$PBASIC 2.5}
{$PORT COM2}

=====
-----INTRODUCTION - cutisfirm070709 pg 0 of 0/2 -----
=====
This program runs the complete control system for the Cutisfirm Skin Tension Measurement
System. The system contains a IR proximity sensor for skin deformation measurement when
under suction and a 6VDC micropump which creates the vacuum inside a probe attached to
the skin. The control system also consists of a normally open pushbutton activator.
When the button is depressed, the vacuum pump is activated for a preset time. The pump
is automatically disabled after a test by an electronic shut off of the voltage supply
using a subordinate BASIC Stamp 2 module. This program also sets up the Basic Stamp 2px to
control a uM-FPU math co-processor chip to perform a decimal conversion of the IR proximity
sensor voltage output. The chip records 8 readings of 100 averaged, then a digital filter
removing the minimum noise dips is used to reduce the noise from the analog signal.
Skin deformation height is calculated from a quadratic calibration equation obtained
from experiments at known distances using a precision automated stage (Velmex, Inc.)
Data is also sent to microSD card using the uDRIVE-USD-G1 DOS micro-Drive module from 4D
Systems Pty Ltd (Sydney, Australia).
=====
-----VARIABLES-----
=====
BS2 Output Variables
-----
reading  VAR  word  ' IRread cycle counter for For/Next loop

Input Variables
-----
calib    VAR  Bit   ' input for IR calibration initiation
on1      VAR  Bit   ' input for initiating device warm up
cardin   VAR  Bit   ' input for microSD insertion confirmation

Wiring Pin Location Variables
-----
PinReset PIN  0    ' reset Stamp
FpuOut   PIN  1    ' SPI data out (connects to SIN/SDA on uM-FPU)
FpuIn    PIN  1    ' SPI data in (connects to SOUT on uM-FPU)
FpuClk   PIN  2    ' SPI clock (connects to SCL/SCLK on uM-FPU)
PinIRVdd PIN  3    ' Connects to TIP120 pin 1 then to black wire on IR (pin 2)
PinButton PIN  4    ' Connects to button to complete ground side
PinTxSD  PIN  5    ' Tx wire to SD card module

```

```

PinData      PIN      6      Green wire to SD card module (Rx = Data to SD card)
PinLoopoff  PIN      7      Connects to BASIC Stamp BS2 for power down (BS2_P8)
PinLoopon   PIN      8      Connects to BASIC Stamp BS2 for power on (BS2_P7)
PinLoopp60  PIN      9      Connects to BASIC Stamp BS2 for input on BS2_P6
PinLoopp30  PIN     10     " " " " " " " " BS2_P5
PinLoopp25  PIN     11     " " " " " " " " BS2_P4
PinLoopp20  PIN     12     " " " " " " " " BS2_P3
PinLoopp15  PIN     13     " " " " " " " " BS2_P2
PinLoopp10  PIN     14     " " " " " " " " BS2_P1
PinLoopp05  PIN     15     " " " " " " " " BS2_P0
=====
----uM-FPU V3 SPI definitions-----
=====
uM-FPU V3 opcodes
-----
SELECTA      CON      $01      Select register A
COPYI        CON      $12      Swap reg[nn] and reg[mm]
FWRITEA      CON      $17      write 32-bit float to reg[A]
FCALL        CON      $7E      call user-defined function in Flash memory
LWRITEA      CON      $91      write 32-bit long integer to reg[A]
LTOA         CON      $9B      Convert long integer to ASCII
FSEROUT      CON      $CE      serial output
ADCMODE      CON      $D1      Set A/D trigger mode
STRINS       CON      $E5      Insert string at selection point
SYNC         CON      $F0      Get synchronization byte
READSTATUS   CON      $F1      Read status byte
READSTR      CON      $F2      Read string from string buffer
VERSION      CON      $F3      Copy version string to string buffer
=====
SyncChar     CON      $5C
Time         CON      1      sync character
TimeEnd      CON      2      uM-FPU Registry 1 = millisecond storage
Sample1      CON      3      uM-FPU Registry 2 = millisecond cumulative for reading
Sample2      CON      4      uM-FPU Registry 3 = storage for A/D conversion for IR
Sample3      CON      5      uM-FPU Registry 4 = storage for A/D conversion for IR
Sample4      CON      6      uM-FPU Registry 5 = storage for A/D conversion for IR
Sample5      CON      7      uM-FPU Registry 6 = storage for A/D conversion for IR
Sample6      CON      8      uM-FPU Registry 7 = storage for A/D conversion for IR
Sample7      CON      9      uM-FPU Registry 8 = storage for A/D conversion for IR
Sample8      CON     10     uM-FPU Registry 9 = storage for A/D conversion for IR
Compare1_2   CON     11     uM-FPU Registry 10 = storage for A/D conversion for IR
Compare3_4   CON     12     uM-FPU Registry 11 = Digital filter max of Samples 1,2
Compare5_6   CON     13     uM-FPU Registry 12 = Digital filter max of Samples 3,4
Compare7_8   CON     14     uM-FPU Registry 13 = Digital filter max of Samples 5,6
Comparemax1  CON     15     uM-FPU Registry 14 = Digital filter max of Samples 7,8
             CON     15     uM-FPU Registry 15 = Digital filter min of Samples 1-4max

```



```

Comparemax2      CON      16 = Digital filter min of samples 5-8max
CompareNex      CON      17 = Digital filter averaging
Comparea11      CON      18 = Digitally filtered sample value
SQRD            CON      19 = Square of sample value
MSQ             CON      20 = Quadratic x^2 slope (from calibration)
M               CON      21 = Quadratic x slope (from calibration)
Be              CON      22 = storage for IR calibration y-intercept
Quad           CON      23 = MSQ * Sample^2
Linear         CON      24 = M * Sample
Rest           CON      25 = Quad - Linear
Distance       CON      26 = Rest + Be - Calculated distance
Ca1Dist       CON      27 = storage for 8.000, known height
Ca1Lin        CON      28 = M * Sample for Be calibration
Ca1Nex        CON      29 = Ca1Lin - Ca1Quad for Be calibration
Ca1SQRD       CON      30 = MSQ * Ca1SQRD for Be calibration
Ca1SQRD       CON      31 = Sample^2 for Be calibration
TimeFull1     CON      32 = storage for additional IR process time
TimeElapse    CON      33 = IR reading time total length
SampleCnt     CON      34 = Sample # for each IRread loop
SampleDiv     CON      35 = Sample # same as SampleCnt but formatted
waitCount     CON      36 = Loopcounter to _waitCounter loop
Pressdec      CON      37 = storage for Pressure decimal input
PressM        CON      38 = storage for Pressure calibration slope
PressB        CON      39 = storage for Pressure calibration y-intercept
Pressconv     CON      40 = storage for PressM * Pressdec
Pressure      CON      41 = storage for Pressure data
Divide        CON      42 = storage for 2

UM-FPU variables
-----
dataword      VAR      word      data word
dataHigh     VAR      dataword.HIGHBYTE  high byte of dataword
dataLow      VAR      dataword.LOWBYTE   low byte of dataLow
dataByte     VAR      dataLow           (alternate name)
opcode       VAR      dataHigh          opcode (same as dataHigh)
format       VAR      dataLow           format (same as dataLow)
status       VAR      dataLow           status (same as dataLow)

status_Zero  VAR      status.BIT0       Zero status bit (0-not zero, 1-zero)
status_Sign  VAR      status.BIT1       Sign status bit (0-positive, 1-negative)
status_NaN   VAR      status.BIT2       Not a Number status bit (0-valid number, 1-NaN)
status_Inf   VAR      status.BIT3       Infinity status bit (0-not infinite, 1-infinite)

4D-uDRIVE-USD-G1 variables
-----

```

```

cycle          VAR          word
triggerset    VAR          word
'reset Loopcounter
'

sampleCntCPY  VAR          word

=====
-----CONSTANTS & INITIAL CONDITIONS-----
=====

reading = 0
triggerset = 0

GOSUB Card_Reset
PAUSE 100

LOW PinReset
LOW PinIRVdd
LOW PinButton
LOW PinLoop05
LOW PinLoop10
LOW PinLoop15
LOW PinLoop20
LOW PinLoop25
LOW PinLoop30
LOW PinLoop60
LOW PinLoopon
LOW PinLoopoff

' P0
' P3
' P4
' P15
' P14
' P13
' P12
' P11
' P10
' P9
' P8
' P7

=====
-----uM-FPU initialization -----
=====
Reset the uM-FPU.

Reset:
GOSUB Fpu_Reset
PAUSE 100

' resets the FPU hardware

=====
-----PROGRAM-----
=====
NOTES: CR = carriage return, Serial Baud Rate set to 115.2 kbytes
Initialize instructions:
=====

```

```

'SEROUT 16, 14, ["welcome to the Cutisfirm Skin Tension Measurement System!", CR] ; PCSerial
SEROUT 16, 14, [$A0, $02, $00, $21, $3D] ; LCD page 1
PAUSE 3000
LOW PinIRVdd

GOSUB Fpu_SER57600
PAUSE 100

'SEROUT 16, 14, ["Insert microSD card for data collection. Press any # key + enter to continue.", CR]
; PCSerial
'SERIN 16, 14, [DEC cardin] ; LCD page 2
SEROUT 16, 14, [$A0, $02, $00, $22, $3C]
SERIN 16, 14, [cardin] ; initializes the microsd card
GOSUB Card_IDISK
PAUSE 100

'SEROUT 16, 14, ["Are you ready to warm up the sensor? Press any # key + enter when ready.", CR]
; PCSerial
'SERIN 16, 14, [DEC on1]
SEROUT 16, 14, [$A0, $02, $00, $23, $3B] ; LCD page 3
SERIN 16, 14, [on1]
PAUSE 1000

warmup:
-----
HIGH PinReset
PAUSE 100
LOW PinReset
PAUSE 100

'SEROUT 16, 14, ["warming up...", CR] ; PCSerial
SEROUT 16, 14, [$A0, $02, $00, $24, $3A] ; LCD page 4
HIGH PinIRVdd
PAUSE 100

GOSUB Card_OPEN2
PAUSE 100
GOSUB Card_MESSAGE2
PAUSE 100
GOSUB Card_OPEN1
PAUSE 100
GOSUB Card_MESSAGE
PAUSE 20000
; MAKE 20 SEC WHEN DONE!!
-----

```

```

Calibrate:
'SEROUT 16, 14, ["Attach probe to skin. Press any # key + enter to continue." , CR] ' PCSerial
'SERIN 16, 14, [DEC calib]
SEROUT 16, 14, [$A0, $02, $00, $25, $39]
SERIN 16, 14, [calib]
PAUSE 1000
'SEROUT 16, 14, ["Calibrating IR sensor..." , CR]
SEROUT 16, 14, [$A0, $02, $00, $26, $38]
PAUSE 10

SHIFTOUT FpuOut, FpuClk, MSBFIRST, [SELECTA, TimeFu], LWRITEA, $00, $00, $51, LTOA, 4]
, Sets addon time = 0
SHIFTOUT FpuOut, FpuClk, MSBFIRST, [SELECTA, MSQ, FWRITEA, $37, $C9, $53, $9C]
, IR Quadratic Slope2 = 0.000024
SHIFTOUT FpuOut, FpuClk, MSBFIRST, [SELECTA, M, FWRITEA, $3D, $9E, $F8, $FE]
, IR Linear Slope = 0.0776
SHIFTOUT FpuOut, FpuClk, MSBFIRST, [SELECTA, CaDist, FWRITEA, $41, $00, $00, $00]
, IR Calibration Distance = 8 cm
SHIFTOUT FpuOut, FpuClk, MSBFIRST, [SELECTA, PressB, FWRITEA, $42, $0D, $6B, $85]
, Pressure Y-intercept = 35.355
SHIFTOUT FpuOut, FpuClk, MSBFIRST, [SELECTA, PressM, FWRITEA, $3C, $1B, $A5, $E3]
, Pressure Slope = 0.0095
SHIFTOUT FpuOut, FpuClk, MSBFIRST, [FCALL, 0]
, run funcCALIBRATION program on um-FPU
GOSUB Print_FpuString
, setup output string

PAUSE 1000
LOW PinIRVdd

RUN 1

=====
-----SUBROUTINES-----
=====
-----um-FPU V3 SPI support routines-----
=====
Fpu_Reset:
SHIFTOUT FpuOut, FpuClk, MSBFIRST,
[$FF, $FF, $FF, $FF, $FF, $FF, $FF, $FF, $FF, $FF]
PAUSE 10
RETURN

```



```

Fpu_SER57600:
  SHIFTOUT FpuOut, FpuCLK, MSBFIRST, [FSEROUT, 0, 9]
  RETURN
' sets baudrate for FPU to 57600

Fpu_wait:
  INPUT FpuIn
' (required for 2-wire interface)

Fpu_wait2:
  IF (FpuIn = 1) THEN GOTO Fpu_wait2
  RETURN
' wait until UM-FPU is ready

Print_FpuString:
  GOSUB Fpu_wait
  SHIFTOUT FpuOut, FpuCLK, MSBFIRST, [READSTR]
  DO
    SHIFTOUT FpuIn, FpuCLK, MSBFIRST, [dataByte]
    IF (dataByte = 0) THEN EXIT
    SEROUT PinData, 14, [dataByte]
    PAUSE 10
  'SEROUT 16, 14, [dataByte]
' PCSerial calibration data output

LOOP
RETURN

=====
-----uDRIVE-uSD-G1 support routines -----
=====
Card_RESET:
  Cycle = 0
  FOR Cycle = 0 TO 10 STEP 1
    SEROUT PinData, 14, [$55]
    PAUSE 100
  NEXT
  RETURN

Card_IDISK:
  SEROUT PinData, 14, [$40,$69]
  RETURN

Card_OPEN2:
  SEROUT PinData, 14, [$40,$74,$00,$41,$42,$43,$44,$45,$2E,$74,$78,$74,$00,$00,$00,$03]
  RETURN

Card_MESSAGE2:
  SEROUT PinData, 14, [$31,$0D,$0A]
  RETURN

```

```
Card_OPEN1:
SEROUT PinData, 14, [ $40, $74, $80, $41, $42, $43, $44, $2E, $74, $78, $74, $00, $00, $00, $00, $1C]
RETURN

Card_MESSAGE:
SEROUT PinData, 14, [ $20, $49, $52, $23, $20, $50, $72, $65, $73, $73, $23, $20, $48, $65, $69, $67, $68, $74,
$20, $69, $6E, $48, $67, $20, $6D, $73, $0D, $0A]
RETURN
*END OF PAGE 0 of 0/2
=====
```

```

'Cutisfirm072409-Fpumax-LCD.bpx          'Program Page 1
{$PORT COM2}
{$STAMP BS2px}
{$PBASIC 2.5}

=====
-----cutisfirm072409 pg 1 of 0/2 -----
=====
-----VARIABLES-----
=====
BS2 Output Variables
-----
count1      VAR      Byte      ' button loopcounter
times       VAR      word       ' test cycle limit for IRRead For/Next loop
reading     VAR      word       ' IRRead cycle counter for For/Next loop

Input Variables
-----
secs        VAR      Byte      ' input variable for test time
probe       VAR      Bit        ' input variable for confirming IR turn on safety
cortime     VAR      Bit

Wiring Pin Location Variables
-----
PinReset    PIN      0          ' reset Stamp
FpuOut      PIN      1          ' SPI data out (connects to SIN/SDA on UM-FPU)
FpuIn       PIN      1          ' SPI data in (connects to SOUT on UM-FPU)
FpuClk      PIN      2          ' SPI clock (connects to SCL/SCLK on UM-FPU)
PinIRVdd    PIN      3          ' Connects to TIP120 pin 1 then to black wire on IR (pin 2)
PinButton   PIN      4          ' Connects to button to complete ground side
PinTXSD     PIN      5          ' Tx wire to SD card module
PinData     PIN      6          ' Green wire to SD card module (RX = Data to SD card)
PinLoopoff  PIN      7          ' Connects to BASIC Stamp BS2 for power down (BS2 P8)
PinLoopon   PIN      8          ' Connects to BASIC Stamp BS2 for power on (BS2 P7)
PinLoop60   PIN      9          ' Connects to BASIC Stamp BS2 for input on BS2 P6
PinLoop30   PIN      10         ' BS2 P5
PinLoop25   PIN      11         ' BS2 P4
PinLoop20   PIN      12         ' BS2 P3
PinLoop15   PIN      13         ' BS2 P2
PinLoop10   PIN      14         ' BS2 P1
PinLoop05   PIN      15         ' BS2 P0

-----uM-FPU V3 SPI definitions-----

```



```

CaLSQRD          CON          31 = Sample^2 for Be calibration
TimeFull        CON          32 = storage for additional IR process time
TimeElapse      CON          33 = IR reading time total length
SampleCnt       CON          34 = Sample # for each IRread loop
SampleDiv       CON          35 = Sample # same as SampleCnt but formatted
WaitCount       CON          36 = Loopcounter to _waitCounter loop
Pressdec        CON          37 = storage for Pressure decimal input
PressM          CON          38 = storage for Pressure calibration slope
PressB          CON          39 = storage for Pressure calibration y-intercept
Pressconv       CON          40 = storage for PressM * Pressdec
Pressure        CON          41 = storage for Pressure data
Divide          CON          42 = storage for 2

-----
! uM-FPU Registry 31 = Sample^2 for Be calibration
! uM-FPU Registry 32 = storage for additional IR process time
! uM-FPU Registry 33 = IR reading time total length
! uM-FPU Registry 34 = Sample # for each IRread loop
! uM-FPU Registry 35 = Sample # same as SampleCnt but formatted
! uM-FPU Registry 36 = Loopcounter to _waitCounter loop
! uM-FPU Registry 37 = storage for Pressure decimal input
! uM-FPU Registry 38 = storage for Pressure calibration slope
! uM-FPU Registry 39 = storage for Pressure calibration y-intercept
! uM-FPU Registry 40 = storage for PressM * Pressdec
! uM-FPU Registry 41 = storage for Pressure data
! uM-FPU Registry 42 = storage for 2

-----
uM-FPU variables
-----
dataword        VAR          word          data word
dataHigh        VAR          dataword.HIGHBYTE  high byte of dataword
dataLow         VAR          dataword.LOWBYTE  low byte of dataLow
dataByte        VAR          dataLow          (alternate name)
opcode          VAR          dataHigh         opcode (same as dataHigh)
format          VAR          dataLow          format (same as dataLow)

-----
4D-uDRIVE-uSD-G1 variables
-----
cycle          VAR          word          'Reset Loopcounter
triggerSet     VAR          word
SampleCntCPY   VAR          word

-----
-----CONSTANTS & INITIAL CONDITIONS-----
-----
time05         CON          160          ' number of readings in 5 secs plus a buffer around test
time10         CON          195          "
time15         CON          245          "
time20         CON          285          "
time25         CON          325          "
time30         CON          365          "
time60         CON          610          "
times = 0      ' resets limit for IRread cycles
reading = 0    ' resets For/Next loop in IR calibration
triggerSet = 0
-----

```

```

=====
PROGRAM
=====
=====
MAIN:
=====
PAUSE 1000
GOSUB Card_OPEN3
PAUSE 100
GOSUB Card_MESSAGE3
PAUSE 100

HIGH PinLoopoff
PAUSE 10
LOW PinLoopoff

HIGH PinReset
PAUSE 10
LOW PinReset
PAUSE 1000

LOW PinIRVdd
LOW PinButton
LOW PinLoop05
LOW PinLoop10
LOW PinLoop15
LOW PinLoop20
LOW PinLoop25
LOW PinLoop30
LOW PinLoop60
LOW PinLoopon
LOW PinLoopoff

'SEROUT 16, 14, ["Reattach probe to skin, if necessary. Press any # key + enter to continue" , CR]
, PCSerial
'SERIN 16, 14, [DEC probe]
SEROUT 16, 14, [$A0, $02, $00, $27, $37] ' LCD page 7
SERIN 16, 14, [probe]

PAUSE 100
HIGH PinIRVdd
PAUSE 100

backtime:
=====
'SEROUT 16, 14, ["Enter time length option: 05, 10, 15, 20, 25, 30 ,or 60 seconds: " , CR] ' PCSerial

```

```

'SERIN 16, 14, [DEC secs]
SEROUT 16, 14, [$A0, $02, $00, $28, $36] 'LCD page 8
SERIN 16, 14, [secs]
PAUSE 100
'SEROUT 16, 14, ["You picked: ", DEC secs, " seconds.", CR] ' PCSerial
'PAUSE 100
'SEROUT 16, 14, ["Correct Time? Yes=1, No=0", CR] ' PCSerial
'SERIN 16, 14, [DEC cortime]
SEROUT 16, 14, [$A0, $02, $00, $29, $35] ' LCD page 9
SERIN 16, 14, [cortime]
' for multiple tests
IF cortime=0 THEN
  GOTO backtime
ELSEIF cortime=1 THEN
  ENDIF
GOSUB timecheck
PAUSE 100
' subroutine to convert secs for timers
'SEROUT 16, 14, ["Initializing...", CR]
SEROUT 16, 14, [$A0, $02, $00, $2A, $34]
PAUSE 100
SEROUT PinLoopoon, 396, ["XYZ", CR]
PAUSE 2000
' turns on BASIC Stamp program
' 2 seconds for Stamp initialization
-----
Operation:
'SEROUT 16, 14, ["Press button to test.", CR] ' PCSerial
SEROUT 16, 14, [$A0, $02, $00, $2B, $33]
' LCD page 11
GOTO buttonloop
' subroutine for button operation
topump:
GOSUB pumptime
'SEROUT 16, 14, ["Reading...", CR]
SEROUT 16, 14, [$A0, $02, $00, $2C, $32]
PAUSE 10
' returns to prgm once button is pressed
' subroutine for Stamp control of pump
'SEROUT 16, 14, ["Reading...", CR]
SEROUT 16, 14, [$A0, $02, $00, $2C, $32]
PAUSE 10
' PCSerial
' LCD page 12
GOSUB IRREAD
PAUSE 1000
' sub for converting IR volts to height
=====
RUN 2
=====

```



```

-----SUBROUTINES-----
Timer set program:
timecheck:
SELECT secs
CASE 1
    times = time05
CASE 2
    times = time10
CASE 3
    times = time15
CASE 4
    times = time20
CASE 5
    times = time25
CASE 6
    times = time30
CASE 7
    times = time60
ENDSELECT
' For LCD

'IF secs = 05 THEN
    times = time05
' ELSEIF secs = 10 THEN
    times = time10
' ELSEIF secs = 15 THEN
    times = time15
' ELSEIF secs = 20 THEN
    times = time20
' ELSEIF secs = 25 THEN
    times = time25
' ELSEIF secs = 30 THEN
    times = time30
' ELSEIF secs = 60 THEN
    times = time60
' ELSE
    SEROUT 16, 14, ["Pick from the list!", CR]
    GOTO Main
' ENDIF
RETURN
' For PCSerial

Button operation:

```



```

buttonloop:
  BUTTON PinButton, 1, 80, 40, count1, 1, pump1 'button pin, downstate(0/1), delay(0-255),
  'rate(0-255), loopcounter, targetstate (1=when pressed), target
  GOTO buttonloop

pump1:
  HIGH PinButton
  GOTO topump

-----
Pump timing subroutine:
-----
pumptime:
  SELECT secs
  CASE 1
    HIGH PinLoop05
    PAUSE 10
    LOW PinLoop05
  CASE 2
    HIGH PinLoop10
    PAUSE 10
    LOW PinLoop10
  CASE 3
    HIGH PinLoop15
    PAUSE 10
    LOW PinLoop15
  CASE 4
    HIGH PinLoop20
    PAUSE 10
    LOW PinLoop20
  CASE 5
    HIGH PinLoop25
    PAUSE 10
    LOW PinLoop25
  CASE 6
    HIGH PinLoop30
    PAUSE 10
    LOW PinLoop30
  CASE 7
    HIGH PinLoop60
    PAUSE 10
    LOW PinLoop60
  ENDSELECT

' IF secs = 05 THEN
' For PCSerial
' For LCD

```

```

HIGH PinLoop05
PAUSE 10
LOW PinLoop05
ELSEIF secs = 10 THEN
HIGH PinLoop10
PAUSE 10
LOW PinLoop10
ELSEIF secs = 15 THEN
HIGH PinLoop15
PAUSE 10
LOW PinLoop15
ELSEIF secs = 20 THEN
HIGH PinLoop20
PAUSE 10
LOW PinLoop20
ELSEIF secs = 25 THEN
HIGH PinLoop25
PAUSE 10
LOW PinLoop25
ELSEIF secs = 30 THEN
HIGH PinLoop30
PAUSE 10
LOW PinLoop30
ELSEIF secs = 60 THEN
HIGH PinLoop60
PAUSE 10
LOW PinLoop60
ELSE
SEROUT 16, 14, ["Error! ", CR]
ENDIF
RETURN
-----
Subroutine for GP2D120 IR sensor voltage to skin height conversion using uM-FPU chip:
IRREAD:
FOR reading = 0 TO times STEP 1 'step 1 = increment the For/Next Loop by ones
GOSUB Card_OPEN
SHIFTOUT FpuOut, FpuClk, MSBFIRST, [SELECTA, samplediv, LWRITEA, $00, $00, $00, $64]
'100 samples
SHIFTOUT FpuOut, FpuClk, MSBFIRST, [SELECTA, waitCount, LWRITEA, $00, $00, $02, $58]
'600 = 40ms
SHIFTOUT FpuOut, FpuClk, MSBFIRST, [FCALL, 1] ' runs funcGETSAMPLE on uM-FPU
GOSUB Print_Fpustring ' sets up output string
NEXT

```

```

RETURN
=====
----um-FPU V3 SPI support routines -----
=====

Fpu_wait:
INPUT FpuIn          ' (required for 2-wire interface)

Fpu_wait2:
IF (FpuIn = 1) THEN GOTO Fpu_wait2 ' wait until um-FPU is ready
RETURN

Print_FpuString:
GOSUB Fpu_wait
SHIFTOUT FpuOut, FpuCk, MSBFIRST, [READSTR]
DO
  SHIFTOIN FpuIn, FpuCk, MSBPRES, [dataByte]
  IF (dataByte = 0) THEN EXIT
  SEROUT PinData, 14, [dataByte]
  PAUSE 2
'SEROUT 16, 14, [dataByte] ' For PCserial string output
LOOP
RETURN
=====
----uDRIVE-USD-G1 support routines -----
=====

Card_IDISK:
SEROUT PinData, 14, [$40,$69]
RETURN

Card_OPEN3:
SEROUT PinData, 14, [$40,$74,$80,$41,$42,$43,$44,$2E,$74,$78,$74,$00,$00,$00,$03]
RETURN

Card_MESSAGE3:
SEROUT PinData, 14, [$20,$0D,$0A]
RETURN

Card_OPEN: ' opens ABCD.txt, 28bytes: IR dec, Pressure dec, Height calc, Pressure calc, time ms
SEROUT PinData, 14, [$40,$74,$80,$41,$42,$43,$44,$2E,$74,$78,$74,$00,$00,$00,$03,$1C]
RETURN
'END OF PAGE 1 of 0/2
=====

```

```

{ $STAMP BS2px}
{ $PBASIC 2.5}
{ $PORT COM2}
-----cutisfirm072409 pg 2 of 0/2 -----
=====
-----VARIABLES-----
=====
Input Variables
-----
yn      VAR      Bit      ' input variable for performing multiple tests
-----
Wiring Pin Location Variables
-----
PinReset  PIN      0      ' reset Stamp
FpuOut    PIN      1      ' SPI data out (connects to SIN/SDA on uM-FPU)
FpuIn     PIN      1      ' SPI data in (connects to SOUT on uM-FPU)
FpuClk    PIN      2      ' SPI clock (connects to SCL/SCLK on uM-FPU)
PinIRVdd  PIN      3      ' Connects to TIP120 pin 1 then to black wire on IR (pin 2)
PinButton PIN      4      ' Connects to button to complete ground side
PinTXSD   PIN      5      ' TX wire to SD card module
PinData   PIN      6      ' Green wire to SD card module (RX = Data to SD card)
PinLoopoff PIN      7      ' Connects to BASIC Stamp BS2 for power down (BS2 P8)
PinLoopon  PIN      8      ' Connects to BASIC Stamp BS2 for power on (BS2 P7)
PinLoop60  PIN      9      ' Connects to BASIC Stamp BS2 for input on BS2 P6
PinLoop30  PIN     10      ' " " " " " " " " " " " "
PinLoop25  PIN     11      ' " " " " " " " " " " " "
PinLoop20  PIN     12      ' " " " " " " " " " " " "
PinLoop15  PIN     13      ' " " " " " " " " " " " "
PinLoop10  PIN     14      ' " " " " " " " " " " " "
PinLoop05  PIN     15      ' " " " " " " " " " " " "
=====
-----PROGRAM-----
'SEROUT 16, 14, ["Another test? Y=1 or N=0? ", CR] ' PCSerial
'SERIN 16, 14, [DEC yn]
SEROUT 16, 14, [$A0, $02, $00, $2D, $31] ' LCD page 13
SERIN 16, 14, [yn] ' for multiple tests
PAUSE 100

```

```

' for multiple tests

IF yn=0 THEN
  GOTO Done
ELSEIF yn=1 THEN
  RUN 1
ENDIF

Done:
SEROUT 16, 14, [ $A0, $02, $00, $2E, $30 ]
LOW PinIRvdd
HIGH PinLoopoff
PAUSE 10
LOW PinLoopoff
END

'END OF PAGE 2 of 0/2
' shut down procedure
' LCD page 14, "Goodbye"

```

APPENDIX F: BASIC STAMP 2 OPERATIONAL PROGRAM

```
' BASIC Stamp 2 Program for Pump Timer control
' {$STAMP BS2}
' {$PBASIC 2.5}
' {$PORT COM1}
' Program Description: The BASIC Stamp 2 waits for a string instruction from
' the BS2px microcontroller to initiate operation. The BS2 then receives the
' time choice from the BS2px by choice of which I/O pin. Then the BS2 serves
' as a switch and time counter for the Hargraves CE103E-12 Minature Pump and
' the Clippard Solenoid Valve.
```

```
'----- INITIALIZATION -----
DEBUG "Pump is running."
SEROUT 16, 84, ["Hello", CR]      'For serial diagnostic purposes
INPUT 0                          'Configuring Pins
INPUT 1
INPUT 2
INPUT 3
INPUT 4
INPUT 5
INPUT 6
INPUT 7
INPUT 8
LOW 14
LOW 15
SERIN 7,84,[WAIT("XYZ")]         'Waiting for input string from BS2px
SEROUT 16, 84, ["on", CR]       'String received
```

```
'----- PROGRAM -----
Pump:
IF (IN0 = 1) THEN Second5
IF (IN1 = 1) THEN Second10
IF (IN2 = 1) THEN Second15
IF (IN3 = 1) THEN Second20
IF (IN4 = 1) THEN Second25
IF (IN5 = 1) THEN Second30
IF (IN6 = 1) THEN Second60
IF (IN8 = 1) THEN off
GOTO Pump
```

```
'----- SUB-ROUTINES -----
Second5:
SEROUT 16, 84, ["5sec", CR]
PAUSE 5000
HIGH 14
PAUSE 5000
```

LOW 14
PAUSE 100
HIGH 15
PAUSE 9000
LOW 15
GOTO Pump

Second10:
SEROUT 16, 84, ["10sec", CR]
PAUSE 5000
HIGH 14
PAUSE 10000
LOW 14
PAUSE 100
HIGH 15
PAUSE 9000
LOW 15
GOTO Pump

Second15:
SEROUT 16, 84, ["15sec", CR]
PAUSE 5000
HIGH 14
PAUSE 15000
LOW 14
PAUSE 100
HIGH 15
PAUSE 9000
LOW 15
GOTO Pump

Second20:
SEROUT 16, 84, ["20sec", CR]
PAUSE 5000
HIGH 14
PAUSE 20000
LOW 14
PAUSE 100
HIGH 15
PAUSE 9000
LOW 15
GOTO Pump

Second25:
SEROUT 16, 84, ["25sec", CR]
PAUSE 5000
HIGH 14

PAUSE 25000
LOW 14
PAUSE 100
HIGH 15
PAUSE 9000
LOW 15
GOTO Pump

Second30:
SEROUT 16, 84, ["30sec", CR]
PAUSE 5000
HIGH 14
PAUSE 30000
LOW 14
PAUSE 100
HIGH 15
PAUSE 9000
LOW 15
GOTO Pump

Second60:
SEROUT 16, 84, ["60sec", CR]

PAUSE 5000
HIGH 14
PAUSE 60000
LOW 14
PAUSE 100
HIGH 15
PAUSE 9000
LOW 15
GOTO Pump

off:
SEROUT 16, 84, ["off", CR]
LOW 14
LOW 15
END

APPENDIX G: uM-FPU MATH CO-PROCESSOR IDE PROGRAM

```
-----
;-----uM-FPU Math Co-Processor IDE Program-----
;-----Register Definitions-----
Time          equ L1
TimeEnd      equ L2
Sample       equ F3
M            equ F4
Be           equ F5
K            equ F6
Linear       equ F7
Rest         equ F8
Distance     equ F9
CalDist     equ F10
CalLin       equ F11
CalNex       equ F12
TimeFull     equ L13
TimeElapse   equ L14
SampleCnt    equ L15
SampleDiv    equ L16
WaitCount    equ L17
Pressdec     equ F18
PressM       equ F19
PressB       equ F20
Pressconv    equ F21
Pressure     equ F22

;-----
;-----Function Protoypes-----
funcCALIBRATION func %
funcGETSAMPLE   func %
;-----
;-----
#function funcCALIBRATION
; input:  none
; output: none

#asm
    ADCMODE, $10
    ADCTRIG
    SELECTA, 3
    ADCLONG, 0
    LSET0
    FLOAT
    FTOA, 50
    SELECTA, 11
    FSET, 10
    FADD, 6
    LSET, 11
    SELECTA, 11
    FINV
    SELECTA, 12
    FSET, 3
    FMUL, 4
    LSET, 12
    SELECTA, 5
    FSET, 11
    FSUB, 12
    LSET, 5
    FTOA, 96
    STRINS, "\0D\0A"
    ADCMODE, $00
```

```
#endasm
```

```
;
```

```
;
```

```
#function funcGETSAMPLE
```

```
; input: none
```

```
; output: none
```

```
#asm
```

```
CLR, 3
```

```
CLR, 18
```

```
TIMESET
```

```
SELECTA, 1
```

```
TICKLONG
```

```
LSET0
```

```
ADCMODE, $10
```

```
_SampleLoop:
```

```
ADCTRIG
```

```
SELECTA, 3
```

```
ADCLONG, 0
```

```
LADDO
```

```
LDEC, 15
```

```
BRA, GT, _SampleLoop
```

```
SELECTA, 3
```

```
LUDIV, 16
```

```
FLOAT
```

```
FTOA, 50
```

```
ADCTRIG
```

```
SELECTA, 18
```

```
ADCLONG, 1
```

```
LSET0
```

```
FLOAT
```

```
FTOA, 50
```

```
SELECTA, 7
```

```
FSET, 3
```

```
FMUL, 4
```

```
LSET, 7
```

```
SELECTA, 8
```

```
FSET, 7
```

```
FADD, 5
```

```
LSET, 8
```

```
SELECTA, 8
```

```
FINV
```

```
SELECTA, 9
```

```
FSET, 8
```

```
FSUB, 6
```

```
LSET, 9
```

```
FTOA, 73
```

```
SELECTA, 21
```

```
FSET, 18
```

```
FMUL, 19
```

```
LSET, 21
```

```
SELECTA, 22
```

```
FSET, 20
```

```
FSUB, 21
```

```
LSET, 22
```

```
FTOA, 51
```

```
_WaitLoop:
```

```
LDEC, 17
```

```
BRA, GT, _WaitLoop
```

```
SELECTA, 2
```

```
TICKLONG
LSUB, 1
LSET0
SELECTA, 14
LSET, 2
LADD, 13
LSET, 14
LTOA, 4
STRINS, "\\0D\\0A"
SEROUT, 2
ADCMODE, $00
CLR, 15
#endasm
;-----
```

APPENDIX H: MICROSOFT OFFICE EXCEL VBA PROGRAM

```
Sub AAIndex1()  
,  
'Overall Program:  
,  
    Application.Run "Shuffleheight"  
    Application.Run "Shufflepressure"  
    Application.Run "Time1"  
    Application.Run "Time2"  
    Application.Run "Time3"  
    Application.Run "Time4"  
    Application.Run "Time5"  
    Application.Run "Time6"  
    Application.Run "Labels1"  
    Application.Run "Labels2"  
    Application.Run "Labels3"  
    Application.Run "Labels4"  
    Application.Run "Labels5"  
    Application.Run "Labels6"  
    Application.Run "AVERAGE1"  
    Application.Run "AVERAGE2"  
    Application.Run "AVERAGE3"  
    Application.Run "AVERAGE4"  
    Application.Run "AVERAGE5"  
    Application.Run "AVERAGE6"  
    Application.Run "STDEV1"  
    Application.Run "STDEV2"  
    Application.Run "STDEV3"  
    Application.Run "STDEV4"  
    Application.Run "STDEV5"  
    Application.Run "STDEV6"  
    Application.Run "Normal1"  
    Application.Run "Normal2"  
    Application.Run "Stder1"  
    Application.Run "Graph1"  
    Sheets("Data Subj #").Select  
    Application.Run "Graph3"  
    Sheets("Data Subj #").Select  
    Application.Run "Graph5"  
    Sheets("Data Subj #").Select  
    Application.Run "Graph6"  
    Sheets("Data Subj #").Select  
    Application.Run "Graph7"  
    Sheets("Data Subj #").Select  
    Application.Run "Graph9"  
    Sheets("Data Subj #").Select  
    Application.Run "Graph11"  
    Sheets("Data Subj #").Select  
    Application.Run "Graph12"  
    Exit Sub  
End Sub
```

Sub Shuffleheight()

'Reorganizes the height data

```
Range("C3:C2956").Select
Selection.Copy
Range("H3").Select
ActiveSheet.Paste
Range("H200:H2956").Select
Application.CutCopyMode = False
Selection.Cut
Range("I3").Select
ActiveSheet.Paste
Range("I200:I2956").Select
Selection.Cut
Range("J3").Select
ActiveSheet.Paste
Range("J200:J2956").Select
Selection.Cut
Range("K3").Select
ActiveSheet.Paste
Range("K200:K2956").Select
Selection.Cut
Range("L3").Select
ActiveSheet.Paste
Range("L200:L2956").Select
Selection.Cut
Range("R3").Select
ActiveSheet.Paste
Range("R200:R2956").Select
Selection.Cut
Range("S3").Select
ActiveSheet.Paste
Range("S200:S2956").Select
Selection.Cut
Range("T3").Select
ActiveSheet.Paste
Range("T200:T2956").Select
Selection.Cut
Range("U3").Select
ActiveSheet.Paste
Range("U200:U2956").Select
Selection.Cut
Range("V3").Select
ActiveSheet.Paste
Range("V200:V1200").Select
Selection.Cut
Range("AB3").Select
ActiveSheet.Paste
Range("AB200:AB1200").Select
Selection.Cut
Range("AC3").Select
ActiveSheet.Paste
Range("AC200:AC1200").Select
Selection.Cut
```

```

Range("AD3").Select
ActiveSheet.Paste
Range("AD200:AD1200").Select
Selection.Cut
Range("AE3").Select
ActiveSheet.Paste
Range("AE200:AE1200").Select
Selection.Cut
Range("AF3").Select
ActiveSheet.Paste
Range("H2").Select
ActiveSheet.Name = "Data Subj #"
End Sub

```

```

Sub Shufflepressure()

```

```

' Reorganizes the pressure data

```

```

Range("D3:D2956").Select
Selection.Copy
Range("AL3").Select
ActiveSheet.Paste
Range("AL200:AL2956").Select
Application.CutCopyMode = False
Selection.Cut
Range("AM3").Select
ActiveSheet.Paste
Range("AM200:AM2956").Select
Selection.Cut
Range("AN3").Select
ActiveSheet.Paste
Range("AN200:AN2956").Select
Selection.Cut
Range("AO3").Select
ActiveSheet.Paste
Range("AO200:AO2956").Select
Selection.Cut
Range("AP3").Select
ActiveSheet.Paste
Range("AP200:AP2956").Select
Selection.Cut
Range("AV3").Select
ActiveSheet.Paste
Range("AV200:AV2000").Select
Selection.Cut
Range("AW3").Select
ActiveSheet.Paste
Range("AW200:AW2000").Select
Selection.Cut
Range("AX3").Select
ActiveSheet.Paste
Range("AX200:AX2000").Select
Selection.Cut
Range("AY3").Select

```

```

ActiveSheet.Paste
Range("AY200:AY2000").Select
Selection.Cut
Range("AZ3").Select
ActiveSheet.Paste
Range("AZ200:AZ1200").Select
Selection.Cut
Range("BF3").Select
ActiveSheet.Paste
Range("BF200:BF1200").Select
Selection.Cut
Range("BG3").Select
ActiveSheet.Paste
Range("BG200:BG1200").Select
Selection.Cut
Range("BH3").Select
ActiveSheet.Paste
Range("BH200:BH1200").Select
Selection.Cut
Range("BI3").Select
ActiveSheet.Paste
Range("BI200:BI1200").Select
Selection.Cut
Range("BJ3").Select
ActiveSheet.Paste
Range("AL2").Select
End Sub

```

```

Sub Time1()
'
' Creates the time column
'
Range("G3").Select
ActiveCell.FormulaR1C1 = "=ROUND(((RC[-2]/1000)-5.082),3)"
Range("G4").Select
ActiveCell.FormulaR1C1 = "=ROUND((R[-1]C+(RC[-2]/1000)),3)"
Range("G4").Select
Selection.AutoFill Destination:=Range("G4:G198")
Range("G2").Select
End Sub

```

```

Sub Time2()
'
Range("G3:G198").Select
Selection.Copy
Range("Q3").Select
Selection.PasteSpecial Paste:=xlPasteValues, Operation:=xlNone, SkipBlanks _
:=False, Transpose:=False
Range("Q2").Select
End Sub

```

```

Sub Time3()
'
Range("G3:G198").Select

```

```
Selection.Copy
Range("AA3").Select
Selection.PasteSpecial Paste:=xlPasteValues, Operation:=xlNone, SkipBlanks _
:=False, Transpose:=False
Range("AA2").Select
End Sub
```

```
Sub Time4()
'
Range("G3:G198").Select
Selection.Copy
Range("AK3").Select
Selection.PasteSpecial Paste:=xlPasteValues, Operation:=xlNone, SkipBlanks _
:=False, Transpose:=False
Range("AK2").Select
End Sub
```

```
Sub Time5()
'
Range("G3:G198").Select
Selection.Copy
Range("AU3").Select
Selection.PasteSpecial Paste:=xlPasteValues, Operation:=xlNone, SkipBlanks _
:=False, Transpose:=False
Range("AU2").Select
End Sub
```

```
Sub Time6()
'
Range("G3:G198").Select
Selection.Copy
Range("BE3").Select
Selection.PasteSpecial Paste:=xlPasteValues, Operation:=xlNone, SkipBlanks _
:=False, Transpose:=False
Range("BE2").Select
End Sub
```

```
Sub Labels1()
'
' Adds the labels to columns for height
'
Range("G1").Select
ActiveCell.FormulaR1C1 = "TIME (sec)"
Range("H2").Select
ActiveCell.FormulaR1C1 = "TRIAL 1"
Range("I2").Select
ActiveCell.FormulaR1C1 = "TRIAL 2"
Range("J2").Select
ActiveCell.FormulaR1C1 = "TRIAL 3"
Range("K2").Select
```



```

ActiveCell.FormulaR1C1 = "TRIAL 4"
Range("L2").Select
ActiveCell.FormulaR1C1 = "TRIAL 5"
Columns("G:G").EntireColumn.AutoFit
Columns("H:H").EntireColumn.AutoFit
Columns("I:I").EntireColumn.AutoFit
Columns("J:J").EntireColumn.AutoFit
Columns("K:K").EntireColumn.AutoFit
Columns("L:L").EntireColumn.AutoFit
Range("H1:O1").Select
With Selection
    .HorizontalAlignment = xlCenter
    .VerticalAlignment = xlBottom
    .WrapText = False
    .Orientation = 0
    .AddIndent = False
    .IndentLevel = 0
    .ShrinkToFit = False
    .ReadingOrder = xlContext
    .MergeCells = False
End With
Selection.Merge
ActiveCell.FormulaR1C1 = "RUN 1, HEIGHT (cm)"
Range("G2").Select
End Sub

```

```

Sub Labels2()
'
' Adds the labels to columns for height
'
Range("Q1").Select
ActiveCell.FormulaR1C1 = "TIME (sec)"
Range("R2").Select
ActiveCell.FormulaR1C1 = "TRIAL 1"
Range("S2").Select
ActiveCell.FormulaR1C1 = "TRIAL 2"
Range("T2").Select
ActiveCell.FormulaR1C1 = "TRIAL 3"
Range("U2").Select
ActiveCell.FormulaR1C1 = "TRIAL 4"
Range("V2").Select
ActiveCell.FormulaR1C1 = "TRIAL 5"
Columns("Q:Q").EntireColumn.AutoFit
Columns("R:R").EntireColumn.AutoFit
Columns("S:S").EntireColumn.AutoFit
Columns("T:T").EntireColumn.AutoFit
Columns("U:U").EntireColumn.AutoFit
Columns("V:V").EntireColumn.AutoFit
Range("R1:Y1").Select
With Selection
    .HorizontalAlignment = xlCenter
    .VerticalAlignment = xlBottom
    .WrapText = False
    .Orientation = 0

```

```

        .AddIndent = False
        .IndentLevel = 0
        .ShrinkToFit = False
        .ReadingOrder = xlContext
        .MergeCells = False
    End With
    Selection.Merge
    ActiveCell.FormulaR1C1 = "RUN 2, HEIGHT (cm)"
    Range("Q2").Select
End Sub

```

```

Sub Labels3()
'
' Adds the labels to columns for pressure
'
    Range("AA1").Select
    ActiveCell.FormulaR1C1 = "TIME (sec)"
    Range("AB2").Select
    ActiveCell.FormulaR1C1 = "TRIAL 1"
    Range("AC2").Select
    ActiveCell.FormulaR1C1 = "TRIAL 2"
    Range("AD2").Select
    ActiveCell.FormulaR1C1 = "TRIAL 3"
    Range("AE2").Select
    ActiveCell.FormulaR1C1 = "TRIAL 4"
    Range("AF2").Select
    ActiveCell.FormulaR1C1 = "TRIAL 5"
    Columns("AA:AA").EntireColumn.AutoFit
    Columns("AB:AB").EntireColumn.AutoFit
    Columns("AC:AC").EntireColumn.AutoFit
    Columns("AD:AD").EntireColumn.AutoFit
    Columns("AE:AE").EntireColumn.AutoFit
    Columns("AF:AF").EntireColumn.AutoFit
    Range("AB1:AI1").Select
    With Selection
        .HorizontalAlignment = xlCenter
        .VerticalAlignment = xlBottom
        .WrapText = False
        .Orientation = 0
        .AddIndent = False
        .IndentLevel = 0
        .ShrinkToFit = False
        .ReadingOrder = xlContext
        .MergeCells = False
    End With
    Selection.Merge
    ActiveCell.FormulaR1C1 = "RUN 3, HEIGHT (cm)"
    Range("AA2").Select
End Sub

```

```

Sub Labels4()
'
' Adds the labels to columns for pressure

```

```

Range("AK1").Select
ActiveCell.FormulaR1C1 = "TIME (sec)"
Range("AL2").Select
ActiveCell.FormulaR1C1 = "TRIAL 1"
Range("AM2").Select
ActiveCell.FormulaR1C1 = "TRIAL 2"
Range("AN2").Select
ActiveCell.FormulaR1C1 = "TRIAL 3"
Range("AO2").Select
ActiveCell.FormulaR1C1 = "TRIAL 4"
Range("AP2").Select
ActiveCell.FormulaR1C1 = "TRIAL 5"
Columns("AK:AK").EntireColumn.AutoFit
Columns("AL:AL").EntireColumn.AutoFit
Columns("AM:AM").EntireColumn.AutoFit
Columns("AN:AN").EntireColumn.AutoFit
Columns("AO:AO").EntireColumn.AutoFit
Columns("AP:AP").EntireColumn.AutoFit
Range("AL1:AS1").Select
With Selection
    .HorizontalAlignment = xlCenter
    .VerticalAlignment = xlBottom
    .WrapText = False
    .Orientation = 0
    .AddIndent = False
    .IndentLevel = 0
    .ShrinkToFit = False
    .ReadingOrder = xlContext
    .MergeCells = False
End With
Selection.Merge
ActiveCell.FormulaR1C1 = "RUN 1, PRESSURE (inHg)"
Range("AK2").Select
End Sub

```

Sub Labels5()

```

Range("AU1").Select
ActiveCell.FormulaR1C1 = "TIME (sec)"
Range("AV2").Select
ActiveCell.FormulaR1C1 = "TRIAL 1"
Range("AW2").Select
ActiveCell.FormulaR1C1 = "TRIAL 2"
Range("AX2").Select
ActiveCell.FormulaR1C1 = "TRIAL 3"
Range("AY2").Select
ActiveCell.FormulaR1C1 = "TRIAL 4"
Range("AZ2").Select
ActiveCell.FormulaR1C1 = "TRIAL 5"
Columns("AU:AU").EntireColumn.AutoFit
Columns("AV:AV").EntireColumn.AutoFit
Columns("AW:AW").EntireColumn.AutoFit
Columns("AX:AX").EntireColumn.AutoFit

```

```

Columns("AY:AY").EntireColumn.AutoFit
Columns("AZ:AZ").EntireColumn.AutoFit
Range("AV1:BC1").Select
With Selection
    .HorizontalAlignment = xlCenter
    .VerticalAlignment = xlBottom
    .WrapText = False
    .Orientation = 0
    .AddIndent = False
    .IndentLevel = 0
    .ShrinkToFit = False
    .ReadingOrder = xlContext
    .MergeCells = False
End With
Selection.Merge
ActiveCell.FormulaR1C1 = "RUN 2, PRESSURE (inHg)"
Range("AU2").Select
End Sub

```

```

Sub Labels6()
    Range("BE1").Select
    ActiveCell.FormulaR1C1 = "TIME (sec)"
    Range("BF2").Select
    ActiveCell.FormulaR1C1 = "TRIAL 1"
    Range("BG2").Select
    ActiveCell.FormulaR1C1 = "TRIAL 2"
    Range("BH2").Select
    ActiveCell.FormulaR1C1 = "TRIAL 3"
    Range("BI2").Select
    ActiveCell.FormulaR1C1 = "TRIAL 4"
    Range("BJ2").Select
    ActiveCell.FormulaR1C1 = "TRIAL 5"
    Columns("BE:BE").EntireColumn.AutoFit
    Columns("BF:BF").EntireColumn.AutoFit
    Columns("BG:BG").EntireColumn.AutoFit
    Columns("BH:BH").EntireColumn.AutoFit
    Columns("BI:BI").EntireColumn.AutoFit
    Columns("BJ:BJ").EntireColumn.AutoFit
    Range("BF1:BM1").Select
    With Selection
        .HorizontalAlignment = xlCenter
        .VerticalAlignment = xlBottom
        .WrapText = False
        .Orientation = 0
        .AddIndent = False
        .IndentLevel = 0
        .ShrinkToFit = False
        .ReadingOrder = xlContext
        .MergeCells = False
    End With
    Selection.Merge
    ActiveCell.FormulaR1C1 = "RUN 3, PRESSURE (inHg)"
    Range("BE2").Select
End Sub

```

```

Sub AVERAGE1()
'
' Averages the points of the different trials
'
Range("M2").Select
ActiveCell.FormulaR1C1 = "AVERAGE"
Range("M3").Select
ActiveCell.FormulaR1C1 = "=ROUND(AVERAGE(RC[-5]:RC[-1]),3)"
Range("M3").Select
Selection.AutoFill Destination:=Range("M3:M198")
Range("M3:M198").Select
Columns("M:M").EntireColumn.AutoFit
End Sub

```

```

Sub AVERAGE2()
'
' Averages the points of the different trials
'
Range("W2").Select
ActiveCell.FormulaR1C1 = "AVERAGE"
Range("W3").Select
ActiveCell.FormulaR1C1 = "=ROUND(AVERAGE(RC[-5]:RC[-1]),3)"
Range("W3").Select
Selection.AutoFill Destination:=Range("W3:W198")
Range("W3:W198").Select
Columns("W:W").EntireColumn.AutoFit
End Sub

```

```

Sub AVERAGE3()
'
Range("AG2").Select
ActiveCell.FormulaR1C1 = "AVERAGE"
Range("AG3").Select
ActiveCell.FormulaR1C1 = "=ROUND(AVERAGE(RC[-5]:RC[-1]),3)"
Range("AG3").Select
Selection.AutoFill Destination:=Range("AG3:AG198")
Range("AG3:AG198").Select
Columns("AG:AG").EntireColumn.AutoFit
End Sub

```

```

Sub AVERAGE4()
'
Range("AQ2").Select
ActiveCell.FormulaR1C1 = "AVERAGE"
Range("AQ3").Select
ActiveCell.FormulaR1C1 = "=ROUND(AVERAGE(RC[-5]:RC[-1]),3)"
Range("AQ3").Select
Selection.AutoFill Destination:=Range("AQ3:AQ198")
Range("AQ3:AQ198").Select
Columns("AQ:AQ").EntireColumn.AutoFit
End Sub

```

```

Sub AVERAGE5()
'
Range("BA2").Select
ActiveCell.FormulaR1C1 = "AVERAGE"
Range("BA3").Select
ActiveCell.FormulaR1C1 = "=ROUND(AVERAGE(RC[-5]:RC[-1]),3)"
Range("BA3").Select
Selection.AutoFill Destination:=Range("BA3:BA198")
Range("BA3:BA198").Select
Columns("BA:BA").EntireColumn.AutoFit
End Sub

```

```

Sub AVERAGE6()
'
Range("BK2").Select
ActiveCell.FormulaR1C1 = "AVERAGE"
Range("BK3").Select
ActiveCell.FormulaR1C1 = "=ROUND(AVERAGE(RC[-5]:RC[-1]),3)"
Range("BK3").Select
Selection.AutoFill Destination:=Range("BK3:BK198")
Range("BK3:BK198").Select
Columns("BK:BK").EntireColumn.AutoFit
End Sub

```

```

Sub STDEV1()
'
' Computes standard deviation of average curve
'
Range("N2").Select
ActiveCell.FormulaR1C1 = "STDEV"
Range("N3").Select
ActiveCell.FormulaR1C1 = "=ROUND(STDEV(RC[-6]:RC[-2]),4)"
Range("N3").Select
Selection.AutoFill Destination:=Range("N3:N198")
Range("N2").Select
Columns("N:N").EntireColumn.AutoFit
End Sub

```

```

Sub STDEV2()
Range("X2").Select
ActiveCell.FormulaR1C1 = "STDEV"
Range("X3").Select
ActiveCell.FormulaR1C1 = "=ROUND(STDEV(RC[-6]:RC[-2]),4)"
Range("X3").Select
Selection.AutoFill Destination:=Range("X3:X198")
Range("X2").Select
Columns("X:X").EntireColumn.AutoFit
End Sub

```

```

Sub STDEV3()
Range("AH2").Select

```

```

ActiveCell.FormulaR1C1 = "STDEV"
Range("AH3").Select
ActiveCell.FormulaR1C1 = "=ROUND(STDEV(RC[-6]:RC[-2]),4)"
Range("AH3").Select
Selection.AutoFill Destination:=Range("AH3:AH198")
Range("AH2").Select
Columns("AH:AH").EntireColumn.AutoFit
End Sub

```

```

Sub STDEV4()
Range("AR2").Select
ActiveCell.FormulaR1C1 = "STDEV"
Range("AR3").Select
ActiveCell.FormulaR1C1 = "=ROUND(STDEV(RC[-6]:RC[-2]),4)"
Range("AR3").Select
Selection.AutoFill Destination:=Range("AR3:AR198")
Range("AR2").Select
Columns("AR:AR").EntireColumn.AutoFit
End Sub

```

```

Sub STDEV5()
Range("BB2").Select
ActiveCell.FormulaR1C1 = "STDEV"
Range("BB3").Select
ActiveCell.FormulaR1C1 = "=ROUND(STDEV(RC[-6]:RC[-2]),4)"
Range("BB3").Select
Selection.AutoFill Destination:=Range("BB3:BB198")
Range("BB2").Select
Columns("BB:BB").EntireColumn.AutoFit
End Sub

```

```

Sub STDEV6()
Range("BL2").Select
ActiveCell.FormulaR1C1 = "STDEV"
Range("BL3").Select
ActiveCell.FormulaR1C1 = "=ROUND(STDEV(RC[-6]:RC[-2]),4)"
Range("BL3").Select
Selection.AutoFill Destination:=Range("BL3:BL198")
Range("BL2").Select
Columns("BL:BL").EntireColumn.AutoFit
End Sub

```

```

Sub Graph1()
'
' Graphs the output of the trials and the average curve with error bars in standard deviation
'
Dim MyChart As Chart
Dim DataRange As Range
Set DataRange = ActiveSheet.Range("G2:M198")
Set MyChart = Charts.Add
MyChart.SetSourceData Source:=DataRange

```

```

ActiveChart.ApplyChartTemplate ("C:\Documents and Settings\Anna\Application
Data\Microsoft\Templates\Charts\Resultsgraph")
ActiveChart.Axes(xlValue).AxisTitle.Select
ActiveChart.Axes(xlValue, xlPrimary).AxisTitle.Text = "DEFORMATION (cm)"
ActiveChart.Name = "RUN 1 TRIES Subj #"
End Sub

```

Sub Graph2()

```

Dim MyCharta As Chart
Dim DataRangea As Range
Set DataRangea = ActiveSheet.Range("G2:G198, M2:M198")
Set MyCharta = Charts.Add
MyCharta.SetSourceData Source:=DataRangea
ActiveChart.ApplyChartTemplate ("C:\Documents and Settings\Anna\Application
Data\Microsoft\Templates\Charts\Resultsgraph")
ActiveChart.Axes(xlValue).AxisTitle.Select
ActiveChart.Axes(xlValue, xlPrimary).AxisTitle.Text = "DEFORMATION (cm)"
ActiveChart.Legend.Select
Selection.Delete
ActiveChart.ChartTitle.Select
Selection.Delete
ActiveChart.SeriesCollection(1).Select
ActiveChart.SeriesCollection(1).HasErrorBars = True
ActiveChart.Name = " RUN 1 DEFORM Subj #"
End Sub

```

Sub Graph3()

```

Dim MyChart As Chart
Dim DataRange As Range
Set DataRange = ActiveSheet.Range("Q2:W198")
Set MyChart = Charts.Add
MyChart.SetSourceData Source:=DataRange
ActiveChart.ApplyChartTemplate ("C:\Documents and Settings\Anna\Application
Data\Microsoft\Templates\Charts\Resultsgraph")
ActiveChart.Axes(xlValue).AxisTitle.Select
ActiveChart.Axes(xlValue, xlPrimary).AxisTitle.Text = "DEFORMATION (cm)"
ActiveChart.Name = "RUN 2 TRIALS Subj #"
End Sub

```

Sub Graph4()

```

Dim MyCharta As Chart
Dim DataRangea As Range
Set DataRangea = ActiveSheet.Range("Q2:Q198, W2:W198")
Set MyCharta = Charts.Add
MyCharta.SetSourceData Source:=DataRangea
ActiveChart.ApplyChartTemplate ("C:\Documents and Settings\Anna\Application
Data\Microsoft\Templates\Charts\Resultsgraph")
ActiveChart.Axes(xlValue).AxisTitle.Select
ActiveChart.Axes(xlValue, xlPrimary).AxisTitle.Text = "DEFORMATION (cm)"

```



```

ActiveChart.Legend.Select
Selection.Delete
ActiveChart.ChartTitle.Select
Selection.Delete
ActiveChart.SeriesCollection(1).Select
ActiveChart.SeriesCollection(1).HasErrorBars = True
ActiveChart.Name = "RUN 2 DEFORMATION Subj #"
End Sub

```

```

Sub Graph5()

```

```

Dim MyChart As Chart
Dim DataRange As Range
Set DataRange = ActiveSheet.Range("AA2:AG198")
Set MyChart = Charts.Add
MyChart.SetSourceData Source:=DataRange
ActiveChart.ApplyChartTemplate ("C:\Documents and Settings\Anna\Application
Data\Microsoft\Templates\Charts\Resultsgraph")
ActiveChart.Axes(xlValue).AxisTitle.Select
ActiveChart.Axes(xlValue, xlPrimary).AxisTitle.Text = "DEFORMATION (cm)"
ActiveChart.Name = "RUN 3 Ht Ts Subj #"
End Sub

```

```

Sub Graph6()

```

```

' Outputs chart of average with error bars in standard deviation FOR BOTH

```

```

Dim MyCharta As Chart
Dim DataRangea As Range
Set DataRangea = ActiveSheet.Range("G2:G198,M2:M198,Q2:Q198, W2:W198, AA2:AA198, AG2:AG198")
Set MyCharta = Charts.Add
MyCharta.SetSourceData Source:=DataRangea
ActiveChart.ApplyChartTemplate ("C:\Documents and Settings\Anna\Application
Data\Microsoft\Templates\Charts\Resultsgraph")
ActiveChart.Axes(xlValue).AxisTitle.Select
ActiveChart.Axes(xlValue, xlPrimary).AxisTitle.Text = "DEFORMATION (cm)"
ActiveChart.SeriesCollection(1).Name = "RUN 1"
ActiveChart.SeriesCollection(3).Name = "RUN 2"
ActiveChart.SeriesCollection(5).Name = "RUN 3"
ActiveChart.SeriesCollection(4).Select
Selection.Delete
ActiveChart.SeriesCollection(2).Select
Selection.Delete
ActiveChart.Name = "DEFORMATION COMPARISON Subj #"
End Sub

```

```

Sub Graph7()

```

```

Dim MyChart As Chart
Dim DataRange As Range
Set DataRange = ActiveSheet.Range("AK2:AQ198")
Set MyChart = Charts.Add

```

```

MyChart.SetSourceData Source:=DataRange
ActiveChart.ApplyChartTemplate ("C:\Documents and Settings\Anna\Application
Data\Microsoft\Templates\Charts\Resultsgraph")
ActiveChart.Axes(xlValue).AxisTitle.Select
ActiveChart.Axes(xlValue, xlPrimary).AxisTitle.Text = "PRESSURE (inHg)"
ActiveChart.Name = "RUN 1 PRESS TRIALS Subj #"
End Sub

```

Sub Graph8()

```

Dim MyCharta As Chart
Dim DataRangea As Range
Set DataRangea = ActiveSheet.Range("AK2:AK198, AQ2:AQ198")
Set MyCharta = Charts.Add
MyCharta.SetSourceData Source:=DataRangea
ActiveChart.ApplyChartTemplate ("C:\Documents and Settings\Anna\Application
Data\Microsoft\Templates\Charts\Resultsgraph")
ActiveChart.Axes(xlValue).AxisTitle.Select
ActiveChart.Axes(xlValue, xlPrimary).AxisTitle.Text = "PRESSURE (inHg)"
ActiveChart.Legend.Select
Selection.Delete
ActiveChart.ChartTitle.Select
Selection.Delete
ActiveChart.SeriesCollection(1).Select
ActiveChart.SeriesCollection(1).HasErrorBars = True
ActiveChart.Name = "RUN 1 PRESSURE Subj #"
End Sub

```

Sub Graph9()

```

Dim MyChart As Chart
Dim DataRange As Range
Set DataRange = ActiveSheet.Range("AU2:BA198")
Set MyChart = Charts.Add
MyChart.SetSourceData Source:=DataRange
ActiveChart.ApplyChartTemplate ("C:\Documents and Settings\Anna\Application
Data\Microsoft\Templates\Charts\Resultsgraph")
ActiveChart.Axes(xlValue).AxisTitle.Select
ActiveChart.Axes(xlValue, xlPrimary).AxisTitle.Text = "PRESSURE (inHg)"
ActiveChart.Name = "RUN 2 PRESS TRIALS Subj #"
End Sub

```

Sub Graph10()

```

Dim MyCharta As Chart
Dim DataRangea As Range
Set DataRangea = ActiveSheet.Range("AU2:AU198, BA2:BA198")
Set MyCharta = Charts.Add
MyCharta.SetSourceData Source:=DataRangea
ActiveChart.ApplyChartTemplate ("C:\Documents and Settings\Anna\Application
Data\Microsoft\Templates\Charts\Resultsgraph")
ActiveChart.Axes(xlValue).AxisTitle.Select

```

```

ActiveChart.Axes(xlValue, xlPrimary).AxisTitle.Text = "PRESSURE (inHg)"
ActiveChart.Legend.Select
Selection.Delete
ActiveChart.ChartTitle.Select
Selection.Delete
ActiveChart.SeriesCollection(1).Select
ActiveChart.SeriesCollection(1).HasErrorBars = True
ActiveChart.Name = "RUN 2 PRESS Subj #"
End Sub

```

```

Sub Graph11()
'
Dim MyChart As Chart
Dim DataRange As Range
Set DataRange = ActiveSheet.Range("BE2:BK198")
Set MyChart = Charts.Add
MyChart.SetSourceData Source:=DataRange
ActiveChart.ApplyChartTemplate ("C:\Documents and Settings\Anna\Application
Data\Microsoft\Templates\Charts\Resultsgraph")
ActiveChart.Axes(xlValue).AxisTitle.Select
ActiveChart.Axes(xlValue, xlPrimary).AxisTitle.Text = "PRESSURE (inHg)"
ActiveChart.Name = "RUN 3 Pres Ts Subj #"
End Sub

```

```

Sub Graph12()
'
' Outputs chart of average with error bars in standard deviation FOR BOTH
'
Dim MyCharta As Chart
Dim DataRangea As Range
Set DataRangea = ActiveSheet.Range("AK2:AK198, AQ2:AQ198, AU2:AU198, BA2:BA198, BE2:BE198,
BK2:BK198")
Set MyCharta = Charts.Add
MyCharta.SetSourceData Source:=DataRangea
ActiveChart.ApplyChartTemplate ("C:\Documents and Settings\Anna\Application
Data\Microsoft\Templates\Charts\Resultsgraph")
ActiveChart.Axes(xlValue).AxisTitle.Select
ActiveChart.Axes(xlValue, xlPrimary).AxisTitle.Text = "PRESSURE (inHg)"
ActiveChart.SeriesCollection(1).Name = "RUN 1"
ActiveChart.SeriesCollection(3).Name = "RUN 2"
ActiveChart.SeriesCollection(5).Name = "RUN 3"
ActiveChart.SeriesCollection(4).Select
Selection.Delete
ActiveChart.SeriesCollection(2).Select
Selection.Delete
ActiveChart.Name = "PRESSURE COMPARISION Subj #"
End Sub

```

```

Sub Normal2()
'
Range("CG1").Select
ActiveCell.FormulaR1C1 = "Normalization:"

```

```

Range("CA2:CE2").Select
Selection.Copy
Range("CG2").Select
ActiveSheet.Paste
Range("CG3").Select
ActiveCell.FormulaR1C1 = "=ROUND(AVERAGE(RC[-18]:R[40]C[-18]),3)"
Range("CH3").Select
ActiveCell.FormulaR1C1 = "=ROUND(AVERAGE(RC[-18]:R[40]C[-18]),3)"
Range("CI3").Select
ActiveCell.FormulaR1C1 = "=ROUND(AVERAGE(RC[-18]:R[40]C[-18]),3)"
Range("CJ3").Select
ActiveCell.FormulaR1C1 = "=ROUND(AVERAGE(RC[-18]:R[40]C[-18]),3)"
Range("CK3").Select
ActiveCell.FormulaR1C1 = "=ROUND(AVERAGE(RC[-18]:R[40]C[-18]),3)"
Range("CF2").Select
ActiveCell.FormulaR1C1 = "RUN 1"
Range("CF3").Select
ActiveCell.FormulaR1C1 = "AVG"
Range("CF4").Select
ActiveCell.FormulaR1C1 = "DIFF"
Range("CF5").Select
ActiveCell.FormulaR1C1 = "Value"
Range("CG4").Select
ActiveCell.FormulaR1C1 = "=8-R[-1]C"
Range("CG4").Select
Selection.AutoFill Destination:=Range("CG4:CK4"), Type:=xlFillDefault
Range("CG4:CK4").Select
Selection.Copy
Range("CG5").Select
Selection.PasteSpecial Paste:=xlPasteValues, Operation:=xlNone, SkipBlanks _
:=False, Transpose:=False
Range("CG1").Select
Range("CA2:CE2").Select
Selection.Copy
Range("CG8").Select
ActiveSheet.Paste
Range("CG9").Select
ActiveCell.FormulaR1C1 = "=ROUND(AVERAGE(R[-6]C[-12]:R[34]C[-12]),3)"
Range("CH9").Select
ActiveCell.FormulaR1C1 = "=ROUND(AVERAGE(R[-6]C[-12]:R[34]C[-12]),3)"
Range("CI9").Select
ActiveCell.FormulaR1C1 = "=ROUND(AVERAGE(R[-6]C[-12]:R[34]C[-12]),3)"
Range("CJ9").Select
ActiveCell.FormulaR1C1 = "=ROUND(AVERAGE(R[-6]C[-12]:R[34]C[-12]),3)"
Range("CK9").Select
ActiveCell.FormulaR1C1 = "=ROUND(AVERAGE(R[-6]C[-12]:R[34]C[-12]),3)"
Range("CF8").Select
ActiveCell.FormulaR1C1 = "RUN 2"
Range("CF9").Select
ActiveCell.FormulaR1C1 = "AVG"
Range("CF10").Select
ActiveCell.FormulaR1C1 = "DIFF"
Range("CF11").Select
ActiveCell.FormulaR1C1 = "Value"
Range("CG10").Select

```

ActiveCell.FormulaR1C1 = "=8-R[-1]C"
 Range("CG10").Select
 Selection.AutoFill Destination:=Range("CG10:CK10"), Type:=xlFillDefault
 Range("CG10:CK10").Select
 Selection.Copy
 Range("CG11").Select
 Selection.PasteSpecial Paste:=xlPasteValues, Operation:=xlNone, SkipBlanks _
 :=False, Transpose:=False
 Range("CA2:CE2").Select
 Selection.Copy
 Range("CG14").Select
 ActiveSheet.Paste
 Range("CG15").Select
 ActiveCell.FormulaR1C1 = "=ROUND(AVERAGE(R[-12]C[-6]:R[28]C[-6]),3)"
 Range("CH15").Select
 ActiveCell.FormulaR1C1 = "=ROUND(AVERAGE(R[-12]C[-6]:R[28]C[-6]),3)"
 Range("CI15").Select
 ActiveCell.FormulaR1C1 = "=ROUND(AVERAGE(R[-12]C[-6]:R[28]C[-6]),3)"
 Range("CJ15").Select
 ActiveCell.FormulaR1C1 = "=ROUND(AVERAGE(R[-12]C[-6]:R[28]C[-6]),3)"
 Range("CK15").Select
 ActiveCell.FormulaR1C1 = "=ROUND(AVERAGE(R[-12]C[-6]:R[28]C[-6]),3)"
 Range("CF14").Select
 ActiveCell.FormulaR1C1 = "RUN 3"
 Range("CF15").Select
 ActiveCell.FormulaR1C1 = "AVG"
 Range("CF16").Select
 ActiveCell.FormulaR1C1 = "DIFF"
 Range("CF17").Select
 ActiveCell.FormulaR1C1 = "Value"
 Range("CG16").Select
 ActiveCell.FormulaR1C1 = "=8-R[-1]C"
 Range("CG16").Select
 Selection.AutoFill Destination:=Range("CG16:CK16"), Type:=xlFillDefault
 Range("CG16:CK16").Select
 Selection.Copy
 Range("CG17").Select
 Selection.PasteSpecial Paste:=xlPasteValues, Operation:=xlNone, SkipBlanks _
 :=False, Transpose:=False
 Range("CG1").Select
 Range("H3").Select
 ActiveCell.FormulaR1C1 = "=RC[59]+R5C[77]"
 Range("H3").Select
 Selection.AutoFill Destination:=Range("H3:L3"), Type:=xlFillDefault
 Range("H3:L3").Select
 Selection.AutoFill Destination:=Range("H3:L198")
 Range("R3").Select
 ActiveCell.FormulaR1C1 = "=RC[55]+R11C[67]"
 Range("R3").Select
 Selection.AutoFill Destination:=Range("R3:V3"), Type:=xlFillDefault
 Range("R3:V3").Select
 Selection.AutoFill Destination:=Range("R3:V198")
 Range("AB3").Select
 ActiveCell.FormulaR1C1 = "=RC[51]+R17C[57]"
 Range("AB3").Select

```
Selection.AutoFill Destination:=Range("AB3:AF3"), Type:=xlFillDefault
Range("AB3:AF3").Select
Selection.AutoFill Destination:=Range("AB3:AF198")
Range("AB3").Select
End Sub
```

```
Sub Normal1()
,
Range("H2:L198").Select
Selection.Copy
Range("BO2").Select
ActiveSheet.Paste
Range("BO1").Select
ActiveCell.FormulaR1C1 = "RUN 1"
Range("R2:V198").Select
Selection.Copy
Range("BU2").Select
ActiveSheet.Paste
Range("BU1").Select
ActiveCell.FormulaR1C1 = "RUN 2"
Range("AB2:AF198").Select
Selection.Copy
Range("CA2").Select
ActiveSheet.Paste
Range("CA1").Select
ActiveCell.FormulaR1C1 = "RUN 3"
End Sub
```

END OF PROGRAM

VITA

Anna Charron Dugas was born as Anna Renae Charron in Aurora, Nebraska in 1979. She grew up on a small family farm near Central City, Nebraska where she gained a passion for learning how equipment works and interacts with humans and animals. After graduating from Central City High School, she earned her Bachelor of Sciences in biological systems engineering at the University of Nebraska-Lincoln in 2002. She worked as a biomedical engineering research assistant at Evanston Northwestern Healthcare in Evanston, Illinois, where she studied the transdermal (skin) toxicity dependence of pesticides on society behaviors (e.g., drinking alcohol, smoking, and using sunscreen). In 2005, she moved to Baton Rouge, Louisiana to be the teaching associate in the Department of Biological and Agricultural Engineering at Louisiana State University. While at LSU, she instructed most of the undergraduate students taking the biological engineering curriculum through the several laboratory classes required for the major.

After the completion of her Master of Science in biological and agricultural engineering, she will move to Dallas, Texas with her husband, Joseph, and plans to continue her research career in the Department of Pharmacology at the University of Texas – Southwestern Medical Center.